ÉCOLE DE TECHNOLOGIE SUPÉRIEURE
UNIVERSITÉ DU QUÉBEC

MANUSCRIPT-BASED THESIS PRESENTED TO
ÉCOLE DE TECHNOLOGIE SUPÉRIEURE

IN PARTIAL FULFILLMENT OF THE REQUIREMENTS FOR
THE DEGREE OF DOCTOR OF PHILOSOPHY
Ph.D.

BY
Cristóbal OCHOA LUNA

NONLINEAR CONTROL OF A SEVEN DEGREES-OF-FREEDOM EXOSKELETON ROBOT ARM

MONTREAL, MARCH 21, 2016

BOARD OF EXAMINERS

THIS THESIS HAS BEEN EVALUATED

BY THE FOLLOWING BOARD OF EXAMINERS

Mr. Maarouf Saad, Thesis Supervisor
Department de genie électrique, École de technologie supérieure

Mr. Guy Gauthier, Chair, Board of Examiners
Département de génie de la production automatisée, École de technologie supérieure

Mr. Vahé Nerguizian, Member of the jury
Département de génie électrique, École de technologie supérieure

Mr. Philippe S. Archambault, Member of the jury
School of Physical & Occupational Therapy, McGill University
and Centre of Interdisciplinary Research in Rehabilitation (CRIR)

Mr. Wael Suleiman, Independent External Evaluator
Electrical and Computer Engineering Department, Engineering Faculty,
Université de Sherbrooke

THIS THESIS WAS PRESENTED AND DEFENDED

IN THE PRESENCE OF A BOARD OF EXAMINERS AND THE PUBLIC

ON JANUARY 21, 2016

AT ÉCOLE DE TECHNOLOGIE SUPÉRIEURE

FOREWORD

The present work is part of the project that has as final objective to develop an upper arm robotic exoskeleton to perform a variety of rehabilitation tasks as well as help in daily life activities. Design and construction of the robot as well as the first control approaches and passive rehabilitation schemes were developed in the work of Mohammad H. Rahman in his Ph.D. studies at École de technologie supérieure (ETS), research summarized in the thesis cited below. Also the work of Thierry Kittel-Ouimet in his M.Sc. studies at ETS yielding to the thesis also cited below.

1. Kittel-Ouimet, Thierry. 2012. « Commande d'un bras exosquelette robotique à sept degrés de liberté ». Master in electric engineering thesis. Montréal, École de technologie supérieure, 154 p.

2. Rahman, Mohammad Habibur. 2012. « Development of an exoskeleton robot for UPPER-LIMB rehabilitation ». Doctor of Philosophy thesis. Montréal, École de technologie supérieure, 206 p.

ACKNOWLEDGMENTS

I wish to express my deepest gratitude to my advisor, Dr. Maarouf Saad for all his teachings and the shared knowledge; but especially his invaluable guidance, patience and his enormous qualities as a mentor and as a person. Without them, the achievement of the present work would have not been possible.

I want to thank as well all my research team: Dr. Philippe S. Archambault, Dr. Jawhar Ghommam, Dr. Wen-Hong Zhu, Dr. Mohammad H. Rahman, Abdelkrim Brahmi, Thierry Kittel-Ouimet and Bruce S. Ferrer for their important contributions to this research. Also I want to thank Dr. Guy Gauthier, Dr. Aimé Francis Okou and Dr. Ilian Bonev for their teaching during the initial part of my studies. I wish to express my gratitude to Dr. Maarouf Saad, Dr. Guy Guthier, Dr. Philippe S. Archambault, Dr. Vahé Nerguizian and Dr. Wael Suleiman for being part of the committee who agreed to review and evaluate this research work. Thanks to Dr. Kash Khorasani for his contribution in my education.

I would like to thank the National Council on Science and Technology of Mexico (CONACYT) for the support under grant No. 211951 jointly with Professor Maarouf Saad and École de technologie supérieure, for the most part of my studies. As well as for the important financial support that Dr. Saad provided in the final part of my studies.

Overall, I want to express my warmest thanks to my parents and sister for their unconditional love and support in all possible ways. To the rest of my family that always supported me in many different means, welcomed me on vacations with all the affection and warmness and forgave the extremely short time that I could spent with them during the last six years.

My most sincere thanks to my friends, back in Mexico and the ones that I made here in Canada; for sharing so many fun and stress-relieving moments, as well as the support and encouragement.

COMMANDE NON LINÉAIRE D'UN BRAS EXOSQUELETTE ROBOTIQUE À SEPT DEGRÉS DE LIBERTÉ

Cristóbal OCHOA LUNA

RÉSUMÉ

Les progrès dans le domaine de la robotique ont permis l'intégration de plus en plus de dispositifs robotisés pour la réadaptation des personnes avec un handicap physique. Ce travail de recherche englobe tout le domaine de la robotique de réadaptation; il présente l'évolution du robot ETS-MARSE, un exosquelette à sept degrés de liberté destiné à être porté par le bras humain. Les développements incluent l'étude et l'implémentation d'une approche de contrôle non linéaire relativement nouvelle, ainsi que différents programmes de réadaptation.

Une des caractéristiques d'un robot de réadaptation est qu'il est utilisé par un grand nombre de patients qui ont des conditions physiologiques et biomécaniques diverses. L'implémentation de la technique de contrôle non linéaire, connue sous le nom de *Virtual Decomposition Control*, atteint cette exigence grâce à son adaptation de paramètres internes qui présente un comportement robuste pour les différentes caractéristiques des utilisateurs de robot. En outre, cette technique simplifie la complexité des robots possédant de hauts degrés de liberté par son innovante décomposition du système. De plus, elle lui assure une stabilité asymptotique et un excellent suivi de trajectoires.

Parmi les différents programmes de réadaptation, nous pouvons nommer : la réadaptation passive, la réadaptation active-assistée et la réadaptation active. La première suit des trajectoires prédéfinies et s'appuie sur l'efficacité du dispositif de commande. Les deux autres programmes ont besoin d'une méthode de compréhension de l'intention du mouvement de l'utilisateur; ils peuvent donc prendre une action de suivre, guider, retenir ou corriger le mouvement. À cet effet, notre première approche utilise un capteur de force comme l'interface humain-robot afin de transformer, par l'intermédiaire d'une fonction d'admittance, les forces que l'utilisateur exerce sur l'effecteur du robot et exécuter la réadaptation active-assistée ou la réadaptation active. Enfin, entre les principaux développements de ce travail, une approche est présentée, dans laquelle la nécessité d'un capteur de force pour effectuer certaines tâches de réadaptation active est supprimée. Au moyen d'un observateur non linéaire, les forces d'interaction sont estimées et l'intention de mouvement de l'utilisateur s'ensuit. Les résultats expérimentaux montrent l'efficacité de toutes les approches proposées. Tous les essais qui ont été faits sur des humains ont été testés avec des sujets qui ne présentent aucun handicap.

Le suivi de trajectoires du robot est exécuté dans l'espace articulaire; certaines trajectoires sont données dans l'espace cartésien et transformées à l'espace articulaire en utilisant la technique du pseudo-inverse de la matrice jacobienne. Cependant, cette option est limitée; la prochaine étape obligatoire pour améliorer les nombreuses fonctions du robot est de résoudre sa cinématique inverse. Parmi les autres progrès qui sont en développement, l'une d'entre

elle est une approche pour la classification et la modélisation des signaux électromyographiques afin d'obtenir des informations auprès des utilisateurs du robot. Les premiers résultats utilisant cette méthodologie sont présentés. La téléopération et les capacités haptiques sont également dans la phase initiale de développement.

Mots-clés: 7DDL réadaptation exosquelette, Virtual Decomposition Control, réadaptation active, réadaptation active-assistée, admittance, observateur non linéaire

NONLINEAR CONTROL OF A SEVEN DEGREES-OF-FREEDOM EXOSKELETON ROBOT ARM

Cristóbal OCHOA LUNA

ABSTRACT

Advances in the field of robotics have allowed increasingly integrating robotic devices for rehabilitation of physical disabilities. This research work is encompassed into the field of rehabilitation robotics; it presents the development of the robot ETS-MARSE, a seven degrees-of-freedom exoskeleton designed to be worn in the human arm. The developments include the study and implementation of a relatively novel nonlinear control approach, as well as different rehabilitation schemes.

One of the characteristics of a rehabilitation robot is that it deals with a wide number of patients that have different biomechanical and physiological conditions. The implementation of the nonlinear control technique known as Virtual Decomposition Control addresses this issue with its internal parameters' adaptation that presents a robust behavior to different characteristics of the robot users. Besides, this technique simplifies the complexity of high degree-of-freedom robots by its innovative sub-systems decomposition. All of above, while ensuring the system asymptotic stability and excellent trajectory tracking.

Between the different rehabilitation schemes, we can mention: passive, active-assistive and active rehabilitation. The first one follows predefined trajectories and relies on the efficiency of the controller. The two other schemes require understanding the user's intention of movement and take an action in order to guide, restrain, correct or follow it. For this purpose, we present an approach that utilizes a force sensor as the human-robot interface in order to transform, via an admittance function, the forces that the user exert to the robot end-effector (handle), and execute active-assisted or active rehabilitation. Finally among the main developments of this work, an approach is presented in which the need of a force sensor to perform some active rehabilitation tasks is removed. By means of a nonlinear observer, the interaction forces are estimated and the user's intention of movement followed. Experimental results show the effectiveness of all the proposed approaches. All the tests involving humans were tested with healthy subjects.

Trajectory tracking of the robot is executed in joint space; some trajectories are given in Cartesian space and transformed to joint space by means of the pseudoinverse of the Jacobian technique. However this option is limited; a mandatory next step to improve many functionalities of the robot is to solve its inverse kinematics. Between other progresses that are in development, is an approach to process electromyographic signals in order to obtain information from the robot's users. First results on this methodology are presented. Teleoperation and haptic capabilities are also in the initial stage of development.

Keywords: 7DOF rehabilitation exoskeleton, Virtual Decomposition Control, active rehabilitation, active-assistive rehabilitation, admittance, nonlinear observer

TABLE OF CONTENTS

LIST OF TABLES

Page

LIST OF FIGURES

Page

LIST OF ABBREVIATIONS AND ACRONYMS

DOF	Degrees-of-freedom
CRIR	Interdisciplinary Research Center in Rehabilitation
CTC	Computed Torque Control
DC	Direct Current
EBC	Electromyographic Based Control
EMG	Electromyographic
ETS	École de technologie supérieure
FBC	Force Based Control
FPGA	Field Programmable Gate Array
HMI	Human Machine Interface
MARSE	Motion Assistive Robotic-exoskeleton for Superior Extremity
mDH	Modified Denavit-Hartenberg parameters
PD	Proportional-Derivative
PI	Proportional-Integral
PID	Proportional-Integral-Derivative
RMS	Root-Mean-Square
SMC	Sliding Mode Control
SCARA	Selective Compliant Assembly (or Articulated) Robot Arm
UE	Upper Extremity
US	United States
VDC	Virtual Decomposition Control

LIST OF SYMBOLS AND UNITS OF MEASUREMENTS

UNITS OF MEASUREMENT

° or deg	degree
μs	microsecond
σ	standard deviation
A	ampere
cm	centimeter
g	gram
Kg	kilogram
m	meter
mNm	millinewton meter
ms	millisecond
N	newton
Nm	newton meter
rpm	revolutions per minute
s or sec	second
V	volt
W	watt

SYMBOLS

α_{i-1}	angle from $\hat{Z}_i$ to $\hat{Z}_{i+1}$, measured about $\hat{X}_i$
a_{i-1}	length from $\hat{Z}_i$ to $\hat{Z}_{i+1}$, measured about $\hat{X}_i$
d_i	distance from $\hat{X}_{i-1}$ to $\hat{X}_i$ measured about $\hat{Z}_i$
θ_i	joint angle from $\hat{X}_{i-1}$ to $\hat{X}_i$ measured positive about $\hat{Z}_i$

$\hat{X}_i, \hat{Y}_i, \hat{Z}_i$	Unitary vectors of the Cartesian coordinate system main axes.
${}^{B_i}\boldsymbol{U}_{B_{i+1}}$	force/moment transformation matrices from frame B_i to frame B_{i+1}
${}^{B_i}V$	linear/angular velocity vector of frame $\{B_i\}$
$\mathcal{V}_7$	augmented velocity vector
$\boldsymbol{J}_7$	VDC Jacobian matrix
$\mathcal{V}_{7r}$	augmented required velocity vector
θ_A	link parameters vector
$\hat{\theta}_i$	estimated parameters vector
${}^{B_i}F_r^*$	required net force/moment vector
${}^{B_i}F_r$	required force/moment vector
τ_{ir}^*	net torque for the joint
τ_{air}	link force/moment vector
τ_i	control torque in Nm

INTRODUCTION

Since the beginnings of robotics, robots have been associated with human beings. In fact, their first activity was their use in the industrial environment to replace or help people in repetitive, dangerous or tedious tasks, and those that require high precision. Subsequently the relation was enriched with a greater exchange of information, for example in areas as robot teleoperation and service robots; nowadays, the relation has arrived at the level of cognitive and physical interaction in the called wearable robots. These robots can be defined as: "those worn by human operators, whether to supplement the function of a limb or to replace it completely" (Pons, 2008).

We can classify wearable robots into two general types, prosthetic and orthotic robots. The first ones have the purpose of replacing a member lost by amputation; the second ones, also called exoskeletons, map the structure of the limb and adapt to it to re-establish or to complete some functional lost. Among the purposes for the wearable robots we can mention: the increase of power, e.g. military applications; teleoperation, e.g. aerospace industry; and rehabilitation, in which our research work is focused. Additionally we can classify them, in a general way, as upper-limb and lower-limb exoskeletons, depending if they are worn in the arms or in the legs respectively.

This thesis presents the development of a robotic orthosis for the upper-limb to be used in rehabilitation, the robot ETS-MARSE (Motion Assistive Robotic-exoskeleton for Superior Extremity). The ETS-MARSE has seven degrees of freedom (DOF) designed to correspond with the main DOF of the human arm at shoulder (3DOF), elbow (1DOF) and wrist (3DOF) levels. The developments included in this work are the study and implementation of a novel control approach and some passive, active-assisted and active rehabilitation schemes. In rehabilitation when assistance is mandatory or might be needed, a therapist, apparatus or robot could participate; in our case, the proposed robot will be in charge of the assistance according to the necessary rehabilitation scheme. Passive rehabilitation is the kind of rehabilitation in which the subject should not provide effort and the rehabilitation task is

carried out by the robot. Active-assisted rehabilitation is the kind of rehabilitation where the subject receives partial assistance from the robot. In active rehabilitation, the subject performs the exercise by itself and the robot became the object of the exercise and an excellent way to measure the subject's performance.

The ETS-MARSE is commanded in passive mode by pre-generated trajectories, either in joint space or Cartesian space, which correspond to different rehabilitation exercises. In active-assisted mode the predefined trajectory is followed by the robot, but it is allowed to be modified by the user in variable degrees. In active mode, the robot responds to the user intention of movement by following it and only assists according with time and spatial constrains.

The first chapter of this document describes the research problem. First, the chapter presents the identification and justification of the research problem, where the problematic that validates the present project is presented. A review of the existing literature is given and the outline of the state of the art of this area of research. Immediately, the objectives of the project, so much general as specific, are declared. Finally, it is presented an overview of the methodology used.

The second chapter presents the first paper of this research work. It is called "Virtual Decomposition Control of an Exoskeleton Robot Arm" and was published in *Robotica* in October, 2014 (Ochoa Luna et al., 2014b) (on-line version). This paper deals with two important issues in rehabilitation robotics: The first one is the capacity to adapt to different patients without significantly varying its performance. It is demonstrated that VDC through its internal parameter adaptation is capable to adapt to the whole robot-human system and have a robust behavior in comparison with Computed Torque control and PID control. The second is that with the novel subsystem decomposition of the VDC, the dynamics of the ETS-MARSE (a 7DOF robot) results in simpler dynamics to be handled by the control computation.

The third chapter is the second journal paper titled “Admittance-Based Upper Limb Robotic Active and Active-Assistive Movements” and was published online in the *International Journal of Advanced Robotic Systems* in September, 2015 (Ochoa Luna et al., 2015). It deals with the first approach to active-assisted and active rehabilitation modes. Both approaches uses the VDC control encompassed in a compliant control. The active-assistive approach uses the virtual work principle and an admittance function to transform the measurements from a force sensor (in the handle of the robot) into trajectory variations that allows the system to understand the user’s intention of movement. The admittance is anchored to a predefined trajectory; this allows, by changing its coefficients (spring and damping) to provide more or less degree of help to the user. In the active approach, this anchor is detached and the force transformation results on real-position differentials instead of trajectory ones; allowing the subject to move freely in space. A virtual environment is presented to guide the movement in the first case and in the second to restrain the free environment by virtual walls.

The fourth chapter contains the third research paper titled “Compliant Control of a Rehabilitation Exoskeleton Robot Arm with Force Observer” that was send to the *IEEE/ASME Transactions on Mechatronics* in March 2016. In our research we realised that the use of a force sensor to guide the movements of the robot, especially at the handle level, could easily result in the damage of such sensor. Also the high cost of elaborated sensors presents a problem for this kind of robots, among other complications. This third paper shows how a nonlinear observer could be used to estimate the user intention of movement instead of a force sensor. The observer successfully estimates the interaction forces between the subject and the robot, and uses this information through a compliant control, as in the second paper, to follow the user’s intention of movement.

After, the discussion of the results and the conclusion of the thesis based in the manuscripts described above are given. Finally, to present the additional content, Annex I presents results of this research that were not encompassed in the three main papers product of this thesis; as well as the present and future work for the ETS-MARSE. Between the results shown is an

approach to process and read information from electromyographic (EMG) signals. This method was used in another journal paper: “EMG Based Control of a Robotic Exoskeleton for Shoulder and Elbow Motion Assist”, published in the *Journal of Automation and Control Engineering* in 2015 (Rahman et al., 2015a); as well as in combination with the force sensor control described in Chapter 3, in the paper: “Force-Position Control of a Robotic Exoskeleton to Provide Upper Extremity Movement Assistance” published in the *International Journal of Modelling Identification and Control* in 2014 (Rahman et al., 2014). The EMG approach is also used in the development of a Neuro-Fuzzy controller to command the ETS-MARSE with the EMG signals from the user’s arm. An approach using a haptic device for teleoperation and eventually haptic capabilities for the ETS-MARSE is also described. Annex II presents an overview (not centered in the ETS-MARSE) of the implementation of VDC for manipulator-like robots.

CHAPTER 1

RESEARCH PROBLEM

In everyday life as consequence of traumas, accidents, work-related injuries, geriatric disorders, sport injuries, among others, diverse types of physiological consequences exist that bring limitations of diverse kind. Between them we can mention: social, occupational, and personal, that result into a decrease in the quality of life of large number of people. Among the main causes, one of the more important nowadays is stroke; it is considered by the World Health Organization (WHO) as a global epidemic. According with the WHO each year 15 million people suffer a stroke worldwide; of them 5 million die and another 5 million are left permanently disabled (Mackay and Mensah, 2004). In Canada, the amount of people suffering consequences of stroke is very large. In 2003, the number of people from 12 years of age and older that were living with the effects of a stroke was 272 000; and yearly, between 40 000 and 50 000 are hospitalized by this condition (Health Canada, 2006).

Among the survivors of a stroke often a burden is placed on their life (physical, emotional and cognitive effects). One of the most common effects after a stroke is weakness or inability to move one side of the body (hemiparesis), which affects up to 90 percent of stroke survivors (Van der Loos and Reinkensmeyer, 2008). Spasticity affects roughly 40 percent of stroke survivors, and is characterized by stiff or tight muscles that constraint movement (National Stroke Association®, 2012). The main treatment for these cases is rehabilitation: the process of helping a patient to achieve the highest level of independence and quality of life possible. When rehabilitation is possible, implies many hours of highly skilled and extensive physiotherapy procedures; the amount of people that can bring this support are not sufficient to carry out with all the patients (Bureau of Labor Statistics, 2015; Gupta, Castillo-Laborde and Landry, 2011; Landry, Ricketts and Verrier, 2007). Hence, the use of robots in rehabilitation is a very important point of interest; in fact, in rehabilitation for the arm for example, it has shown promising results (Klamroth-Marganska et al., 2014; Norouzi-Gheidari, Archambault and Fung, 2012; Patton et al., 2006). The aim of the proposed exoskeleton is to be able to supply robotic rehabilitation and contribute to help people to

reduce the disability consequences or the disability period and make a significant improvement on their quality of life.

1.1 Literature review

The idea to utilize orthoses is not a recent idea. In 1883 professor H. Wangenstein stated the concept of a light-weight exoskeleton that would allow to walk about normality, designed with the purpose that the scientists with some injuries that cannot be healed could continue their noble work, controlled by the power of the user's mind (Pons, 2008). This description, referred to a pneumatic orthosis for the legs, can be considered as the first one where the characteristics existing in the current exoskeletons developments were mentioned.

The studies in the field of upper-limb robotic rehabilitation, the subject of this research work, have been conducted since the middle of the 20th century. The first rehabilitation robots came in the 60's and early 70's with the Case Western University Arm and the Rancho Los Amigos Golden Arm (drove joint by joint by a series of tongue-operated switches) respectively (Siciliano and Khatib, 2008). In the mid 70's in the Department of Veterans Affairs the first command type interface appeared (Seamone and Schmeisser, 1985). In relatively recent dates, an increase number of efficient experimental implementations of rehabilitation robots for the upper-limb have been obtained; among them, there are still different purposes and diverse number of human joints actuated. We find some examples that are focused only on the hand (Chiri et al., 2012; Hu et al., 2013; Jiang et al., 2005; Wege, Kondak and Hommel, 2006), that is by itself a very complex area. Some others are focused in just some of the degrees of freedom of the arm, like elbow (Hu et al., 2007; Vitiello et al., 2013) or wrist training (Hu et al., 2009; Krebs et al., 2007). Some are combined, as shoulder and elbow (Masiero et al., 2007) or forearm and wrist (Gopura and Kiguchi, 2007) or elbow, forearm and wrist (Rocon et al., 2007). Finally there are some robots, as the ETS-MARSE, that deal with the entire arm (shoulder, elbow, forearm and wrist), which will be described in the next subsections of this chapter. Besides rehabilitation, we have upper-limb orthoses for purposes like power augmentation (Kazerooni and Guo, 1993; Sankai, 2006) or as haptic

devices for virtual reality and teleoperation (Tsagarakis, Caldwell and Medrano-Cerda, 1999).

In the study of the state of the art that follows, only robots that are aimed to provide rehabilitation to the whole arm (shoulder, elbow, forearm and wrist) are mentioned. We classify them into two main types: end-effector type and exoskeleton type. The first ones attach to the human arm at specific contact points and manipulate it by applying forces to the distal segments of the arm; the second ones, are designed to be worn by the users and model the human arm mechanics and axis of movement. This analysis starts with a brief description of the main approaches in control inputs and control strategies.

1.1.1 Overview of control inputs and control strategies

The source that commands the robot behavior has evolved greatly since the first developments in the area. It has advanced through joysticks, sensors operated by another part of the body, preprogrammed routines and others, to reach nowadays high-order schemes that mimic with human physiological actions and responses. Two of the techniques most used in our days are force control (Perry and Rosen, 2006) and EMG-based control. Work in the subject of EMG signals has shown that an active EMG-driven robotic rehabilitation has some advantages over the passive robotic rehabilitation; e.g. reducing the spasticity on the elbow joint compared against passive rehabilitation (Hu et al., 2008). Also, the use of EMG signals to study the arm motion provided an improve continuous-profile of force and motion (Artemiadis and Kyriakopoulos, 2008), over previous work that deals only with the initiation and ending of the motion.

With respect to the control strategies, we can find PD controllers used in combination with nonlinear techniques as Computed Torque Control (CTC) (Brackbill et al., 2009), Neuro-Fuzzy controllers (Rahman et al., 2006), Fuzzy Controllers based on Sliding Mode (Sun, Sun and Feng, 1999), CTC combined with Fuzzy Control (Song et al., 2005) to overcome the CTC disadvantage of requiring precise knowledge of the dynamical model of the robot.

1.1.2 End-effector type upper-limb rehabilitation robots state of the art

Table 1.1 End-effector type upper-limb rehabilitation state-of-the-art robots

Robot	DOF	Institute	Year of studied publication
MIT-MANUS	2	Massachusetts Institute of Technology	2003
iPAM	3	University of Leeds	2007
MIME	3	VA Palo Alto and Stanford University	2004
GENTLE/s	3	University of Reading	2003

Among some of the end-effector based devices for rehabilitation we can mention: The MIT-MANUS, a 2DOF planar robot to provide physical rehabilitation with extremely low inertia and friction that has presented successful results in tests at the Burke Rehabilitation Hospital (Krebs et al., 2003). The iPAM robotic system, it uses two manipulator-like robots aimed to provide assistive upper-limb therapeutic exercises for post-stroke patients. It has a total of 6DOF and holds patient's arm at that upper arm and forearm level (Jackson et al., 2007). The MIME system; in it, a robot manipulator (PUMA-560) applies forces to the patient that would normally be provided by a therapist. It restricts hand and wrist movement and the focus of the rehabilitation task is aimed to the forearm using goal-oriented movements. It has also been tested to prove the efficiency of robotic rehabilitation in post-stroke hemiparesis (Lum et al., 2002; Lum, Burgar and Shor, 2004). The GENTLE/s system, it utilizes an active 3DOF haptic master robot attached to the wrist of the patient. It uses tele-presence and virtual reality as the method to provide rehabilitation. This approach encourages the patients to exercise for longer periods of time; it has been tested with stroke patients (Coote et al., 2008; Loureiro et al., 2003). A very important characteristic of this type of robotic devices is that they do not actively support the extremity. Table 1.1 lists the systems described above.

1.1.3 Exoskeleton type upper-limb rehabilitation state of the art robots

Table 1.2 Exoskeleton type upper-limb rehabilitation state-of-the-art robots

Robot	DOF	Institute	Year of studied publication
ETS-MARSE	7	École de technologie supérieure	2015
CADEN-7	7	University of Washington	2007
ABLE	4	Interactive Robotics Unit of CEA-LIST	2010
SARCOS	7	University of Southern California	2005

Between some of the exoskeletons devices for rehabilitation we can mention: ETS-MARSE, our project, a 7DOF manipulator-like exoskeleton (Rahman et al., 2015b). It has been developed to the point of having passive, active-assisted and active rehabilitation routines. It remains pending to improve security protocols for the human-machine interaction and to initiate tests with patients to validate the effectiveness of such schemes to provide rehabilitation. The CADEN-7 (Perry, Rosen and Burns, 2007), a 7DOF exoskeleton currently in the third generation of this project. It is controlled by two PCs, one for the low level control (servo control) and the other that calculates the force feedbacks that need to be rendered and applied by the exoskeleton arm, retrieving information from three multi-axis force/torque sensors and can run the virtual environment to be simulated to the user. It can perform different tasks, under four modalities: active and passive mode of rehabilitation, assistive device, haptic device and master device. The ABLE robot, an anthropomorphic upper limb exoskeleton which innovative actuators design allows it to be highly reversible (Garrec, 2010). The 4DOF version was being tested for rehabilitation proposes and the design to create a forearm-wrist module with the remaining 3DOF was under development. The Sarcos Master Arm system (Mistry, Mohajerian and Schaal, 2005), a 7DOF hydraulic model. Besides rehabilitation, it is used to model and study issues of motor control in the human arm by applying forces in the joints as perturbations to learn about the human use of arm redundancy to adapt to this constrains. Table 1.2 lists the systems described above.

1.1.4 Limitations of current approaches

Besides the extensive research and great progress in the field of upper-limb robotic rehabilitation, we still can mention a list of limitations that encompass both hardware design and control algorithms. As the main hardware limitations, we can mention:

- Limited degrees of freedom;
- Limited range of motion with respect to human range of motion;
- Complex and robust structures;
- Big-sized joint actuators;
- Weak joint mechanisms;
- Inadequate or not-present safety measurements;
- Lack of adequate gravity compensation;
- Complex coupling mechanisms for arm attachment;
- Use of wires with intricate routing mechanisms for power transmission.

As the main limitations in control approaches we can mention:

- Use of linear control techniques as PD and PID;
- Very heavy computational demands to handle very complex dynamic models;
- Use of simplified models that can introduce lack of robustness and decrease tracking performance;
- Chattering when Sliding Mode Control is used.

1.2 Research objectives and methodology

The global objective of this project is to obtain an arm orthosis that can offer passive, active-assistive and active rehabilitation to physically disable people, with full shoulder, elbow and wrist rehabilitation capabilities. To achieve this main objective the ETS-MARSE exoskeleton was used, developed in its mechanical part and first control approaches in a preceding research work of our research group (Rahman, 2012). The focus of the work described in this thesis is to apply a suitable control algorithm for the robot positioning and to develop a sensing interface between the human and the robot that can provide the control of the

exoskeleton by direct command from the person; i.e., to capture the intension of movement of the user to provide active-assisted and active rehabilitation. To that purpose, the following specific objectives with the described methodology were applied during this research project:

1.2.1 Development of the nonlinear control law

Different control techniques were studied. Because the nonlinear nature of the kinematic chain model of a human arm, the resultant model is nonlinear. Nevertheless, approaches as regular and enhanced PID were studied as well as the most used nonlinear control techniques as computed torque control and sliding mode control. A relatively new technique was implemented: Virtual Decomposition Control. A direct comparison between VDC, CTC and SMC was done. Because its advantages, already described, VDC is now used as the main nonlinear control law of the ETS-MARSE.

1.2.2 The sensing interface

This objective involved the analysis, study and implementation of the human-machine interface to obtain the motion intention for the active-assisted and active rehabilitation modes. Force control was implemented by means of the virtual work principle transformation and an admittance function. As the input to the controller, a force sensor was used as well as a nonlinear perturbation observer. Studies in the area of EMG signals were started and the first result towards control directed by means of these signals were implemented and presented. Teleoperation was begun to be studied.

1.2.3 Inverse Kinematics

In order to perform rehabilitation tasks, some trajectories must be provided in Cartesian space. Although the redundancy problem was not solved, an approach to manage some Cartesian trajectories through the Jacobian pseudo-inverse technique was implemented.

1.2.4 Implementation and experimentation

Besides design and simulation with a variety of tools (MATLAB, Mathematica, and LabVIEW), all the control techniques and methods studied in this research work were implemented on the ETS-MARSE.

To summarize the structure of the present work, Figure 1.1 condenses the methodology described above.

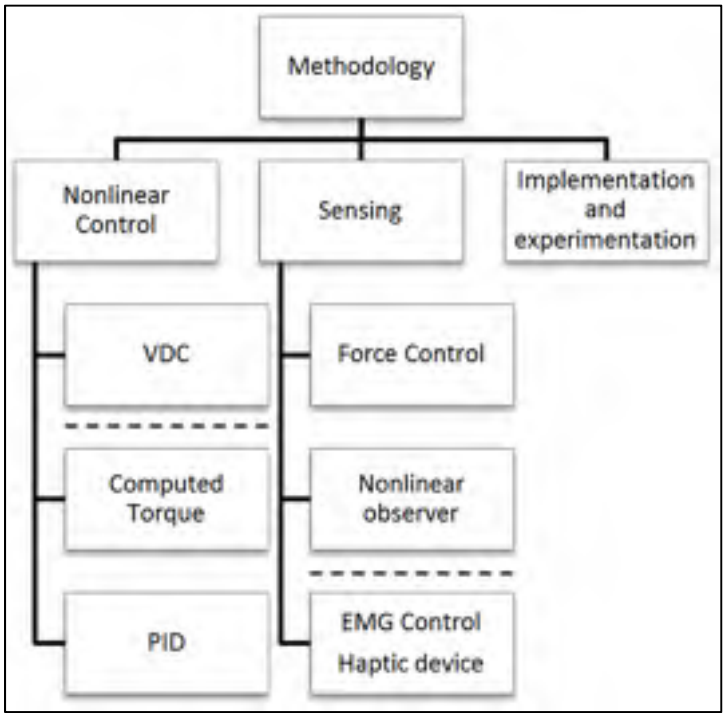

Figure 1.1 Methodology

1.3 Originality of the research and contribution

Besides that in this area extensive studies, models, and projects have been done, still remain in front many options to improve and contribute to this technology as well as many problems and areas of opportunity that need to be solved. Particularly, completely satisfactory results that offer passive, active-assisted an active rehabilitation to the 7DOF of the human arm are

not available yet commercially. One of the important contributions of this work is that our robot covers the main seven degrees-of-freedom of the human arm and it presents passive, active-assisted and active rehabilitation schemes. In the particular case of the control, the integration to the ETS-MARSE of the Virtual Decomposition Control, a relatively new approach that showed advantages over other classic techniques, is an important aspect of this research.

In general, the results contribute in an area of constant growth, permitting to complement the existing knowledge in the field. Finally, the most important contribution will be to help people with physical disability to assist the rehabilitation process, helping them to return to a productive and more independent life, improving in a significant way its quality of life.

CHAPTER 2

VIRTUAL DECOMPOSITION CONTROL OF AN EXOSKELETON ROBOT ARM

Cristóbal Ochoa Luna[1], Mohammad Habibur Rahman[1, 2], Maarouf Saad[1], Philippe Archambault[2, 3], and Wen-Hong Zhu[4]

[1]Department of Electrical Engineering, École de technologie supérieure,
1100 Notre-Dame West, Montreal, Quebec (H3C 1K3) Canada.

[2]School of Physical & Occupational Therapy, McGill University,
3654 Prom Sir-William-Osler, Montréal, Québec (H3G 1Y5) Canada.

[3]Centre for Interdisciplinary Research in Rehabilitation (CRIR),
2275 Laurier Avenue East, Montréal, Quebec (H2H 2N8) Canada.

[4]Space Exploration, Canadian Space Agency,
6767 Route de l'Aéroport, Longueuil (St-Hubert), Quebec (J3Y 8Y9) Canada.

This paper was published in *Robotica* on October 14, 2014

Abstract:

Exoskeleton robots, which can be worn on human limbs to improve or to rehabilitate their function, are currently of great importance. When these robots are used in rehabilitation, one aspect that must be fulfilled is their capacity to adapt to different patients without significantly varying their performance. This paper describes the application of a relatively new control technique called Virtual Decomposition Control (VDC) to a seven degrees-of-freedom (DOF) exoskeleton robot arm, named ETS-MARSE. The VDC approach mainly involves decomposing complex systems into subsystems, and using the resulting simpler dynamics to conduct control computation, while strictly ensuring global stability and having the subsystem dynamics interactions rigorously managed and maintained by means of virtual power flow. This approach is used to deal with different masses, joint stiffness and biomechanical variations of diverse subjects, allowing the control technique to naturally adapt to the variances involved and to maintain a successful control task. The results

obtained in real time on a 7DOF exoskeleton robot arm show the effectiveness of the approach.

Keywords: Exoskeleton robot, Virtual Decomposition Control, passive rehabilitation, active rehabilitation, upper-limb impairment, dynamic variations.

2.1 Introduction

Orthotic robots, or exoskeletons, mimic and adapt to the structure of an injured limb to improve, re-establish or complete some of its functionality (Pons, 2008). Following occupational and sport injuries, traumas, geriatric disorders (Department of Economic and Social Affairs, 2013) and strokes (Mackay and Mensah, 2004), etc., diverse types of physiological complications can arise, possibly leading to social, labour and personal limitations, and consequently decreasing the quality of life of a large number of individuals. One of the symptoms most often diagnosed as a result of a stroke is the loss of function on one side of the body. The main treatment for this is rehabilitation, which requires hours of highly skilled and extensive procedures. The number of people qualified to provide such support is hardly enough to treat all patients affected. Rehabilitation can be supplemented with the use of robots, especially wearable (orthotic or prosthetic) robots (Garrec et al., 2008; Nef et al., 2009; Rahman et al., 2012c). These robots can help people by reducing the impacts of their disabilities and by significantly improving their quality of life.

Passive arm movement therapy is a form of treatment used among patients who are unable to actively move their arms throughout their complete range of motion, following a neurological insult, such as a stroke, which can lead to weakness or paralysis. In passive rehabilitation, the affected limb is moved by external forces (therapist or robot) while the patient relaxes. Active rehabilitation for its part focuses on long-term results; it encourages subjects to move their arms by themselves in order to build muscle strength and flexibility. These issues must therefore be properly addressed in rehabilitation robotics. In the area of upper limb rehabilitation, which was initialized in the middle of the twentieth century (Van

der Loos and Reinkensmeyer, 2008), it was not until very recently that truly functional experimental implementations were obtained with the full capabilities of the whole arm (shoulder, elbow and wrist) (Perry and Rosen, 2006; Tsagarakis, Caldwell and Medrano-Cerda, 1999). Different studies have shown that the use of robotic tools in rehabilitation provides intensive therapy that leads to measurable functional gains (Eschweiler et al., 2014; Lo and Xie, 2012; Norouzi-Gheidari, Archambault and Fung, 2012; Sarakoglou et al., 2007). To that end, work in our laboratory has led to the development of a seven DOF exoskeleton robot to ultimately assist patients with shoulder (3DOF), elbow (1DOF), and wrist (3DOF) movements (Rahman et al., 2015b). The primary objective of this research is to develop a robotic device that can offer passive and active rehabilitation, as well as daily assistance of the upper limbs, to physically disabled people.

A wide range of approaches have been proposed to control rehabilitation robots, ranging from simple PD controllers to nonlinear techniques such as Computed Torque Control (CTC) and Neuro-Fuzzy controllers. Some attractive combined approaches, such as an adaptive Fuzzy controller based on Sliding Mode Control (SMC), for example, was presented by Sun et al (Sun, Sun and Feng, 1999), and seems to be able to deal with the inherent chattering of the SMC, subject to model uncertainties and external disturbances. A combination of adaptive and robust control (Uzmay and Burkan, 2002) merges the advantages of both control laws, eliminating the disadvantage of adaptive controllers in transient behaviour and suppressing the steady-state error. Furthermore, a CTC with Fuzzy Control (Song et al., 2005) provides satisfactory results, subject to manipulator-structured and unstructured uncertainties. An adaptive control with an Artificial Neural Network was presented by Ciliz (Ciliz, 2005) for dealing with frictional uncertainties, which are highly difficult to model. Some other approaches use robust adaptive control that indicate an interesting way of dealing with system uncertainties and external disturbances (Li et al., 2008; Zhijun et al., 2008). However, some fundamental problems are yet to be solved.

In CTC, the main concern is that the control only shows moderate performance improvement when the dynamical model is not exactly known, and this is true even for robots with

relatively small numbers of DOF, such as 4DOF orthosis (Brackbill et al., 2009) for example. Neuro-fuzzy controllers are highly complex, and use different sets of rules and layers involving switching in different regions of operation. This is true even for 3DOF arm exoskeletons (Rahman et al., 2006). In most of the above-mentioned approaches (Ciliz, 2005; Li et al., 2008; Song et al., 2005; Sun, Sun and Feng, 1999; Uzmay and Burkan, 2002; Zhijun et al., 2008), the results are mainly restricted to simulations (i.e., a 2DOF manipulator (Sun, Sun and Feng, 1999), a two-link planar robot (Uzmay and Burkan, 2002) and a two-link elbow planar manipulator (Song et al., 2005)) or implementation on simple robots (i.e., successfully tested on a two-link SCARA type direct drive arm (Ciliz, 2005)).

As can be seen, two specific problems need to be considered together in exoskeleton research: the high number of degrees-of-freedom and the system variability (biomechanical and physiological). For these reasons, a novel application of the Virtual Decomposition Control (VDC) technique is introduced in this paper for the control of exoskeleton robots, in order to address two important issues: a) to facilitate the implementation of a high degree-of-freedom robot (7DOF in this case), and b) to cope with the changes in the dynamics of the robot-human system, due to the biomechanical and physiological characteristics of different patients. As robots become more complex, the complexity of the control task increases as well. Indeed, the complexity of the computation of robot dynamics is proportional to the fourth power of the number of degrees-of-freedom in Lagrangian dynamics (Zhu, Piedboeuf and Gonthier, 2006). This research deals with a complex 7DOF robot. The VDC approach allows us to break the system down into subsystems with relatively simpler dynamics and to apply the control directly over those subsystems. The Virtual Decomposition Control uses the dynamics of subsystems (rigid links and joints) to conduct control design, while rigorously maintaining the L_2 and L_∞ stability of the entire robotic system (Zhu and De Schutter, 2002). This virtual decomposition yields simpler dynamic equations, both in their formulation and implementation. Proceeding as such maintains the complexity of the dynamics of the subsystems constant, meaning that as more and more DOF are added to the robot, the complexity of the total system increases linearly. With the system broken down into simpler subsystems, the VDC handles the dynamic interactions among subsystems

mathematically through the definition of virtual power flows. Thus, even with the subsystem decomposition, the highly nonlinear dynamics of the robotic system are not decoupled, thereby maintaining the control and stability of the entire system.

An additional advantage of the VDC is its ability to manage, through its parameter adaptation, the inherent variability that is present in human dynamics. In addition to the imperfect knowledge of the dynamics of the body structures, different individuals will display differences in body mass, weight distribution, limb length, etc. Moreover, muscular and neurological conditions can change the visco-elastic properties of muscles and joints. For controllers that need to know the dynamical model of the system (e.g., CTC), variations in all these parameters could have a negative impact on the performance of the robot. In our previous research (Rahman et al., 2012b), SMC was implemented for dynamic trajectory tracking corresponding to typical passive rehabilitation exercises. Though SMC performed well, it also showed some limitations in dealing with different subjects. The adaptive characteristics of the VDC overcome this limitation by dealing with biomechanical and physiological variations, providing a better and constant performance of the exercises.

The original contribution of this paper is the application of the VDC to address the issue of dynamic variability, due to individual differences, in order to obtain constant performance by a rehabilitation exoskeleton arm. As well, the simplification of the control task of these multi-articulated robots, through the virtual decomposition process and the use of virtual stability and virtual power flows, allows a simpler computation for systems with high numbers of degrees-of-freedom. The experiments were carried out on different healthy subjects with the ETS-MARSE exoskeleton robot, designed by our research team.

This paper is organized as follows: section 2.2 presents a brief description of the robot and its characteristics. Section 2.3 lays out a detailed presentation of the control development. Finally, in section 2.4, the implementation of the control and experiments executed are explained and the results are presented and discussed, followed in section 2.5 by the conclusions of the work.

2.2 Characteristics of the Motion Assistive Robotic Exoskeleton for Superior Extremity

The wearable upper-limb exoskeleton robot, named "Motion Assistive Robotic Exoskeleton for Superior Extremity" (ETS-MARSE) has 7DOF, and was designed to correspond to the natural range of movement of the upper extremity of the human body. It is comprised of a shoulder motion support part (which assists in horizontal flexion/extension (Figure 2.1a), vertical flexion/extension (Figure 2.1b), and internal/external rotation (Figure 2.1c) of the shoulder), an elbow motion support part (Figure 2.1d) for elbow flexion/extension, a forearm motion support part which is responsible for forearm pronation/supination (Figure 2.1e), and a wrist motion support part (for flexion/extension (Figure 2.1f) and radial/ulnar deviation (Figure 2.1g) of the wrist).

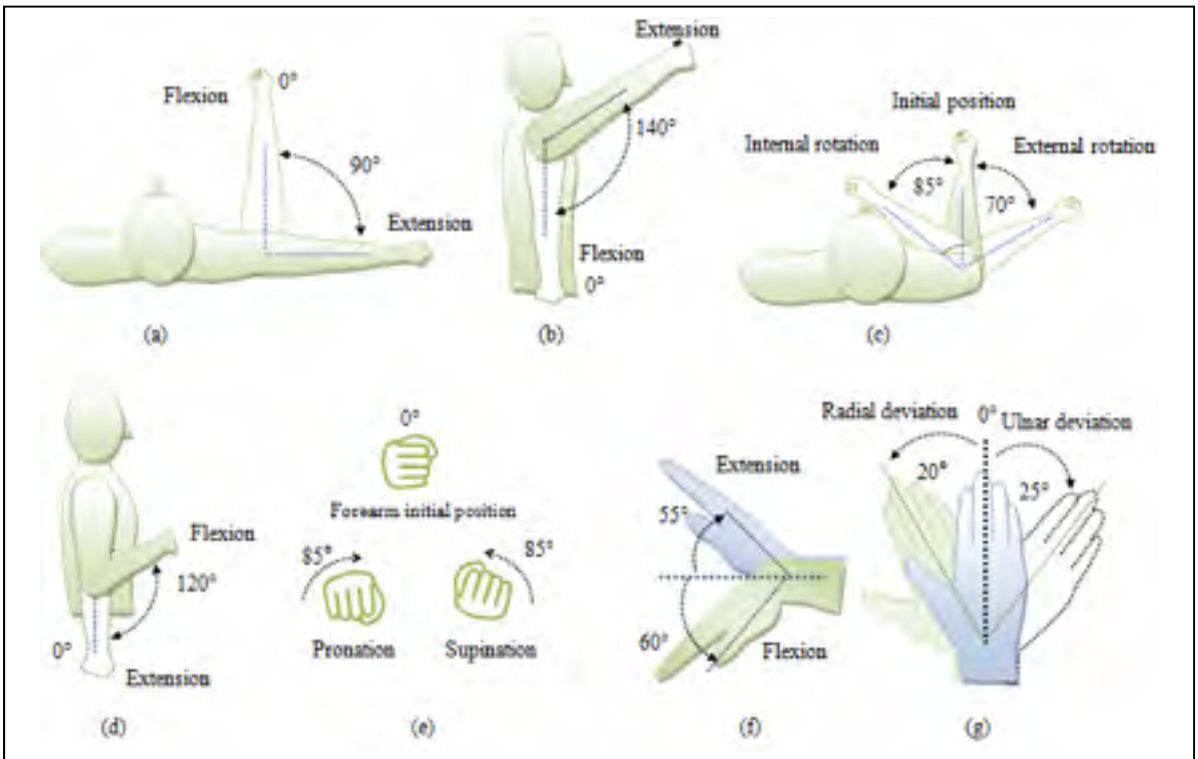

(a) shoulder joint: horizontal flexion/extension; (b) shoulder joint: vertical flexion/extension; (c) shoulder joint: internal/external rotation; (d) elbow flexion/extension; (e) forearm pronation/supination; (f) wrist

Figure 2.1 Joint range of motion of ETS-MARSE

The exoskeleton is an open kinematic chain, manipulator-like robot, with seven revolute DOF ($n = 7$). The kinematics of any robot can be described with four parameters per joint, two describing the joint, and two for its connection with the adjacent joint. One parameter is the joint variable (angle if revolute, distance if prismatic), while the other three are constants (an angle or a distance, opposite of the joint variable and the angle and distance from joint to joint). This convention is known as the Denavit-Hartenberg notation; it has two variations, the original and the modified. As described in Craig (Craig, 2005), with the frames attached to the robot as shown in Figure 2.2, the modified Denavit-Hartenberg parameters are obtained and summarized in Table 2.1.

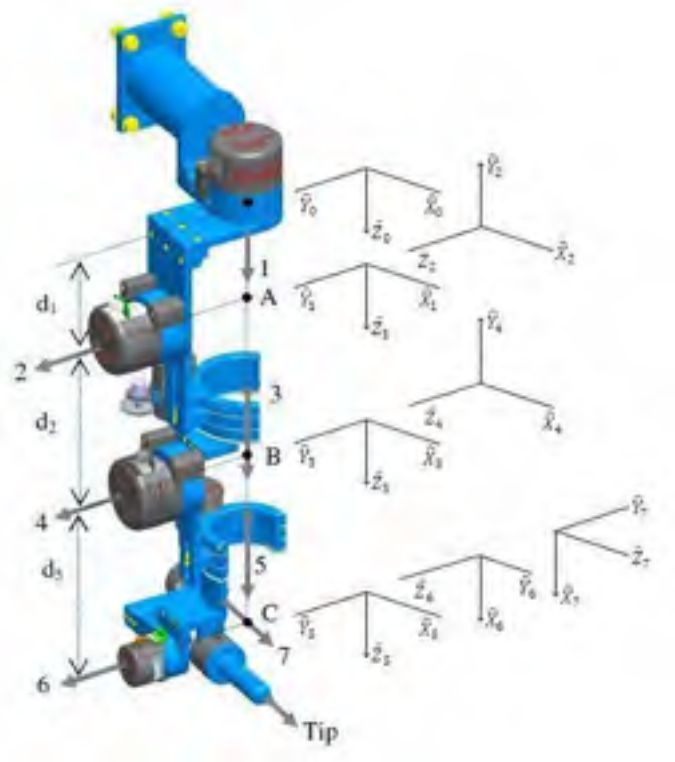

Frame {0} represents the base frame; frame {1}: shoulder horizontal flexion/extension; frame {2}: shoulder vertical flexion/extension; frame {3}: shoulder internal/external rotation; frame {4}: elbow flexion/extension; frame {5}: forearm pronation/supination; frame {6}: wrist flexion/extension and frame {7}: wrist radial/ulnar deviation. Axes shown are in positive direction

Figure 2.2 7DOF Exoskeleton robot arm

Table 2.1 ETS-MARSE Modified
Denavit-HartenbergParameters

i	α_{i-1}	a_{i-1}	d_i	θ_i
1	0°	0	d_1	θ_1
2	-90°	0	0	θ_2
3	90°	0	d_2	θ_3
4	-90°	0	0	θ_4
5	90°	0	d_5	θ_5
6	-90°	0	0	θ_6-90°
7	-90°	0	0	θ_7

2.3 Analysis of the ETS-MARSE robot with Virtual Decomposition Control (Zhu et al., 1997)

The first step in VDC analysis is to perform the virtual decomposition of the robot; in this case, the exoskeleton is a single open chain. This decomposition allows us to base control directly on subsystem dynamics, allowing it to remain relatively simple, i.e., proportional to the number of subsystems. Decomposition is done by placing virtual cutting points separating each joint and link of the system into a subsystem. Although the robot or the human arm does not have seven links (see Figure 2.2), this is a virtual decomposition, and is performed as such to express the system in its most basic operative units. This is a basic approach of VDC to maintain the equations of the system at their most simple expressions for computational handling; another advantage is that if a change is made to any actuator, only the dynamics of that joint will change, not the rest of the system. The result of the system decomposition is illustrated in Figure 2.3: it yielded a decomposition into fourteen subsystems, with the virtual cutting points represented by vertical dotted lines, linked to their respective frames by horizontal dotted lines.

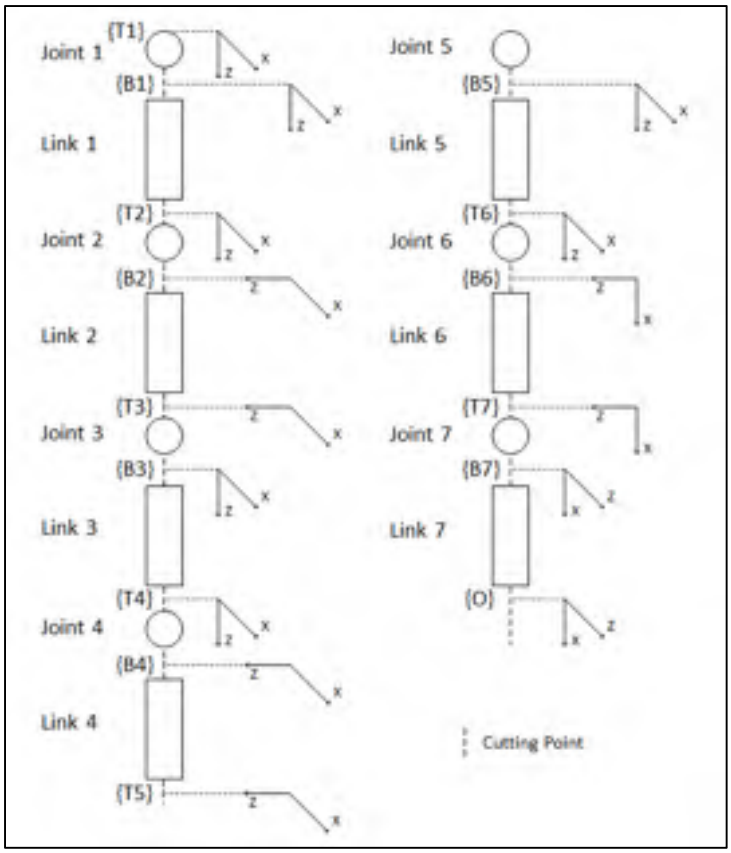

Figure 2.3 Virtual decomposition into 14 subsystems

2.3.1 Kinematics

From the resulting modified Denavit-Hartenberg parameters for the decomposition shown in Figure 2.3, the homogeneous transform matrices of the system are obtained. Using them, it is necessary to calculate the force/moment transformation matrices between any consecutive $\{B\}$ frames ${}^{B_i}\boldsymbol{U}_{B_{i+1}}$ for $i = 1, \dots, 6$ (see Figure 2.3) as follows:

$$ {}^{B_i}\boldsymbol{U}_{B_{i+1}} = \begin{bmatrix} {}^{B_i}\boldsymbol{R}_{B_{i+1}} & \boldsymbol{0}_{3\times 3} \\ ({}^{B_i}r_{B_{i+1}}\times){}^{B_i}\boldsymbol{R}_{B_{i+1}} & {}^{B_i}\boldsymbol{R}_{B_{i+1}} \end{bmatrix} \in \mathbb{R}^{6\times 6} \tag{2.1} $$

where ${}^{B_i}\boldsymbol{R}_{B_{i+1}}$ represents the rotation matrix from frame B_i to frame B_{i+1} and ${}^{B_i}r_{B_{i+1}}$ the vector pointing from B_i to frame B_{i+1}, and:

$$({}^{B_i}r_{B_{i+1}}\times)=\begin{bmatrix}0 & -{}^{B_i}r_{B_{i+1}}(3) & {}^{B_i}r_{B_{i+1}}(2)\\ {}^{B_i}r_{B_{i+1}}(3) & 0 & -{}^{B_i}r_{B_{i+1}}(1)\\ -{}^{B_i}r_{B_{i+1}}(2) & {}^{B_i}r_{B_{i+1}}(1) & 0\end{bmatrix} \tag{2.2}$$

where ${}^{B_i}r_{B_{i+1}}(i)$ represents the ith term of the ${}^{B_i}r_{B_{i+1}}$ vector.

The next step is to calculate ${}^{B_i}V$, the linear/angular velocity vectors of the $\{B_i\}$ frames for $i=1,\dots,7$ as follows:

$${}^{B_i}V=\begin{bmatrix}{}^{B_i}v\\ {}^{B_i}\omega\end{bmatrix}\in\mathbb{R}^6 \tag{2.3}$$

where ${}^{B_i}v$ is the linear velocity vector and ${}^{B_i}\omega$ is the angular velocity vector of the corresponding frame. Defining each joint position (angle) as q_1 to q_7 and using the previous linear/angular velocity vectors in (2.3), the augmented velocity vector is formed as follows:

$$\mathcal{V}_7=[\dot{q}_1\quad\cdots\quad\dot{q}_7\quad{}^{B_1}V^T\quad\dots\quad{}^{B_7}V^T]^T \tag{2.4}$$

Factorizing the joint velocity vector $\dot{q}=[\dot{q}_1\quad\cdots\quad\dot{q}_7]^T$ in (2.4), we obtain:

$$\mathcal{V}_7=\boldsymbol{J}_7\,\dot{q} \tag{2.5}$$

where $\boldsymbol{J}_7$ is the VDC Jacobian matrix of the system:

$$\boldsymbol{J}_7=\begin{bmatrix}\boldsymbol{I}_7 & & & \\ z & 0_6 & \cdots & 0_6\\ {}^{B_1}\boldsymbol{U}_{B_2}^T z & z & \ddots & \vdots\\ \vdots & \ddots & \ddots & 0_6\\ {}^{B_1}\boldsymbol{U}_{B_7}^T z & \dots & {}^{B_6}\boldsymbol{U}_{B_7}^T z & z\end{bmatrix} \tag{2.6}$$

where $z = [0 \quad 0 \quad 0 \quad 0 \quad 0 \quad 1]^T$, $\boldsymbol{I}_7$ represents the 7× 7 identity matrix and 0_6 is a six-element zero vector. Note that the dimension of $\boldsymbol{J}_7$ is 49 × 7; the aforementioned identity matrix and a block of 6 × 7 for each one of the seven degrees-of-freedom of the robot.

Finally, for the kinematics, it is necessary to calculate the required velocities, which are functions of the control requirements. They incorporate terms that allow the tracking of a control objective to the desired velocities obtained from the trajectory generator. In this case, position control is used such that the position is incorporated into the vector of required velocities.

$$\dot{q}_r = \dot{q}_d + \lambda(q_d - q) \tag{2.7}$$

where $\dot{q}_r = [\dot{q}_{1r} \quad \cdots \quad \dot{q}_{7r}]^T$ is a 7×1 reference velocity vector, $\dot{q}_d = [\dot{q}_{1d} \quad \cdots \quad \dot{q}_{7d}]^T$ is the 7×1 desired velocity vector, $\lambda > 0$ is a control parameter, $q_d = [q_{1d} \quad \cdots \quad q_{7d}]^T$ is the 7×1 desired position vector and $q = [q_1 \quad \cdots \quad q_7]^T$ the 7×1 position vector. From (2.6) and (2.7), the 49×1 augmented required velocity vector is obtained as follows:

$$\mathcal{V}_{7r} = \boldsymbol{J}_7 \, \dot{\boldsymbol{q}}_{\boldsymbol{r}} \tag{2.8}$$

From (2.4), it can be established that:

$$\mathcal{V}_{7r} = [\dot{q}_{1r} \quad \cdots \quad \dot{q}_{7r} \quad {}^{B_1}V_r^T \quad \cdots \quad {}^{B_7}V_r^T]^T \tag{2.9}$$

2.3.2 Dynamics

For the simulation, the dynamics of the robot was obtained using the Newton-Euler approach (Craig, 2005). To apply the VDC approach and to obtain the inverse dynamics that takes part in the control of the robot, it was necessary to calculate the required force/moment vectors for the links, ${}^{B_i}F_r$, and then the net torques required by the joints, τ_{ir}^*.

From the general formulation of a rigid body dynamics, in which one frame $\{A\}$ is used as the reference to express the dynamics, and another frame $\{B\}$ is assumed to be located at the centre of mass, the rigid body dynamics can be expressed as:

$$\boldsymbol{M}_A \frac{d}{dt}({}^A V) + \boldsymbol{C}_A({}^A\omega)\,{}^A V + G_A = {}^A F^* \tag{2.10}$$

where (Zhu et al., 1997):

$$\boldsymbol{M}_A = \begin{bmatrix} m_A \boldsymbol{I}_3 & -m_A({}^A r_{AB}\times) \\ m_A({}^A r_{AB}\times) & \boldsymbol{I}_A - m_A({}^A r_{AB}\times)^2 \end{bmatrix} \tag{2.11}$$

$$\boldsymbol{C}_A({}^A\omega) = \begin{bmatrix} m_A({}^A\omega\times) & -m_A({}^A\omega\times)({}^A r_{AB}\times) \\ m_A({}^A r_{AB}\times)({}^A\omega\times) & ({}^A\omega\times)\boldsymbol{I}_A + \boldsymbol{I}_A({}^A\omega\times) - m_A({}^A r_{AB}\times)({}^A\omega\times)({}^A r_{AB}\times) \end{bmatrix} \tag{2.12}$$

$$G_A = \begin{bmatrix} m_A\,{}^A\boldsymbol{R}_I\, g \\ m_A({}^A r_{AB}\times)\,{}^A\boldsymbol{R}_I\, g \end{bmatrix} \tag{2.13}$$

where $m_A \in \mathbb{R}$ is the mass of the rigid body, $\boldsymbol{I}_3$ is a 3×3 identity matrix, $\boldsymbol{I}_A = {}^A\boldsymbol{R}_I \boldsymbol{I}_o(t)\,{}^I\boldsymbol{R}_A$ is time invariant, $\boldsymbol{I}_o(t) \in \mathbb{R}^{3\times 3}$ denotes the moment of inertia matrix around the centre of mass, ${}^A\boldsymbol{R}_I \in \mathbb{R}^{3\times 3}$ is the rotation matrix from frame A to the inertial frame, ${}^{\mathrm{A}}\mathrm{r}_{\mathrm{AB}} \in \mathbb{R}^3$ is the vector pointing from frame A to frame B, ${}^A\omega \in \mathbb{R}^3$ is the angular velocity vector, $g = [0 \quad 0 \quad 9.81]^T \in \mathbb{R}^3$ and $({}^A\omega\times)$ and $({}^A r_{AB}\times)$ are defined as in relation (2.2).

Substituting from (2.10) the dynamic model velocity vector ${}^A V$ by the required velocity vector ${}^A V_r \in \mathbb{R}^6$ defined in (2.9), the following equation is defined:

$$\boldsymbol{M}_A \frac{d}{dt}({}^A V_r) + \boldsymbol{C}_A({}^A\omega)\,{}^A V_r + G_A \stackrel{\text{def}}{=} \boldsymbol{Y}_A\,\theta_A \tag{2.14}$$

where $\boldsymbol{Y}_A \in \mathbb{R}^{6\times13}$ is a regressor matrix composed of elements of $d/dt({}^{A}V_r) \in \mathbb{R}^6$, the velocity vectors ${}^{A}V \in \mathbb{R}^6$ and ${}^{A}V_r \in \mathbb{R}^6$ and terms from the vector of gravity propagation, and $\theta_A \in \mathbb{R}^{13}$ is the vector composed of the mass of the link, the elements of the vector pointing from the origin of the reference frame of the link toward its mass centre, and elements of the inertia tensor of the body. The exact representation of each element of $\boldsymbol{Y}_A$ and θ_A is given in Appendix A.

By means of the linear parameterization expressed above in (2.14), the first step for the link dynamics is to obtain the required net force/moment vectors with the following equation:

$$ {}^{B_i}F_r^* = \boldsymbol{Y}_i\,\hat{\theta}_i + \boldsymbol{K}_{si}({}^{B_i}V_r - {}^{B_i}V) \tag{2.15}$$

for $i = 1, \ldots, 7$ where ${}^{B_i}F_r^*$ are the required net force/moment vectors, $\boldsymbol{K}_{si}$ is a symmetric positive-definite gain matrix, ${}^{B_i}V$ and ${}^{B_i}V_r$ are the velocities defined in (2.4) and (2.9), and $\hat{\theta}_i \in \mathbb{R}^{13}$ is the estimated parameter vector. The estimation of the parameters in $\hat{\theta}_i$ is defined as follows (Zhu et al., 2013):

$$ \hat{\theta}_{i\gamma} = \mathcal{P}\big(s_{i\gamma}(t), \rho_{i\gamma}, a_{i\gamma}(t), b_{i\gamma}(t), t\big) \tag{2.16}$$

for $i = 1, \ldots, 7$ and $\gamma = 1, \ldots, 13$, where $\hat{\theta}_{i\gamma}$ represents the γth parameter of the ith link, $s_{i\gamma}(t) \in \mathbb{R}$ is a scalar variable defined as the γth element in:

$$ s_i = \boldsymbol{Y}_i^T({}^{B_i}V_r - {}^{B_i}V) \tag{2.17}$$

$\rho_{i\gamma}$ is the parameter update gain, $a_{i\gamma}(t)$ and $b_{i\gamma}(t)$ are the lower and upper bounds of $\hat{\theta}_{i\gamma}$ respectively, and the projection function $\mathcal{P}$ is a differentiable scalar function (Zhu and De Schutter, 1999) defined for $t \geq 0$ such that its time derivative is governed by:

$$ \dot{\mathcal{P}} = \rho\, s(t)\, \mathcal{K} \tag{2.18}$$

with:

$$\mathcal{K} = \begin{cases} 0 \;\; if \; \mathcal{P} \leq a(t) and \; s(t) \leq 0 \\ 0 \;\; if \; \mathcal{P} \geq b(t) and \; s(t) \geq 0 \\ 1 \qquad otherwise \end{cases}$$

Once this step is complete, the required force/moment vectors at the cutting points are obtained as follows:

$$\begin{aligned} {}^{B_7}F_r &= {}^{B_7}F_r^* \\ {}^{B_i}F_r &= {}^{B_i}F_r^* + {}^{B_i}\boldsymbol{U}_{B_{i+1}} \, {}^{B_{i+1}}F_r \end{aligned} \tag{2.19}$$

for $i = 6, \dots, 1$. The next step is the calculation of the dynamics of the joints. For $i = 1, \dots, 7$ in (2.20) to (2.24), the following Y vector and parameter vector are defined:

$$Y_{ai} = [\ddot{q}_{ir} \quad sign(\dot{q}_{ir}) \quad \dot{q}_{ir} \quad 1] \tag{2.20}$$

$$\theta_{ai} = [J_{mi} \quad k_{ci} \quad k_{vi} \quad c_i]^T \tag{2.21}$$

where the sub-index a in the vectors is used to differentiate joint variables from the link variables introduced in (2.15), J_{mi} is the equivalent mass or moment of inertia, $k_{ci} > 0$ denotes the Coulomb friction coefficient, $k_{vi} > 0$ is the viscous friction coefficient and c_i denotes an offset that accommodates asymmetric Coulomb frictions. The adaptation of the parameters defined in (2.21) is calculated as:

$$\hat{\theta}_{ai\gamma} = \mathcal{P}\big(s_{ai\gamma}(t), \rho_{ai\gamma}, a_{ai\gamma}(t), b_{ai\gamma}(t), t\big) \tag{2.22}$$

for $i = 1, \dots, 7$ and $\gamma = 1, \dots, 4$, where $\hat{\theta}_{ai\gamma}$ represents the γth parameter of the ith joint, $s_{ai\gamma}(t) \in \mathbb{R}$ is a scalar variable defined as the γth element in:

$$s_{ai} = Y_{ai}^T(\dot{q}_{ir} - \dot{q}_i) \tag{2.23}$$

$\rho_{ai\gamma}$ is the parameter update gain, $a_{ai\gamma}(t)$ and $b_{ai\gamma}(t)$ are the lower and upper bounds of $\hat{\theta}_{ai\gamma}$ respectively, and the projection function $\mathcal{P}$ is a differentiable scalar function defined in (2.18).

Finally, the net torque for the joint τ_{ir}^{*} is obtained as follows:

$$\tau_{ir}^{*} = Y_{ai}\,\hat{\theta}_{ai} + k_{ai}(\dot{q}_{ir} - \dot{q}_{i}) \tag{2.24}$$

where τ_{ir}^{*} is the net torque of the joint, k_{ai} denotes a feedback gain and $\hat{\theta}_{ai} \in \mathbb{R}^4$defined in (2.22) denotes the estimate of $\theta_{ai} \in \mathbb{R}^4$ defined in (2.21).

2.3.3 Control

To develop the control of the entire system, the torques resulting from the link and joint analysis are combined. First, it is necessary to extract the torque of the link force/moment vector τ_{air} as follows:

$$\tau_{air} = z^{T\ B_i} F_r \tag{2.25}$$

for $i = 1, \ldots, 7$. With $z = [0 \quad 0 \quad 0 \quad 0 \quad 0 \quad 1]^T$ that was defined earlier, the control torque τ_i is designed as:

$$\tau_i = \tau_{ir}^{*} + \tau_{air} \tag{2.26}$$

for $i = 1, \ldots, 7$. The flow diagram with the calculations needed in the VDC technique is shown in Figure 2.4.

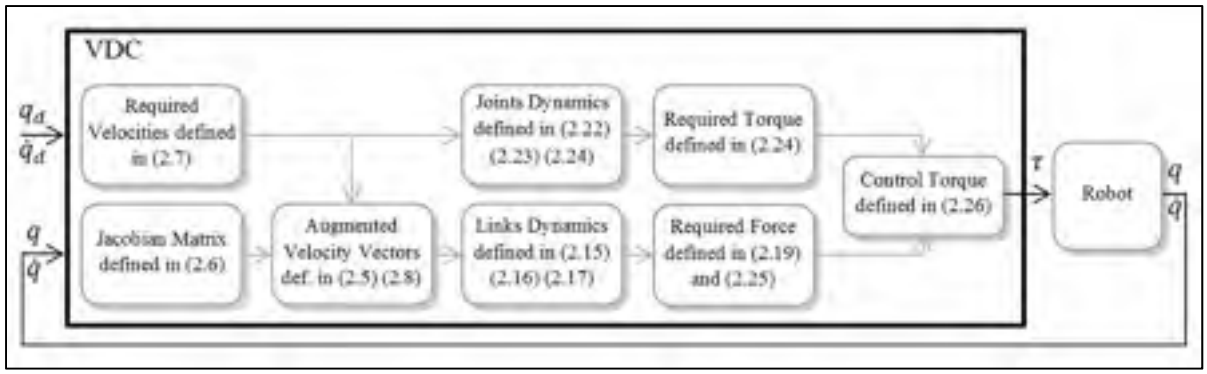

Figure 2.4 Block diagram of the system
(with the equations used in each step in the parentheses)

Associating (2.26) with the traditional dynamic equation of a manipulator:

$$\tau = \boldsymbol{M}(\theta)\ddot{\theta} + V\left(\theta, \dot{\theta}\right) + G(\theta) + F(\theta, \dot{\theta}) \tag{2.27}$$

where $\boldsymbol{M}(\theta)$ is the manipulator's $n \times n$ mass matrix, $V\left(\theta, \dot{\theta}\right)$ the $n \times 1$ Coriolis and centrifugal terms vector, $G(\theta)$ the $n \times 1$ gravity terms vector and $F(\theta, \dot{\theta})$ the $n \times 1$ torque friction vector. It is clear that in the case of VDC, the parameter adaptation that is defined in (2.15) and (2.24) from equations (2.10) to (2.14) for the rigid links and (2.20) to (2.21) for the joints, will incorporate not only the mass, inertia (moments and products) and centre of mass parameters of the links, and the moment of inertia and friction for the joints of the robot, but also the uncertainties and the disturbances introduced by the subject, which are not modelled. For example, the mass of the human arm (different from subject to subject) will be combined with the links' mass; changes or displacements in the position of the arm of the subject, combined with changes in position of the centre of mass; and friction of the joints, combined with constraints of the movement caused by the subject's limitations, such as difficulty to move due to spasticity or altered muscle tone.

2.3.4 Stability Analysis

Given the dynamics expressed in relation (2.27) and the control design given in (2.19) and (2.24), combined as indicated in (2.25) and (2.26), the asymptotic stability is ensured if the position and velocity errors converge asymptotically to zero:

$$lim_{t\to\infty}\|q(t)_d - q(t)\| \to 0 \tag{2.28}$$

$$lim_{t\to\infty}\|\dot{q}(t)_d - \dot{q}(t)\| \to 0 \tag{2.29}$$

with q and q̇ vectors defined in (2.4) and (2.5) and q_d and $\dot{q}_d$ vectors defined in (2.7).

Using the Lyapunov approach, a non-negative candidate function is defined and then it is shown that the variation is a decreasing function. As explained in the previous section, the system dynamics has two parts. The first represents the link dynamics given by:

$$\boldsymbol{M}_{Bi}\frac{d}{dt}\left({}^{Bi}V\right) + \boldsymbol{C}_{Bi}\left({}^{Bi}\omega\right){}^{Bi}V + G_{Bi} = {}^{Bi}F^{*} \qquad i = 1 \dots n \tag{2.30}$$

And the second, given in relation (2.31), represents the joint dynamics, characterized by the torque resultant from the moment of inertia plus the torque from the Coulomb friction:

$$J_{mi}\ddot{q}_i + k_{ci}sign(\dot{q}_i) = \tau_i^{*} \qquad i = 1 \dots n \tag{2.31}$$

Therefore, considering the Lyapunov candidate function for the entire robot as:

$$v_L = \sum_{i=1}^{7} v_i + \sum_{i=1}^{7} v_{ai} \tag{2.32}$$

where v_i represents the non-negative Lyapunov candidate function related to the link dynamics and v_{ai} is the non-negative Lyapunov candidate function related to the joint

dynamics. Combined with the control equation (2.15) and the parameter adaptation defined in (2.16) and (2.17), v_i is defined as follows:

$$v_i = \frac{1}{2}\left({}^{Bi}V_r - {}^{Bi}V\right)^T \boldsymbol{M}\left({}^{Bi}V_r - {}^{Bi}V\right) + \frac{1}{2}\sum_{\gamma=1}^{13}\frac{(\theta_{i\gamma} - \hat{\theta}_{i\gamma})^2}{\rho_{i\gamma}} \tag{2.33}$$

The non-negative Lyapunov candidate function related to v_{ai} can be defined as follows:

$$v_{ai} = \frac{1}{2}J_{mi}(\dot{q}_{ir} - \dot{q}_i)^2 + \frac{1}{2}\sum_{\gamma=1}^{4}\frac{(\theta_{ai\gamma} - \hat{\theta}_{ai\gamma})^2}{\rho_{i\gamma}} \tag{2.34}$$

The derivative of the Lyapunov candidate function (2.32) is given as:

$$\dot{v}_L = \sum_{i=1}^{7}\dot{v}_i + \sum_{i=1}^{7}\dot{v}_{ai} \tag{2.35}$$

Before showing that relation (2.35) is always decreasing, it is necessary to define the virtual power flows as the inner product of the linear/angular velocity vector error and the force/moment vector error (Zhu and Lamarche, 2007; Zhu et al., 1997). With respect to a frame A:

$$p_A \overset{\text{def}}{=} ({}^{A}V_r - {}^{A}V)^T({}^{A}F_r - {}^{A}F) \tag{2.36}$$

virtual power flows characterize the dynamic interaction between subsystems at its cutting points. They are analogue to power flows within a rigid body, but instead of being the inner product of a velocity vector and a force vector, they are the inner product of a velocity vector error and a force vector error. With definition (2.36), it follows that:

$$\dot{v}_i \leq -\left({}^{Bi}V_r - {}^{Bi}V\right)^T K_{si}\left({}^{Bi}V_r - {}^{Bi}V\right) + \left({}^{Bi}V_r - {}^{Bi}V\right)^T\left({}^{Bi}F_r^* - {}^{Bi}F^*\right) \tag{2.37}$$

Considering (2.36) and the force/moment transformation matrices defined in (2.1) to transform the velocities expressed in (2.3) and the required velocities expressed in (2.9), and with the net force/moment and required net force/moment vectors (2.19), this yields:

$$\left({}^{Bi}V_r - {}^{Bi}V\right)^T \left({}^{Bi}F_r^* - {}^{Bi}F^*\right) = p_{B_i} - p_{T_i} \tag{2.38}$$

where the terms on the right side of (2.38) represent the virtual power flows at the two cutting points of each link.

$\dot{v}_{ai}$ can be written (Zhu et al., 1997) as:

$$\dot{v}_{ai} \leq -k_{ai}(\dot{q}_{air} - \dot{q}_{ai})^2 - p_{B_{ai}} + p_{T_{ai}} \tag{2.39}$$

Considering an open chain structure, as is the case in this paper, and with $p_{B_1} = 0$ and $p_{T_n} = 0$, the total virtual power flows gives:

$$\sum_{i=1}^{n} \left(p_{B_i} - p_{T_i}\right) = 0 \tag{2.40}$$

Therefore, relationship (2.37) becomes:

$$\dot{v}_i \leq -\left({}^{Bi}V_r - {}^{Bi}V\right)^T K_{si} \left({}^{Bi}V_r - {}^{Bi}V\right) \tag{2.41}$$

and the function $\dot{v}_{ai}$ becomes:

$$\dot{v}_{ai} \leq -k_{ai}(\dot{q}_{air} - \dot{q}_{ai})^2 \tag{2.42}$$

Finally, from relationships (2.41) and (2.42), and given positive gains K_{si} and k_{ai}, the derivative of the Lyapunov function $\dot{v}_L$, given in (2.43), is always decreasing.

$$\dot{v}_L \leq -\sum_{i=1}^{n}\left(\left({}^{Bi}V_r - {}^{Bi}V\right)^T K_{si}\left({}^{Bi}V_r - {}^{Bi}V\right) + k_{ai}(\dot{q}_{air} - \dot{q}_{ai})^2\right) \tag{2.43}$$

The asymptotic stability in the sense of Lyapunov follows immediately from the bounded reference signals, the bounded control and the bounded joint acceleration.

2.4 Experimental Results

A general overview of the ETS-MARSE robot is shown in Figure 2.5. Brushless DC motors (Maxon EC-45, EC-90) incorporated with harmonic drives (having gear ratio 120:1 for motor 1 and motor 2, and gear ratio 100:1 for motor 3 to motor 7) were used to actuate the ETS-MARSE.

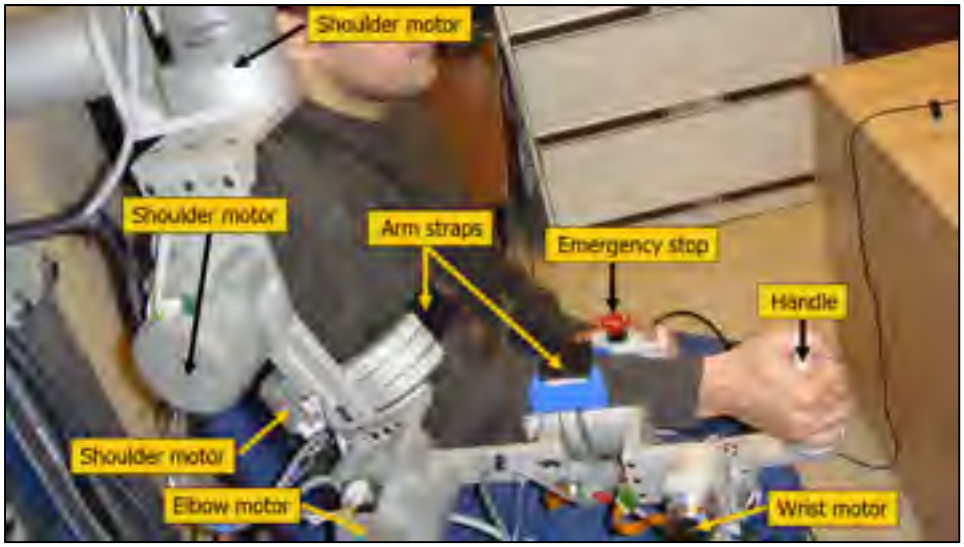

Figure 2.5 ETS-MARSE with human subject

A block diagram of the experimental setup, including the control architecture, for the ETS-MARSE system is depicted in Figure 2.6. For the experimental phase, three control techniques were used: VDC as the focus of this research and CTC and PID as reference control strategies. The outputs of the controllers were the joints' torque commands. However, the torque commands were converted to motor currents, and finally, to reference voltages as

voltage value is the drive command for the motor drivers. The implementation of the system was carried out in a National Instruments PXI system. A PXI-8108 controller card performed the joint-based control (VDC, CTC and PID) and served as the robot operating system. A FPGA (Field Programmable Gate Array) mounted in the NI PXI-7813R remote input-output card, performed the low-level (PI) control, that is, the current loop for the robot actuators and the position feedback control via Hall sensors. The sampling rate for the VDC controller was 1ms and 500µs for the CTC and PID (Figure 2.6, left dotted box). Note that the current loop controller has a sampling time of 50µs (up to 20 times faster) than the torque control loop (Figure 2.6, right dotted box). Also, a host computer was used (not shown in the schematic of Figure 2.6), which displayed the user interface through which it connected to the ETS-MARSE system in order to issue commands (such as selection of exercise or control techniques) to the PXI, and to provide feedback and retrieve experimental data from the system for analysis, as well as the virtual environment used in active rehabilitation.

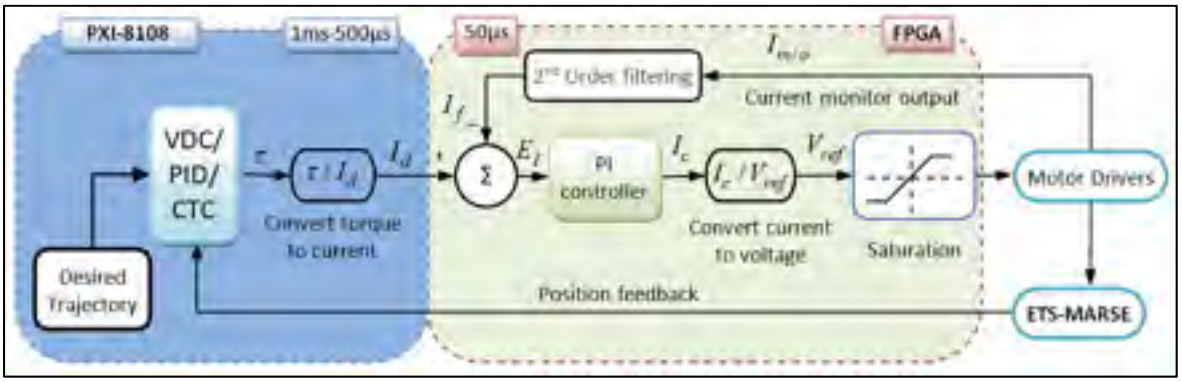

Figure 2.6 Experimental setup with control architecture

2.4.1 Varying subjects experiment

In these experiments, the variation of the trajectory tracking performance of the *ETS-MARSE* was evaluated. The experiment was divided into three scenarios: one with the VDC, another with the PID, and the last with the CTC. Although the CTC controller can include a simple PID controller for the decoupling and cancelation of nonlinear terms, in this case CTC was used with a PD controller. The PID controller described in these tests is different; as a

traditional PID controller, it attempts to minimize the position error through the adjustment of the torque without any need for dynamic modelling of the robot, and only some tuning of the gains is performed. For the CTC controller (with its internal PD), a complete modelling of the robot's dynamics should be done. The trajectory used in this research represents a typical passive rehabilitation exercise (Brigham and Women's Hospital Rehabilitation Services, 2014). It is a joint space trajectory, an outside reaching movement, illustrated in Figure 2.7, and involving the shoulder, elbow and forearm motion: in each exercise, the robot followed the path from A to B (in four seconds) and then reversed direction from B to A (also in four seconds) three times.

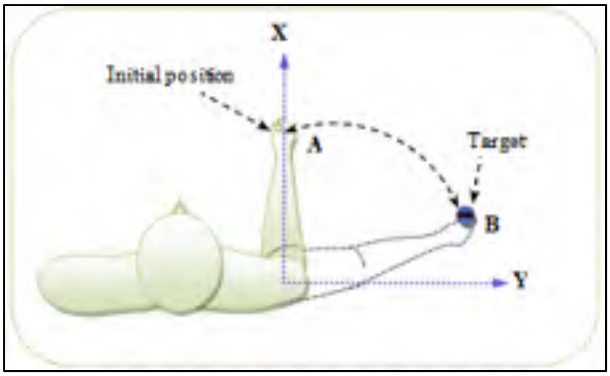

Figure 2.7 Schematic diagram,
reaching movement exercise

The range of motion of each joint is summarized in Table 2.2; since the wrist is not moved in this experiment (joint 6 and joint 7), only joint 1 to joint 5 are presented. To introduce the system variability, this exercise was executed with four different situations: three healthy male human subjects (ages: 24, 33 and 31 years; height: 181, 165 and 182 cm; weight: 75, 63 and 95 Kg) and one scenario without a subject. Experiments with subjects were conducted with them in the seated position, analogous to Figure 2.5. A height-adjustable chair was used to adjust the seating height, i.e., to align the centre of rotation of the shoulder joint of the subject to that of the ETS-MARSE.

Table 2.2 Varying subjects experiment range of motion

Joint	Type of motion	ETS-MARSE Workspace
	Shoulder Joint	
Joint 1	Horizontal Flexion	5°
	Horizontal Extension	60°
Joint 2	Vertical Flexion	60°
	Vertical Extension	0°
Joint 3	Internal Rotation	20°
	External Rotation	0°
	Elbow	
Joint 4	Flexion	90°
	Extension	40°
	Forearm	
Joint 5	Pronation	40°
	Supination	0°

It is important to recall that this rehabilitation movement is a passive one; that is, the robot follows a predefined trajectory with no action from the user. Each condition (i.e., exercises with subjects A, B and C, and without subject) was repeated seven consecutive times, giving a total of 28 trials for each controller. It should be mentioned that no changes were made between the tests, e.g., in terms of gains or parameters in the control strategy.

The experimental results are presented in Figure 2.8. Each plot corresponds to one control strategy, and each one shows the RMS value of the trajectory tracking error for each joint moved, along the 28 tests. It should be recalled that even when all joints are involved in the control, joint 6 and joint 7 of the ETS-MARSE remained at zero degrees, and so were not analysed. It is clear that, in addition to providing a lower tracking error, the VDC controller remained barely affected by variations. Meanwhile, the PID controller presented a more

variable behaviour, and the CTC was the most affected by changes in the subject's characteristics.

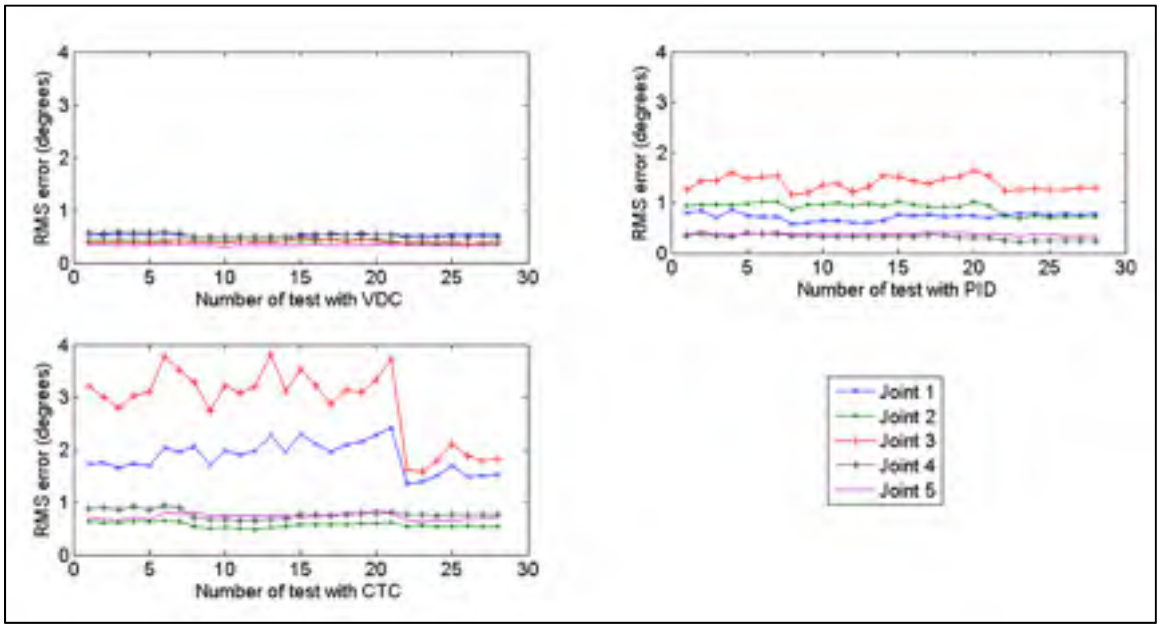

Figure 2.8 RMS joint tracking error along the 28 tests for each controller

The three controllers performed well, but the analysis that is pertinent for this paper is the variation in the performance from one experiment to another due the dynamic variations. In Figure 2.9, the average RMS error (joint 1 to joint 5) of each test and for each controller is shown. It can easily be seen how the VDC results are the more compact, confirming that the controller behaves better over distinct dynamic conditions caused by changes of test subjects. It should be noted that the changes from one condition to the other are also present in the VDC, but the variation is small compared to the other techniques used in this paper. It is also clearly seen that the other controllers changed their behaviour notably even under the same testing condition, that is, with the same subject (or without subject), possibly due to natural, unintended changes in the arm position, relaxation, grip on the handle, etc.

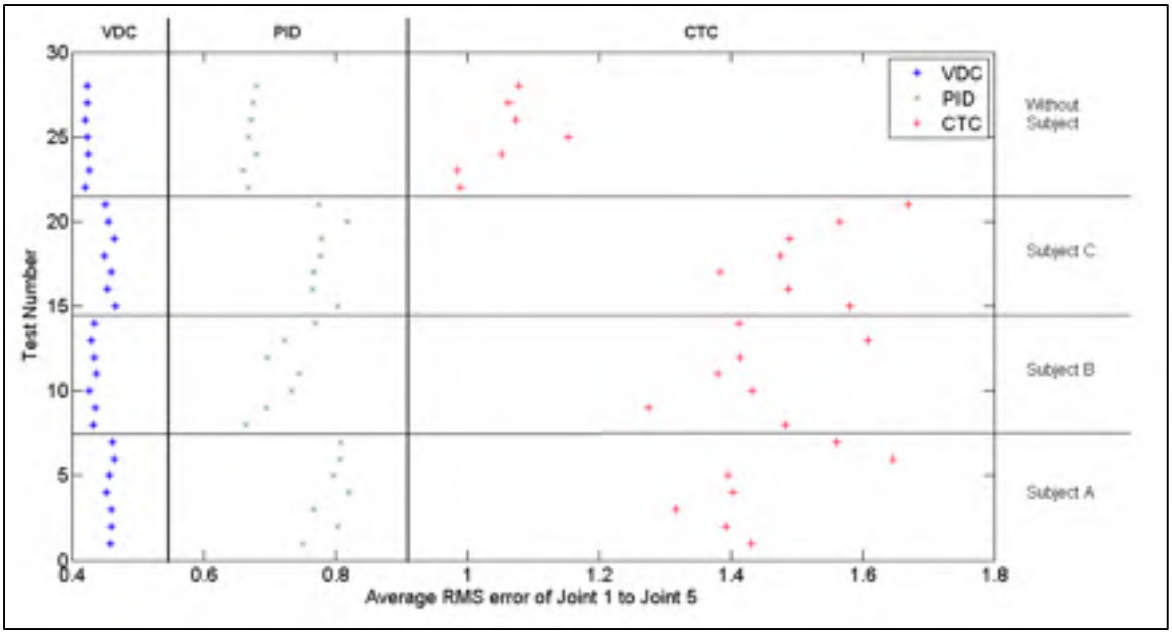

Figure 2.9 Average (joint 1 to joint 5) RMS error of each test

Table 2.3 Statistical analysis of performance variation

Controller	RMS Error σ(°)					Average RMS Error σ(°)	Normalize to VDC RMS Error σ
	Joint 1	Joint 2	Joint 3	Joint 4	Joint 5		
VDC	0.0180	0.0251	0.0243	0.0330	0.0086	0.0218	1.00
PID	0.0703	0.1116	0.1314	0.0483	0.0187	0.0761	3.49
CTC	0.2887	0.0455	0.6731	0.0789	0.0552	0.2283	10.47

Finally, in order to provide a quantitative analysis, Table 2.3 summarizes the standard deviation (σ) of the data plotted in Figure 2.8 and Figure 2.9. The second to the sixth columns represent the standard deviation of the RMS error for each joint (Figure 2.8). The seventh column is the standard deviation of the average RMS error across joints one to five (Figure 2.9). For a better comparison, the average RMS error was normalized to that of the VDC in the last column. The PID showed an average RMS error standard deviation more than three times larger than the VDC; and for the CTC, this was more than 10 times. It can clearly be seen that a controller that depends heavily on the dynamic model of the system

(CTC) is significantly affected by changes and uncertainties caused by the variations in the robot's user.

2.4.2 Varying velocity experiment

Another important concern in rehabilitation is movement velocity. To show the efficiency of the VDC approach in dealing with different velocities, an elbow flexion/extension experiment is shown. The trajectory of joint 4 (elbow joint) passes through 90°, 5°, 115° and 0°. The speed of the movement was increased for each of the three tests performed. In the first one, the maximum speed was 20.63°/sec, it was 45.20°/sec for the second one, and -85.71°/sec for the third test (the minus sign indicates the extension movement). The tests were conducted with no subject wearing the robot. To compare performances, PID and VDC were used in each test. Figure 2.10 shows the results for the VDC controller, where each column displays the position, velocity and error for each movement velocity. Figure 2.11 shows the same for the PID controller. To summarize the performance, Table 2.4 shows the RMS error in each test. It can be seen that the tracking error for the VDC increased by 83% from the slowest to the fastest movement, while for PID the increase was by 204%.

Table 2.4 RMS error of varying velocity experiments

Maximum speed (degrees per second)	**RMS Error J4 (°) VDC**	**RMS Error J4 (°) PID**
20.63	0.3914	0.3695
45.20	0.4719	0.6209
85.71	0.7169	1.1228

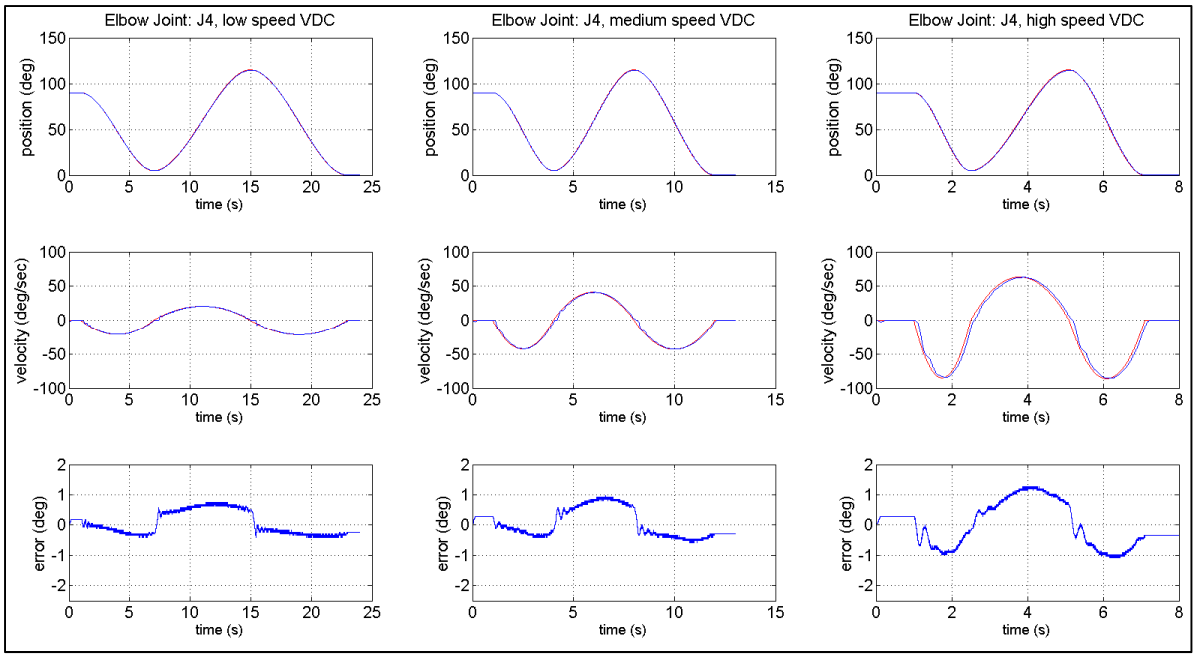

Figure 2.10 VDC results for different speeds test

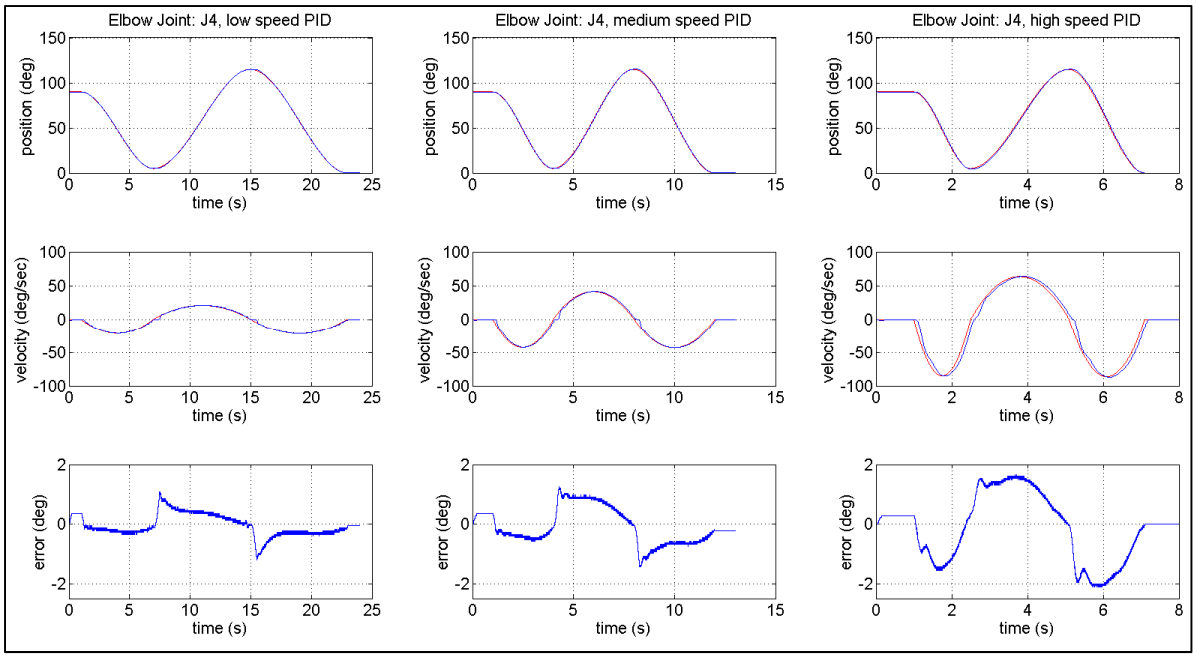

Figure 2.11 PID results for different speeds test

2.4.3 Active rehabilitation experiment

Next in the experiment, an active rehabilitation test is presented. Through a virtual environment as the Human Machine Interface (HMI) (Ferrer et al., 2013), the user's task was to follow a predefined trajectory, in this case, a straight line to the front and back, that is, movement on the X-axis (see Figure 2.7). With the use of a six-axis force sensor mounted on the tip of the robot (refer to Figure 2.2 or Figure 2.5) the trajectory was actively modified by an admittance function to make the robot follow the user's movement intentions. The tip of the robot, the end effector, is in the handle that the user grabs with his hand while wearing the robot. The test was completed with the VDC controller. Figure 2.12 shows the user performing the test with a zoom of the virtual interface in the lower right corner. The red line in the centre represents the path the user should follow; the white sphere represents the user end effector, and the green line, the actual trajectory followed by the subject. Finally, Figure 2.13 shows the movement in the Cartesian space in the first column, the force readings of the force sensor in each Cartesian axis in the second column, and the torque readings in the last column. Thanks to the robustness of the VDC controller described in subsection 2.4.1 and subsection 2.4.2, the variations in trajectory tracking observed in this active rehabilitation exercise were only due to the user's conditions. This will give a more accurate measurement of the user performance from test to test.

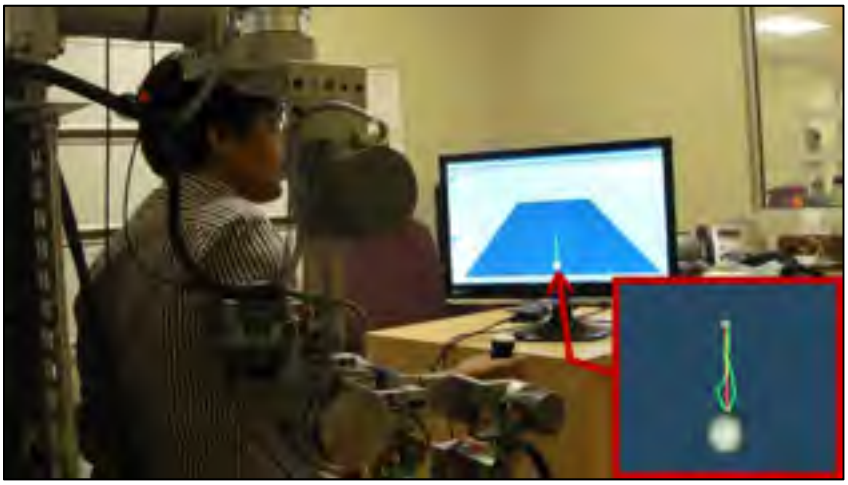

Figure 2.12 Experimental setup for active rehabilitation

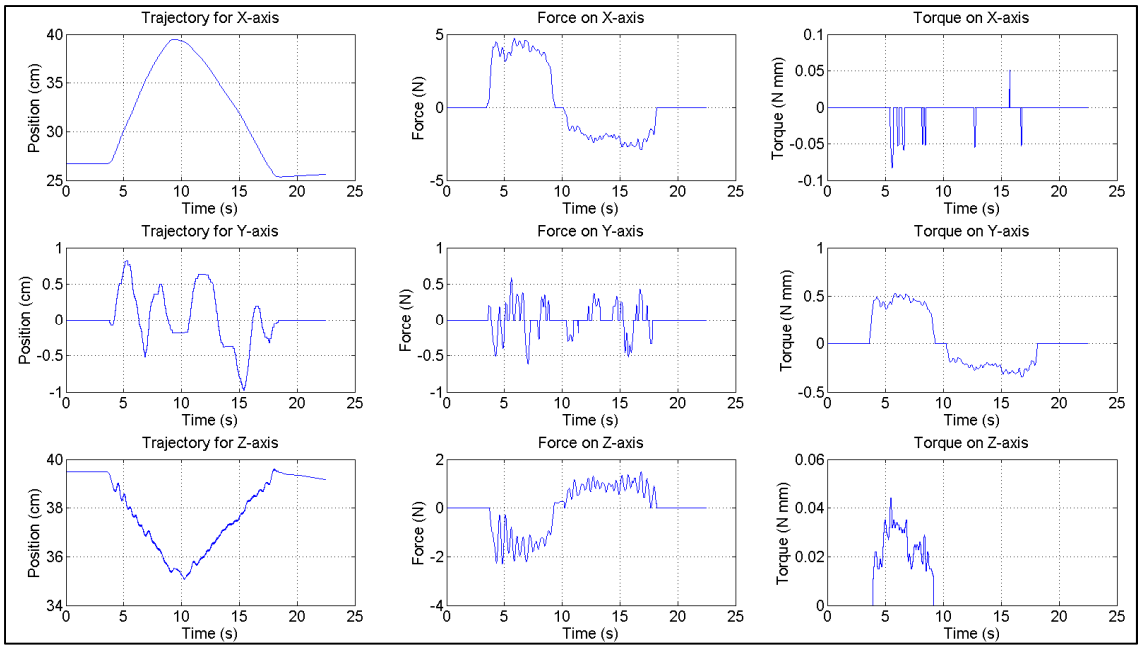

Figure 2.13 Cartesian trajectory, forces and torques for active rehabilitation

2.4.4 Parameter adaptation

Finally, to illustrate the parameter adaptation process, a simple experiment was performed. The adaptation process is shown in the parameters of joint 4. The robot was set at an initial position with all joints as shown in Figure 2.2, except for joint 4, which was set at 90 degrees. All the parameters were then reset to zero and the trajectory commanded to the robot only affected joint 4. The test was performed without a subject. It stayed for one second at the initial position, and then moved from 90 degrees to five degrees in two seconds, and stayed there for another two seconds. The trajectory is shown in Figure 2.14. Next, Figure 2.15 shows the joints parameters adaptation, defined in (2.21), J_{mi}, the equivalent moment of inertia, k_{ci}, the Coulomb friction coefficient, k_{vi}, the viscous friction coefficient and c_i, an offset that accommodates asymmetric Coulomb frictions. It should be recalled that in the VDC, the algorithm guarantees convergence to a certain value that will ensure the fulfilment of the control premise as well as the stability demonstrated in subsection 2.3.4, but these values are not necessarily the real values of the model of the robot. Moreover, it is important to remember that the gain for the parameter adaptation was individually adjusted for each

parameter, as defined in (2.22). The plots show how the first adaptation was done from a zero value to a certain value corresponding to the initial position. From time = 1 s to time = 3 s, the parameters adapted according to the dynamics variations of the system in motion. Finally, arriving at another steady position from time = 3 s onwards, the parameters converge to another value from there to second five.

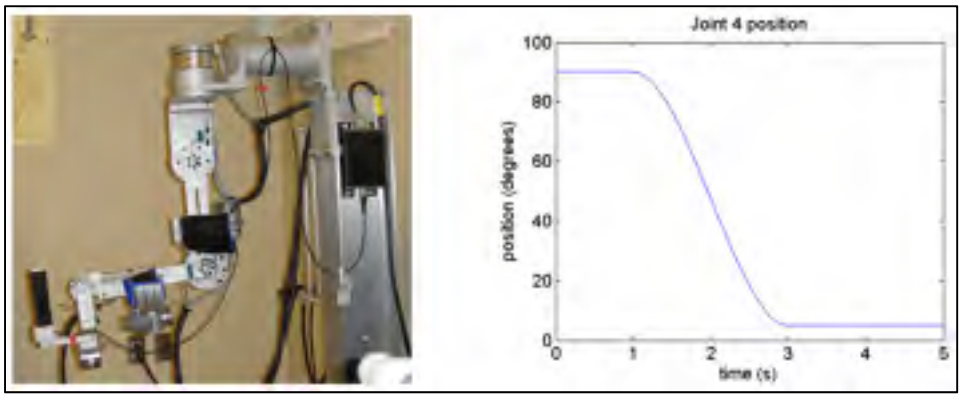

Figure 2.14 Left: Robot initial position. Right: Joint 4 trajectory

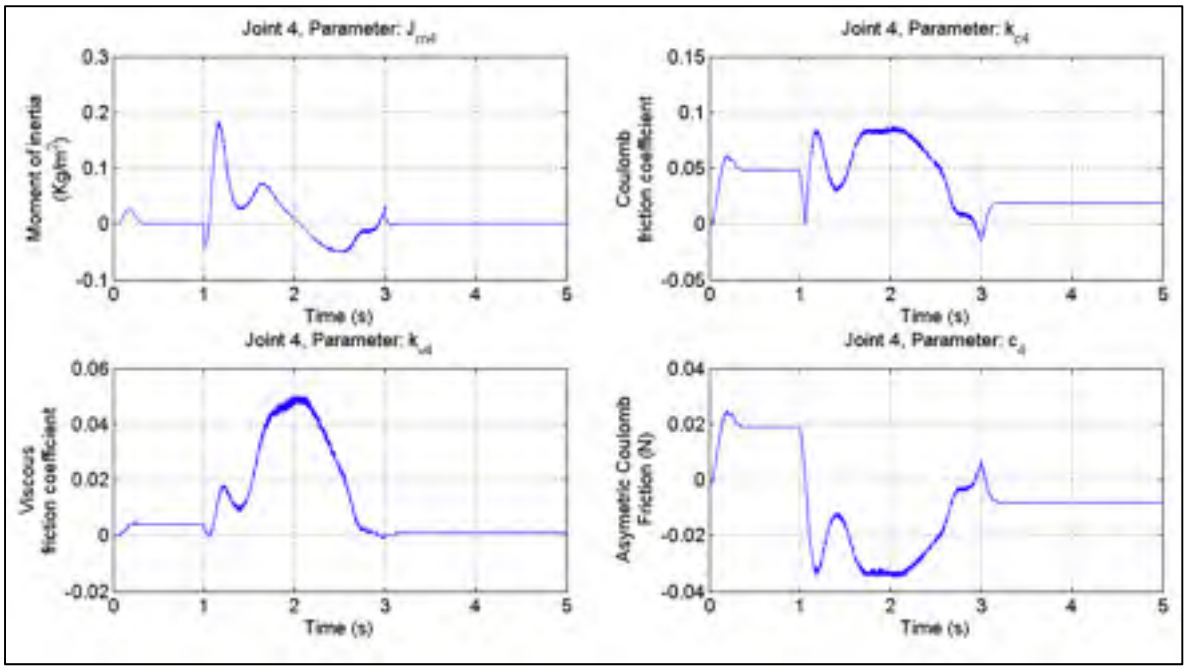

Figure 2.15 Parameter adaptation of joint 4

2.4.5 Discussion of experimental results

The controllers can be tuned in an attempt to achieve a better performance (especially in PID and CTC cases); nevertheless, the tuning process of the gains or changes in the dynamic model would need to be repeated for each user. In rehabilitation, if the PID and the CTC were adjusted for one specific user, this procedure should be repeated for new users with different dynamics (weight, height, neurological condition, etc.). However, this procedure is not needed with the VDC because it is based on an adaptive algorithm; the adaptation process is done online without any manual modification of parameters, which constitutes a big advantage. Making changes to the control system dynamics in controllers like the CTC is an undesirable and time-consuming task for the therapist. Besides, physiological changes due to an improvement in the subjects' condition (such as stiffness) can be another source of periodical variances (reduced resistance with time). These problems are clearly avoided by the use of the VDC. Further, in the experiment presented in subsection 2.4.2, it can be seen that at low velocity, the PID and VDC controllers perform almost equally well. It is crucial to understand that this reflects proper tuning of the gains. Thus, the variations in the system dynamics (in this case, movement velocity) are what lead to a worsening of performance for the PID controller. It should be mentioned that the velocity test was performed without a subject in a bid to specifically isolate the effects of the variations in movement velocity. The results from subsection 2.4.1 and subection 2.4.2 should be considered together, thus supporting the need, in rehabilitation, to have a controller that is robust to changes in biomechanical and physiological conditions. Finally, the active rehabilitation scenario shows that in an active exercise, the tracking of the patient's improvement will be better known, since the uncertainty caused by the system variation will be considerably reduced by the VDC controller approach.

2.4.6 Safety

It is very important to mention that the capacity to deal with the characteristics of different subjects does not mean that regardless of the subjects' capabilities, the robot will force them

to complete the trajectory. The control interface has the provision to modify the position and the velocity limits of the joints, in order to adapt to the different conditions and rehabilitation needs of the subjects. The robot also has mechanical stoppers to maintain the maximum allowable range of motion inside the normal range of human activities of daily living, with these limits illustrated in Figure 2.1.

2.5 Conclusions and Future Work

Trajectory tracking exercises, representing passive and active rehabilitation therapy, were implemented using the VDC approach with trajectories given in joint and in Cartesian space with excellent results. As to their application to rehabilitation, the experimental results show that VDC can respond to subject variations and can effectively accomplish rehabilitation therapy. A performance evaluation against CTC and PID, with all controllers using fixed gains, successfully demonstrated the advantage of the VDC. In experiments, the tracking performance of the robot was compared for different controllers, while varying the subjects' physical characteristics or the movement velocity. The results indicate that the robot under VDC control can better adapt to these variations, as compared to PID and CTC. Thus, we conclude that with this VDC's robustness, a more systematic rehabilitation can be accomplished. The VDC controller will reduce the variation of the trajectory tracking and will provide a better measure of the patient's improvement, as the most important source of variation in movement performance will be the changes in their condition.

A future step in the development of this project is to continue the development of active rehabilitation, where the robot helps the user in completing a given movement. This includes active-assistive rehabilitation, in which the robot can help the subject to different degrees, according to specific rehabilitation needs (time, movement boundaries, etc.). More active rehabilitation work has been developed in our lab, such as changing the effort required of the user to move the robot. Still additional active rehabilitation tasks are to be incorporated, using electromyographic (EMG) signals, to provide the system with another source of information regarding the user's intention of movement. These EMG signals can be used as a

full rehabilitation scheme or combined with force sensor data in order to offer the adequate rehabilitation therapy according to patients' needs. Haptic capabilities are already under development for the ETS-MARSE.

CHAPTER 3

ADMITTANCE-BASED UPPER LIMB ROBOTIC ACTIVE AND ACTIVE-ASSISTIVE MOVEMENTS

Cristóbal Ochoa Luna[1], Mohammad Habibur Rahman[1, 2], Maarouf Saad[1], Philippe S. Archambault[2, 3] and Steven Bruce Ferrer[1]

[1]Department of Electrical Engineering, École de technologie supérieure,
1100 Notre-Dame West, Montreal, Quebec (H3C 1K3) Canada.

[2]School of Physical & Occupational Therapy, McGill University,
3654 Prom Sir-William-Osler, Montréal, Québec (H3G 1Y5) Canada.

[3]Centre for Interdisciplinary Research in Rehabilitation (CRIR),
2275 Laurier Avenue East, Montréal, Quebec (H2H 2N8) Canada.

This paper was published in the *International Journal of Advanced Robotic Systems* on September 01, 2015

Abstract:

This paper presents two rehabilitation schemes for patients with upper limb impairments. The first is an active-assistive scheme based on the trajectory tracking of predefined paths in Cartesian space. In it, the system allows for an adjustable degree of variation with respect to ideal tracking. The amount of variation is determined through an admittance function that depends on the opposition forces exerted on the system by the user, due to possible impairments. The coefficients of the function allow the adjustment of the degree of assistance the robot will provide in order to complete the target trajectory. The second scheme corresponds to active movements in a constrained space. Here, the same admittance function is applied; however, in this case, it is unattached to a predefined trajectory and instead connected to one generated in real time, according to the user's intended movements. This allows the user to move freely with the robot in order to track a given path. The free movement is bounded through the use of virtual walls that do not allow users to exceed certain limits. A human-machine interface was developed to guide the robot's user.

Keywords: Upper limb rehabilitation, active and active-assistive rehabilitation, admittance, 7DOF exoskeleton, human-machine interface

3.1 Introduction

Upper extremity paralysis (the inability of a muscle or group of muscles to move voluntarily) occurs as a consequence of lesions such as injuries to the central or peripheral nervous system. Causes of injuries include strokes, sports mishaps and car or occupational accidents, among others. According with the US National Stroke Association®, approximately 80% of stroke survivors experience hemiparesis, which causes weakness or an inability to move one side of the body. Spasticity affects roughly 40% of stroke survivors and is characterized by stiff or tight muscles that constrain movement (National Stroke Association®, 2012). The primary treatment for these cases is rehabilitation, i.e., the process of helping an individual achieve the highest level of independence and quality of life possible, physically, emotionally, socially and spiritually. Where rehabilitation is possible, it involves many hours of highly skilled procedures. The number of people capable of providing such support is insufficient for adequately covering all patients that need help. Recovery progression varies greatly and while certain people recover relatively quickly, for others, recovery can take a very long time, and can even be a lifelong process.

The use of robotic assistance in rehabilitation is an important point of interest that is attracting significant attention (Feriančik and Líška, 2014; Kurnicki, Stanczyk and Kania, 2014). Many studies have shown that robotic rehabilitation can be effective at improving arm function following a stroke (Hesse, Schmidt and Werner, 2006; Kwakkel, Kollen and Krebs, 2008; Masiero, Armani and Rosati, 2011; Norouzi-Gheidari, Archambault and Fung, 2012; Riener, Nef and Colombo, 2005). However, in studies where participants received an equivalent amount of either robotic or conventional therapy, the improvements in arm function were no longer significant (Norouzi-Gheidari, Archambault and Fung, 2012). One reason for this may be that earlier studies used robotic devices with a limited number of degrees of freedom, such as planar manipulandums. Indeed, a recent study (Klamroth-

Marganska et al., 2014) demonstrated a small but significant improvement in arm function following therapy involving a 7-degree-of-freedom robot (shoulder, elbow and hand opening) when compared to an equivalent amount of conventional therapy. Thus, there is a clinical need for continuing the development of robotic devices that can assist with naturalistic arm movements.

The ETS - Motion Assistive Robotic-exoskeleton for Superior Extremity (ETS-MARSE) was developed in our laboratory (Ochoa Luna et al., 2014a; Rahman et al., 2011b; Rahman et al., 2012b; Rahman et al., 2012c) in order to provide rehabilitation assistance for the upper limbs. Currently, it comprises a seven-degree-of-freedom (DOF) exoskeleton, designed to cope with the full motion capabilities of the human arm; that is, at the shoulder, elbow and wrist levels, combined or individually. Additionally, it contains a graphical user interface that uses a virtual environment with different rehabilitation exercises. To date, work in this regard has been developed to the point of passive rehabilitation, which means that the exoskeleton executes movements along predefined trajectories, while moving the subject's arm with it to help improve the range of movement. This paper describes the next rehabilitation step: active-assistive and active rehabilitation (Brokaw et al., 2011; Dipietro et al., 2005; Krebs et al., 2003).

The methodology presented in this paper combines the advantages of the trajectory tracking control as the inner loop control of the robot and an admittance-based trajectory modifier that performs the outer force control, and which is responsible for the interaction between the robot and user. The admittance is used as a means of modifying the desired trajectory (Culmer et al., 2010; Seraji, 1994). Due to the nonlinear nature of the ETS-MARSE, a nonlinear control technique that has inherent adaptive characteristics has been used, i.e., virtual decomposition control (VDC). VDC is a relatively new approach that can reduce the mathematical complexity of multi-degree of freedom robots and has an adaptive nature that helps to deal with different patients' dynamics (Zhu et al., 1997). As robots become more complex, the computation of robot dynamics is proportional to the fourth power of the number of DOF in Lagrangian dynamics (Zhu, Piedboeuf and Gonthier, 2006). VDC uses the

dynamics of virtually created subsystems to conduct control design; this decomposition yields simpler dynamic equations in formulation and implementation (Zhu and De Schutter, 2002). In previous research with ETS-MARSE, we used different non-linear control strategies, such as computed torque (CTC) (Rahman et al., 2011b) and sliding mode control (SMC) (Rahman et al., 2012b). Though SMC performed well, it showed an approximately 1.5 times increase in end-effector tracking error when the conditions of the subject changed and perturbations were presented, while the same exercise was performed. It also presented the associated chattering, which can be reduced but not eliminated (Rahman et al., 2012b). Conversely, an advantage of the VDC lies in its inherent adaptive capabilities, in the form of internal parameter estimation. It was shown in our previous studies that in direct comparison with CTC and PID, VDC can successfully cope with the physiological variations between different subjects (Ochoa Luna et al., 2014b). Although differences in tracking error were minimal and below the needs dictated by the application, PID showed an average RMS error standard deviation more than three times larger than for VDC; for CTC, this was more than 10 times that of VDC. VDC however, due to control gains and parameter estimation gains, involves a complicated process of initial tuning during the controller design process.

In order to obtain the user's motion intention and modify the robot's trajectory tracking accordingly, the admittance concept is used. This approach has also been proven adequate for high ratio transmissions systems (Calanca and Fiorini, 2014; Seraji, 1994). The robot takes information from the human-machine interaction, in this case through contact force feedback between the structure and the person's arm and uses it to actively modify its rehabilitation task.

In recent years, admittance control for rehabilitation has come to represent a well-known approach and different schemes have been proposed (Colombo et al., 2005; Culmer et al., 2010; Ozkul and Barkana, 2013; Younggeun et al., 2009). One of the main advantages of this type of control is that it offers the possibility of active rehabilitation. This is because it contributes to the rehabilitation process by allowing task repeatability and provides relevant data for the quantification of different outcomes, such as improvement, effort, etc. However,

this approach is limited by the number of degrees of freedom of the robotic device (Ozkul and Barkana, 2013) or has only been employed with end-effector type robots (Colombo et al.; Culmer et al., 2010; Younggeun et al., 2009). The contribution of this paper is to present both active-assistive and active rehabilitation task schemes for the 7DOF ETS-MARSE exoskeleton. These tasks are based on path-tracking game-like exercises that have been successfully employed in neuromuscular rehabilitation (Zhang, Davies and Xie, 2013). The rehabilitation robot works in two different scenarios, both of which make use of a virtual environment as an interface to visualize the movement to be performed. In the first scenario (active-assistive rehabilitation), the robot follows a predefined movement path; however, the system measures the user's force opposing the predetermined movement and allows a certain adjustable degree of trajectory variation. In the active mode, the robot allows the user to freely move in the workspace while trying to achieve a target. In this case, the user's movement is constrained by means of virtual walls that restrain him from exceeding certain limits and mark the point where the system will take corrective or assistive actions to help resolve a collision conflict. At all times, the robot appears weightless to the user and helps to support their arms if they stop in the middle of an exercise. These schemes may encourage the patient to actively participate in the exercise by attempting to follow the target trajectory and motivating them to improve their level of accomplishment.

This paper is organized as follows: section 3.2 describes the ETS-MARSE and the setup of the system. In section 3.3, a general description of the controller (VDC) is given. In section 3.4, the implementations of the active-assistive and active rehabilitation schemes are described. Section 3.5 summarizes the experimental setup and presents the results. Finally, section 3.6 provides conclusions and future work perspectives.

3.2 System Overview

The exoskeleton robot arm ETS-MARSE is shown in Figure 3.1. It is an open chain, all-revolute, 7DOF wearable manipulator-like robot; its joints were designed to correspond to the principal degrees of freedom of the human arm. These are:

- 3DOF at shoulder level for horizontal flexion/extension, vertical flexion/extension and internal/external rotation;
- 1DOF for elbow flexion/extension;
- 1DOF for forearm pronation/supination;
- 2DOF at the wrist level for radial/ulnar deviation and flexion/extension.

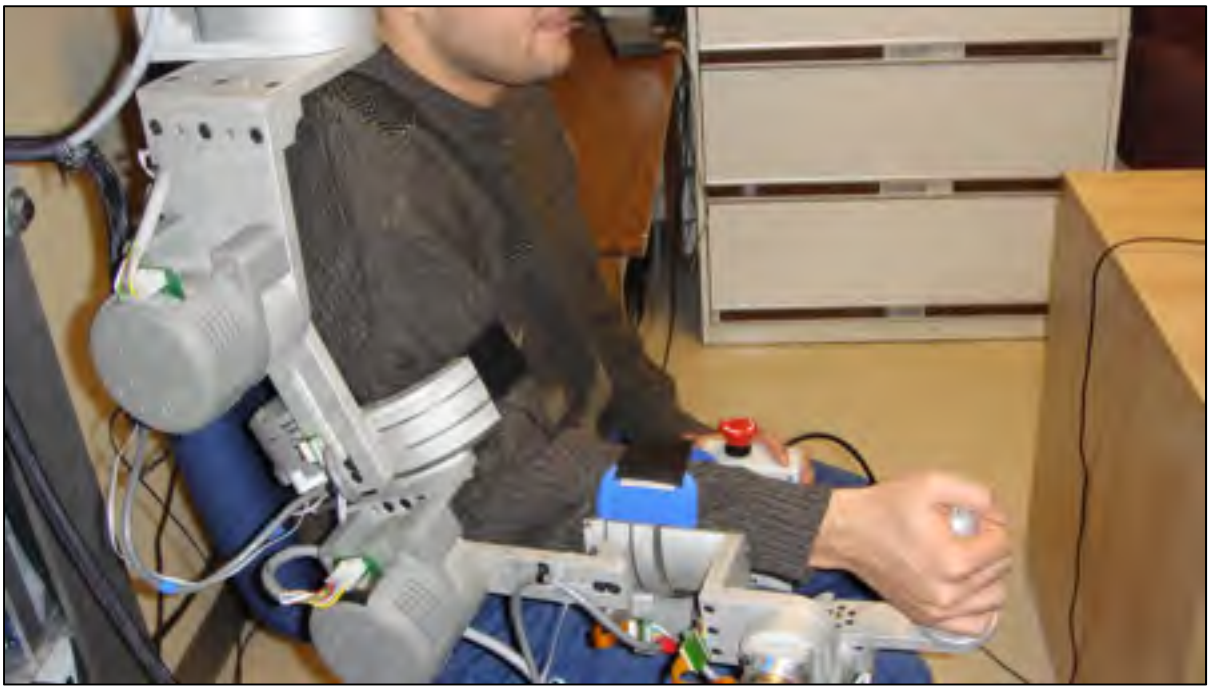

Figure 3.1 Subject wearing ETS-MARSE robot arm

The exoskeleton structure has a six-axis force sensor mounted on the end-effector (tip) of the robot, which is at the base of the handle where the user's hand must be positioned. Each joint is driven by a brushless DC motor that has a Hall effect sensor used for position feedback of the joints. The motors are incorporated with harmonic drives; the specifications for the motors and harmonic drives can be found in Appendix B. A backplane card collects analogue and digital signals and connects through the proper interface cards to an NI PXI-7813R (remote input-output card) placed on an NI PXI-1031 chassis. The card has an integrated FPGA in which low-level control is performed, a PI controller for the current loop of the motors, position feedback via the Hall effect sensors and the collection of force sensor inputs.

A PXI-8108 controller, which performs high-level control (the robot operating system and the trajectory tracking controller) is also mounted on the chassis. In this case, we are using the nonlinear control technique known as virtual decomposition control (VDC) (Zhu et al., 1997), with an update rate of 1 ms. A description of the implementation of the VDC is outlined in section 3.3 of this paper.

A PC runs the human-machine interface virtual environment in which the robot wearer visualizes the rehabilitation exercise. The current architecture of the system is depicted in Figure 3.2. Since the system is a human-machine interface, safety is a major concern and for this reason, a hardware emergency stop button is built into it.

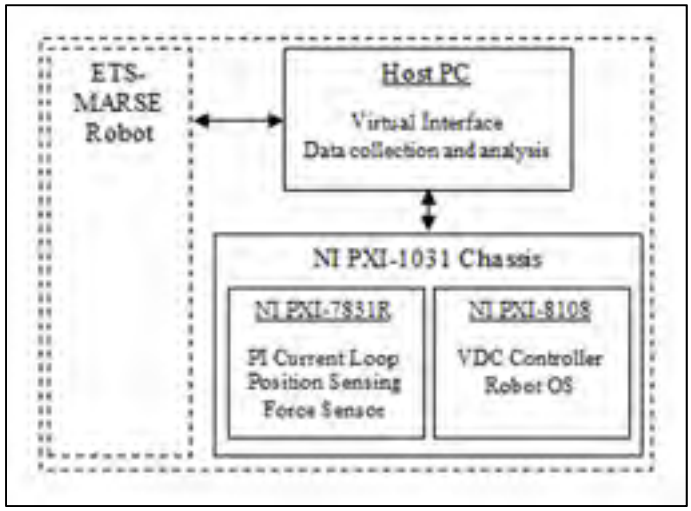

Figure 3.2 ETS-MARSE system hardware overview

3.3 Virtual Decomposition Control of the ETS-MARSE

The control technique we used is presented in this section, but only the steps required to implement VDC are listed. This technique presents an effective approach for dealing with high DOF robots and multi-robot control. A detailed analysis is beyond the scope of this paper; readers interested in such an analysis are referred to other works that address this technique (Zhu and De Schutter, 1999; Zhu et al., 2013). The frame attachment for the DOF of the ETS-MARSE, following the method summarized in (Craig, 2005), is shown in

Figure 3.3. The resulting Denavit-Hartenberg modified parameters are obtained, as described in (Craig, 2005), and are summarized in Table 3.1.

Table 3.1 ETS-MARSE Denavit-Hartenberg modified parameters

i	α_{i-1}	a_{i-1}	d_i	θ_i
1	0°	0	d_1	θ_1
2	-90°	0	0	θ_2
3	90°	0	d_3	θ_3
4	-90°	0	0	θ_4
5	90°	0	d_5	θ_5
6	-90°	0	0	θ_6-90º
7	-90°	0	0	θ_7

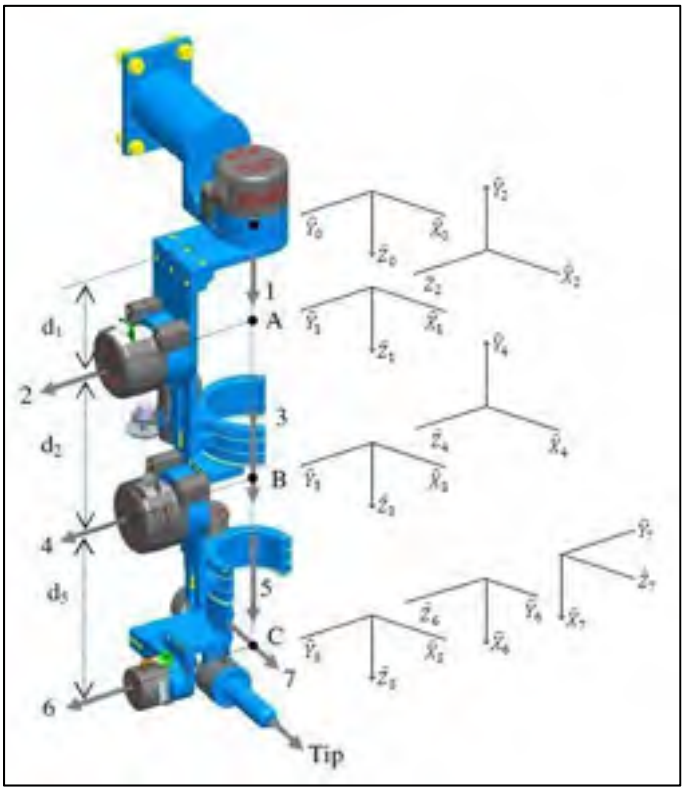

Figure 3.3 7DOF exoskeleton robot arm

3.3.1 Robot subsystem decomposition

The first step in the VDC analysis covers the virtual decomposition of the robot; in our case, we can view the exoskeleton as a single open chain. This results in decomposition into fourteen subsystems, as illustrated in Figure 3.4.

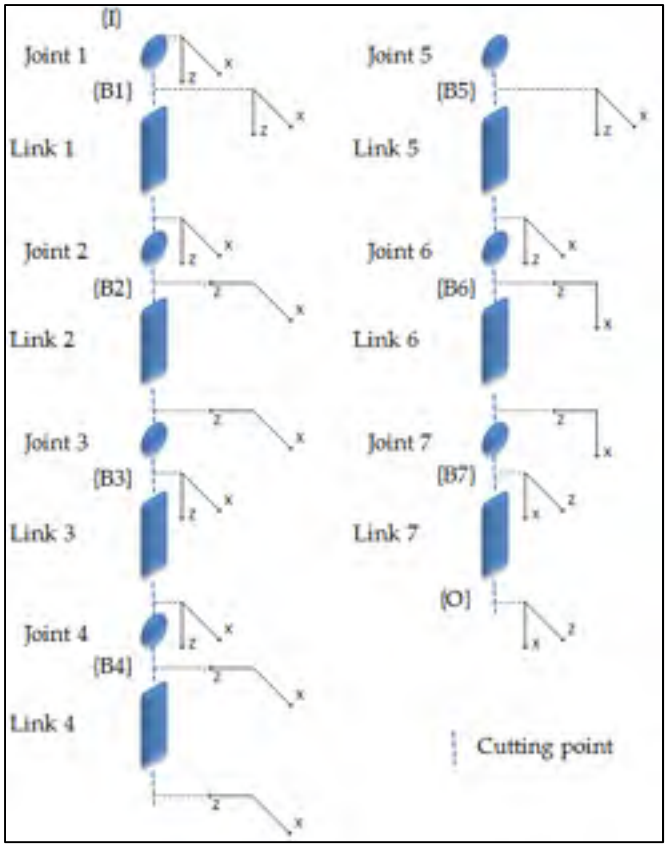

Figure 3.4 Virtual decomposition in 14 subsystems

3.3.2 Kinematics

From the resulting parameters shown in Table 3.1 and the decomposition shown in Figure 3.4, the homogeneous transformation matrices of the system are obtained. From these, the force/moment transformation matrices of the robot are calculated as follows:

$$ {}^{A}U_{B} = \begin{bmatrix} {}^{A}R_{B} & 0_{3\times3} \\ ({}^{A}r_{AB}\times){}^{A}R_{B} & {}^{A}R_{B} \end{bmatrix} \in \mathbb{R}^{6\times6} \tag{3.1} $$

where ${}^{A}R_{B}$ represents the rotation matrix from one frame to the next and ${}^{A}r_{AB}$ is the distance between frames, and:

$$ ({}^{A}r_{AB}\times) = \begin{bmatrix} 0 & -{}^{A}r_{AB}(3) & {}^{A}r_{AB}(2) \\ {}^{A}r_{AB}(3) & 0 & -{}^{A}r_{AB}(1) \\ -{}^{A}r_{AB}(2) & {}^{A}r_{AB}(1) & 0 \end{bmatrix} \tag{3.2} $$

where ${}^{A}r_{AB}(i)$ represents the i_{th} term of the ${}^{A}r_{AB}$ vector.

We calculate each force/moment transformation matrix ${}^{B_i}U_{B_{i+1}}$ for $i = 1, \dots, 6$.

The next step is to calculate ${}^{B_i}V$, the linear/angular velocity vectors of the B_i frames (with $i = 1, \dots, 7$) as follows:

$$ {}^{B_i}V = \begin{bmatrix} {}^{B_i}v \\ {}^{B_i}\omega \end{bmatrix} \in \mathbb{R}^{6} \tag{3.3} $$

where ${}^{B_i}v$ is the linear velocity vector and ${}^{B_i}\omega$ is the angular velocity vector of the corresponding frame. With the previous linear/angular velocity vectors, the augmented velocity vector is formed as:

$$ \mathcal{V}_7 = [\dot{q}_1 \quad \cdots \quad \dot{q}_7 \quad {}^{B_1}V^T \quad \dots \quad {}^{B_7}V^T]^T \tag{3.4} $$

Equation (3.4) can be written in the following form:

$$ \mathcal{V}_7 = J_7 * \dot{q} \tag{3.5} $$

where $\dot{q} = [\dot{q}_1 \quad \cdots \quad \dot{q}_7]^T$ is the velocity vector and J_7 is the VDC-Jacobian matrix of the system:

$$J_7 = \begin{bmatrix} & & I_7 & \\ z & 0_6 & \cdots & 0_6 \\ {}^{B_1}U_{B_2}^T z & z & \ddots & \vdots \\ \vdots & \ddots & \ddots & 0_6 \\ {}^{B_1}U_{B_7}^T z & \ldots & {}^{B_6}U_{B_7}^T z & z \end{bmatrix} \tag{3.6}$$

with $z = [0 \quad 0 \quad 0 \quad 0 \quad 0 \quad 1]^T$, I_7 is a 7×7 identity matrix and 0_6 a 6×1 zero vector.

Finally, the required velocities need to be calculated as a function of the control requirements. Since in our case the robot is required to track a control trajectory, we incorporate the desired position in the vector of required velocities:

$$\dot{q}_r = \dot{q}_d + \lambda(q_d - q) \tag{3.7}$$

where $\dot{q}_r = [\dot{q}_{1r} \quad \cdots \quad \dot{q}_{7r}]^T$ is the required velocity vector, $\dot{q}_d = [\dot{q}_{1d} \quad \cdots \quad \dot{q}_{7d}]^T$ is the desired velocity vector, $\lambda > 0$ is a control parameter, $q_d = [q_{1d} \quad \cdots \quad q_{7d}]^T$ is the desired position vector and $q = [q_1 \quad \cdots \quad q_7]^T$ is the position vector. From (3.5) to (3.7), we obtain the augmented required velocity vector as follows:

$$\mathcal{V}_{7r} = J_7 * \dot{q}_r \tag{3.8}$$

3.3.3 Dynamics

In this paper, only the inverse dynamics that take part in the control of the robot are described. To obtain the inverse dynamics, it is necessary to calculate the forces required for the links and then the torques required by the joints. The first step for the link dynamics is to obtain the required net force/moment vectors using the following equation:

$$^{B_i}F_r^* = Y_i\,\hat{\theta}_i + K_{si}(\,^{B_i}V_r - \,^{B_i}V) \tag{3.9}$$

for $i = 1, \ldots, 7$, where K_{si} is a symmetric positive-definite gain matrix; the velocities $^{B_i}V_r$ and ^{B_i}V are defined in relations (3.3) and (3.8), respectively; $Y_i \in \mathbb{R}^{6\times 13}$ is a regressor matrix and $\hat{\theta}_i \in \mathbb{R}^{13}$ is the estimated parameters vector composed of the mass of the link, the elements of the vector pointing from the origin of the reference frame of the link toward its mass centre, as well as the elements of the inertia tensor of the body. The exact representation of each element of $\hat{\theta}_i$ is given in Appendix A. To estimate the parameters, the following relation is used:

$$\hat{\theta}_{i\gamma} = \mathcal{P}\big(s_{i\gamma}(t), \rho_{i\gamma}, a_{i\gamma}(t), b_{i\gamma}(t), t\big) \tag{3.10}$$

for $i = 1, \ldots, 7$ and $\gamma = 1, \ldots, 13$. Where $\hat{\theta}_{i\gamma}$ represents the γ_{th} parameter of the i_{th} link, $\rho_{i\gamma}$ is the parameter update gain, $a_{i\gamma}(t)$ and $b_{i\gamma}(t)$ are the lower and upper bounds of $\hat{\theta}_{i\gamma}$ respectively and $s(t) \in \mathbb{R}$ is a scalar variable given by:

$$s_i = Y_i^T(\,^{B_i}V_r - \,^{B_i}V) \tag{3.11}$$

The projection function $\mathcal{P}$ is a differentiable scalar function defined for $t \geq 0$, such that its time derivative is governed by:

$$\dot{\mathcal{P}} = \rho\, s(t)\, \mathcal{K} \tag{3.12}$$

with:

$$\mathcal{K} = \begin{cases} 0 & if\ \mathcal{P} \leq a(t) and\ s(t) \leq 0 \\ 0 & if\ \mathcal{P} \geq b(t) and\ s(t) \geq 0 \\ 1 & otherwise \end{cases}$$

Once this step is completed, the required force/moment vectors at the cutting points are obtained as follows:

$$\begin{aligned} {}^{B_7}F_r &= {}^{B_7}F_r^* \\ {}^{B_i}F_r &= {}^{B_i}F_r^* + {}^{B_i}U_{B_{i+1}}\ {}^{B_{i+1}}F_r \end{aligned} \tag{3.13}$$

for $i = 6, \dots, 1$. The next step is the calculation of the dynamics of the joints. Some relations and variables used to calculate the dynamics of the joints were also used in the calculation of the dynamics of the links; therefore, a sub-index, a, is used to refer to the joints' dynamic equations and variables. For $i = 1, \dots, 7$ in (3.14) to (3.18), the following vectors are defined:

$$Y_{ai} = [\ddot{q}_{ir} \quad sign(\dot{q}_{ir}) \quad \dot{q}_{ir} \quad 1] \tag{3.14}$$

$$\theta_{ai} = [J_{mi} \quad k_{ci} \quad k_{vi} \quad c_i]^T \tag{3.15}$$

where J_{mi} is the equivalent mass or moment of inertia, $k_{ci} > 0$ denotes the Coulomb friction coefficient, $k_{vi} > 0$ denotes the viscous friction coefficient and c_i denotes an offset that accommodates asymmetric Coulomb frictions. As in the case of the links, the estimation of the parameters defined in (3.15) is performed as follows:

$$\hat{\theta}_{ai\gamma} = \mathcal{P}\big(s_{ai\gamma}(t), \rho_{ai\gamma}, a_{ai\gamma}(t), b_{ai\gamma}(t), t\big) \tag{3.16}$$

However, in this case, $\gamma = 1, \dots, 4$ and the scalar function s is defined for the joints as:

$$s_{ai} = Y_{ai}^T(\dot{q}_{ir} - \dot{q}_i) \tag{3.17}$$

Thereafter, the net torque for the joint becomes as follows:

$$\tau_{ir}^* = Y_{ai}\ \hat{\theta}_{ai} + k_{ai}(\dot{q}_{ir} - \dot{q}_i) \tag{3.18}$$

where k_{ai} denotes a feedback gain.

Finally, the torques obtained from the link and joint analyses are combined. First, we extract the torque of the link force/moment vector.

$$\tau_{air} = z^T {}^{B_i}F_r \tag{3.19}$$

for $i = 1, \ldots, 7$. With z defined after (3.6), the control torque is then designed for $i = 1, \ldots, 7$ as:

$$\tau_{Ci} = \tau_{ir}^* + \tau_{air} \tag{3.20}$$

For a complete stability analysis of VDC, the reader is referred to (Zhu et al., 2013; Zhu et al., 1997; Zhu, Zeungnam and De Schutter, 1998). Figure 3.5 presents a flow diagram of the VDC architecture applied in the inner position control loop. The interaction between the robot and the human is represented by the human joint position q_h, causing the robot to exert torque τ_h . The human also applies force, $\mathcal{F}$, which will be used in the outer force control loop, as described in the next section.

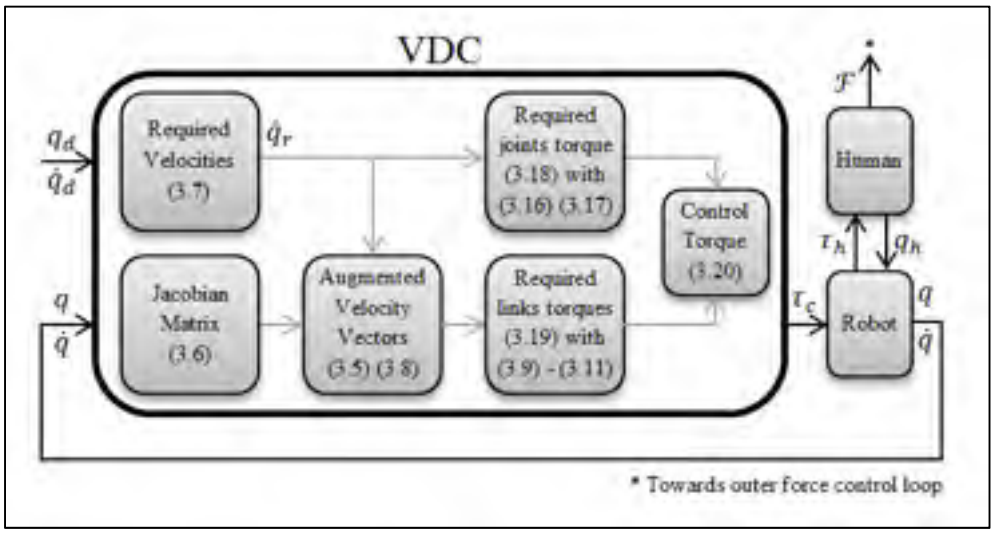

Figure 3.5 Block diagram of the VDC

3.4 Active-assistive and active rehabilitation

In robotics, a trajectory defines movement of a robot in a multidimensional space. This trajectory contains information concerning the position, velocity and acceleration for each degree of freedom in time (Craig, 2005). To control the movement of the robot, the user defines a desired trajectory that includes this information and is usually generated by means of a trajectory planner.

3.4.1 Trajectory planner

The trajectory planner for ETS-MARSE is based on joint-space specification. It is performed in real time on a dedicated processor (PXI-8108), described in section 3.2. Some exercises can comprise different trajectory segments, each specified by initial and final positions for each joint. Each segment of the trajectory for each joint is calculated using a cubic polynomial (Craig, 2005) of the form:

$$q(t) = a_0 + a_1 t + a_2 t^2 + a_3 t^3 \tag{3.21}$$

where a_i for $i = 0, \dots, 3$ are the coefficients of the cubic polynomial to be specified. With initial and final velocities of zero, the initial position defined as $q(0) = q_0$ and the final position defined as $q(t_f) = q_f$, equation (3.21) reduces as follows:

$$q(t) = q_0 + \frac{3(q_f - q_0)}{t_f^2} t^2 - \frac{2(q_f - q_0)}{t_f^3} t^3 \tag{3.22}$$

In order to obtain information on the velocity and acceleration of the trajectory, the corresponding first and second derivatives of (3.22) are used.

In rehabilitation, it is often useful to specify a desired trajectory in Cartesian space in order to specify movements with a physical interpretation. This can be as simple as a straight line, or,

for example, following a geometrical shape such as a triangle, a rectangle, etc. In the case of the ETS-MARSE robot, the trajectory can be specified either in the joint space or in Cartesian space (robot workspace); whatever the case, the trajectory tracking is always executed in joint space. Thus, it is necessary, given a position and orientation of the end-effector in Cartesian space, to find the joint positions of the robot that can accomplish this desired configuration (inverse kinematics problem). In this case, the pseudo-inverse of the Jacobian method is used.

In the dynamic relations of the links of a robot, the reference frame of each link has linear and angular velocities, with respect to the other links and to the robot reference frame. The Jacobian matrix of a robot relates the joint velocities with linear and angular velocities of the Cartesian space as follows:

$$\dot{X} = J(q)\dot{q} \tag{3.23}$$

where $\dot{X} \in \mathbb{R}^6$ is the velocity vector of the end-effector, $\dot{q} \in \mathbb{R}^n$ is the joint velocities vector and $J(q) \in \mathbb{R}^{6 \times n}$ is the robot Jacobian matrix. For the inverse kinematics problem presented, one possible solution can be obtained as follows (Asada and Slotine, 1986):

$$\dot{q} = J(q)^{+}\dot{X} \tag{3.24}$$

where $J(q)^{+} = J(q)^{T}(J(q)J(q)^{T})^{-1}$ is the generalized pseudo-inverse. The method can be enriched by adding null space characteristics to the right side of the equation with the term$(J(q)^{+}J(q) - I)\xi$, where $\xi \in \mathbb{R}^n$ is an arbitrary vector that can be used for tasks such as obstacle avoidance and I is the 6×6 identity matrix. Being a redundant robot, the ETS-MARSE has different solutions for its inverse kinematics problem; currently, to solve that problem, we are developing an inverse kinematics solution (analytical, geometrical or numerical) that will ensure anthropomorphic configurations, as in (Culmer et al., 2010; Zhang, Xiong and Wu, 2011). In the rehabilitation tasks presented here, solving the null space is not necessary, since only predefined Cartesian trajectories were used. These

trajectories were simulated and tested to constantly ensure a configuration of the robot not presenting any non-ergonomic positions. Additionally, singularity avoidance is secured with joint angle limits, both in software and hardware (mechanical stoppers).

3.4.2 Active-assistive rehabilitation based on an admittance-modified trajectory planner

In the case of active-assistive mode, the robot helps the user, at an adjustable level, to achieve the tracking of a trajectory shown in the virtual interface. To do this, the assistive controller somewhat modifies the predefined trajectory in relation to the patient's movement limitations. The system measures the force exerted by the user at the end-effector of the robot, which can be interpreted as the difference between the user's trajectory and the goal trajectory.

The first step is to transform this information into a quantity that specifies how the subject's opposition force affects all the DOF of the exoskeleton (that are related to the human arm joints). As a consequence of the virtual work principle, the Jacobian matrix relates static forces, i.e., it transpose assigns Cartesian forces to joint torques as follows:

$$\tau = J^T \mathcal{F} \tag{3.25}$$

where τ is the 7×1 vector of joint torque and $\mathcal{F}$ is the 6×1 measured force-moment Cartesian vector. This relation gives us the user's opposition force in terms of joint torques.

The second step is to transform these torques into meaningful information for the trajectory that is being followed, that is, information relating to changes in position. Impedance can be defined as a transfer function between the external force acting on the manipulator and its displacement (Gorinevsky, Formalsky and Schneider, 1997). Knowing the result from (3.25) and applying the impedance definition in the form of an admittance relation, which directly

relates an input force to an output position, we have a direct form with which to modify the desired trajectory as follows:

$$q_a = q_d + \tau \left(\frac{1}{K + Cs}\right) \tag{3.26}$$

where q_a is the 7×1 vector of the new desired trajectory defined by the admittance, q_d is the 7×1 vector with the original desired trajectory from the trajectory planner and the final right term of the equation in the parenthesis, the chosen admittance function. It can be seen that the latter has the form of a spring-damper function, in which τ is the 7×1 vector of torques exerted on the robot's joints by the subject, calculated from (3.25) and K and C are the 7×7 gain matrices corresponding to the spring and damper constants, respectively. By adjusting these constants to provide higher or lower opposition to the subjects' disturbances and constraints over movement, this admittance function allows for variation in the amount of help to be provided by the robot. This particular admittance function by means of the damping term also provides smooth movement.

3.4.3 Active rehabilitation based on an admittance-modified trajectory planner

Another application of an admittance function modifying a predefined trajectory involves performing a free trajectory movement. If the spring-damper system introduced by the admittance function in (3.26) is detached from a desired trajectory, it becomes a means of moving the robot freely within its workspace. In this case, the subject is allowed to move in the environment presented by the virtual interface and can try to follow the trajectory without any robotic aid. This rehabilitation option, corresponding to active (unassisted) rehabilitation, is achieved by changing the desired trajectory of the robot, that is, q_d in (3.26). Instead of coming from a trajectory planner, the desired trajectory comes from the robot's previous position, as follows:

$$q_a = q + \tau \left(\frac{1}{K + Cs}\right) \tag{3.27}$$

where q is the 7×1 vector of the joint positions. If the user stops exerting forces on the force sensor, $\tau \to 0$, causing the robot to reduce its movement and gradually, when $q_a = q$, the robot remains in its most recent position. With this mode, the robot is allowed to follow the user‘s movements, while the trajectory tracking ensures the weightless sensation of the robot structure to the subject and provides gravity compensation. In Figure 3.6, a block diagram showing the control architecture is presented. The position of the selector shown in the bottom row of the system corresponds to the case of active-assistive rehabilitation (left position) and active rehabilitation (right position) described earlier. In this case, the desired trajectory that inputs the VDC (see Figure 3.5) is the admittance modified trajectory q_a from (3.26) or (3.27) and Δq is the second term of the right-hand side of the same relations.

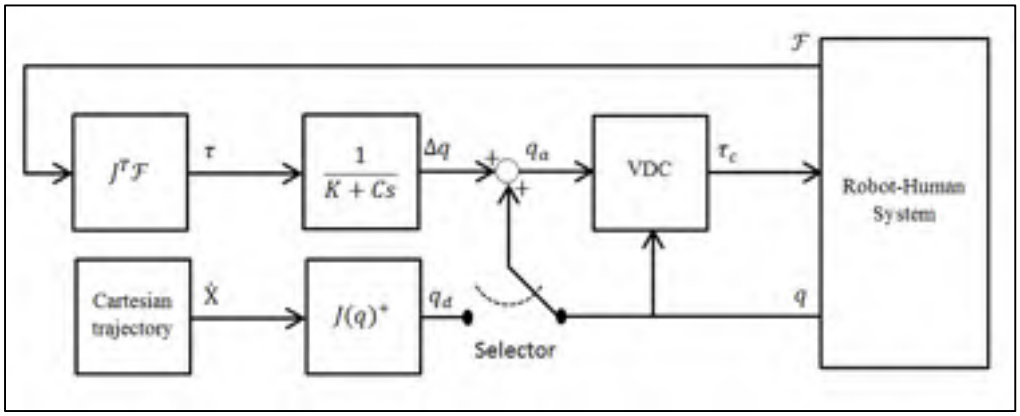

Figure 3.6 Block diagram of the system

The ETS-MARSE works in two different active rehabilitation modes, which use virtual walls added to the environment in order to constrain movement to a confined space. In the first mode, the system restrains movement beyond the wall and only allows movement that corrects the collision situation, i.e., the robot will not allow the user “to slide” through the wall to complete the exercise. The user must return to the inner part of the space in order to continue with the movement. The algorithm used in this rehabilitation mode is presented in Figure 3.7. The second mode of operation is intended for users that need more assistance

once there is a deviation from the main trajectory. Once the user hits a wall, the robot stops for a predetermined time to let the user notice that movement has been stopped by the system. It then goes into passive mode, which means that the robot will help the user by returning automatically to the closest point on the desired trajectory, as illustrated in Figure 3.8. Here, *Pw* represents the point where the user hits the wall, *Pi* the trajectory initial point, *Pf* the final point and *Pr* the point of the position reset. The last one, the closest point to the trajectory, is obtained as follows: first, the cosine of angle α is calculated:

$$cos\,\alpha = \frac{|u_1 \cdot v_1 + u_2 \cdot v_2 + u_3 \cdot v_3|}{\sqrt{u_1^2 + u_2^2 + u_3^2} \cdot \sqrt{v_1^2 + v_2^2 + v_3^2}} \tag{3.28}$$

where $u \in \mathbb{R}^3$ and $v \in \mathbb{R}^3$are the direction vectors of the lines $(\overline{P_i P_w})$ and $(\overline{P_w P_r})$, respectively, and u_i and v_i are the i_{th} elements of the corresponding direction vector. Then, the reset point is calculated as:

$$P_r = cos\,\alpha \cdot \sqrt{u_1^2 + u_2^2 + u_3^2} + P_i \tag{3.29}$$

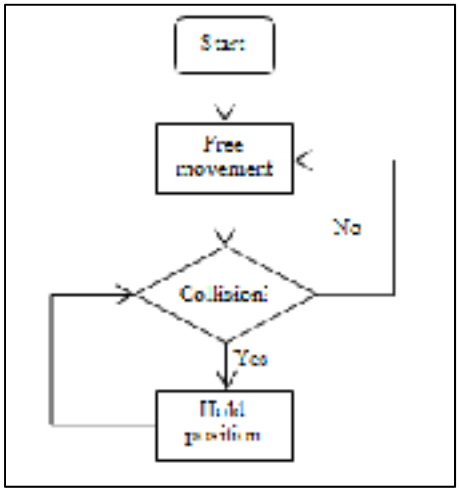

Figure 3.7 Active rehabilitation with walls

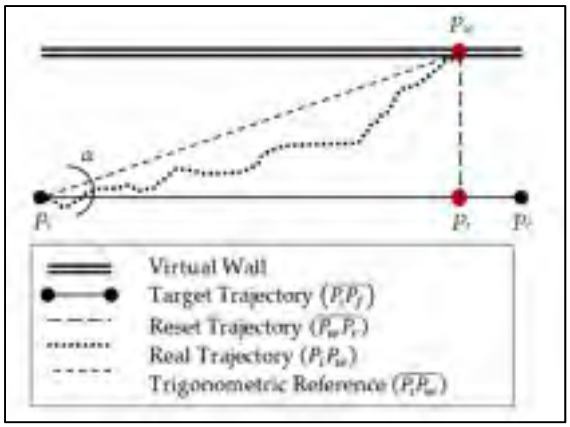

Figure 3.8 Virtual wall collision and reset path

With the final point obtained from (3.29) and the initial point as *Pw*, the passive mode of the system conducts the robot end-effector to this point by means of a trajectory generated as described in subsection 3.4.1. Finally, after another predetermined time to allow the user to be ready, the system allows them to continue. The algorithm followed by this rehabilitation mode is presented in Figure 3.9.

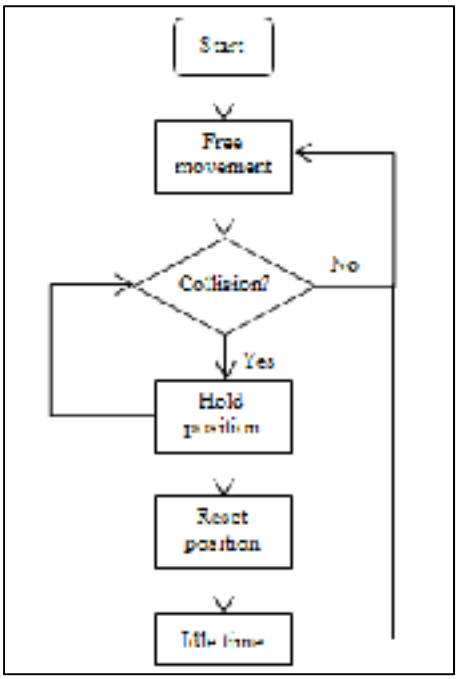

Figure 3.9 Active-assisted rehabilitation with walls

3.5 Experimental results

In this section, we present one scenario for each of the two rehabilitation modes. The first comprises an experiment performed for active-assistive rehabilitation and the second, two tests for active rehabilitation.

3.5.1 Active-assistive rehabilitation

This first scenario comprises three tests based on a tridimensional square trajectory, defined below. The trajectory involves the movement of the seven degrees of freedom of the robot. Test number one is given as a reference of the behaviour of the robot, i.e., without modifying the trajectory tracking. This scenario corresponds to the passive rehabilitation mode in which the patient is guided through a predefined rehabilitation exercise. The result of this test is shown in Figure 3.10. It can be seen that the tracking error is very small and this will be used as a reference value. The initial position of the end-effector of the robot corresponds to point A; it moves to points B – C – D and then returns to A. The points are listed in Table 3.2.

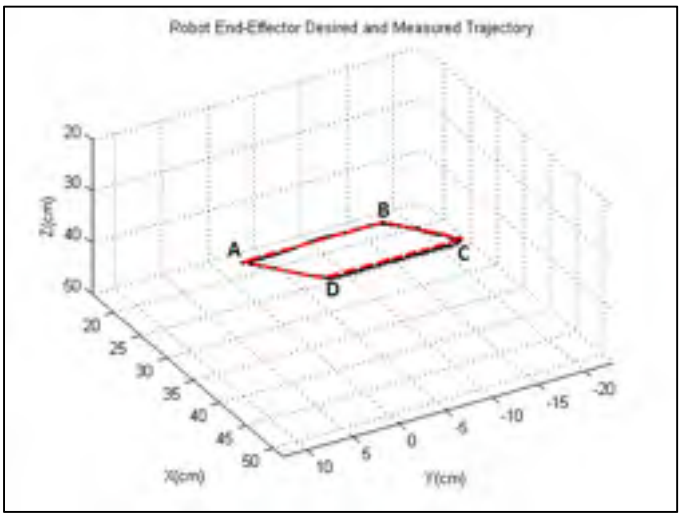

Figure 3.10 Reference trajectory tracking

Table 3.2 Robot active-assistive rehabilitation reference trajectory

Point	X(cm)	Y(cm)	Z(cm)
A	28.67	2.51	37.08
B	28.67	-12.51	37.08
C	43.67	-12.51	27.08
D	43.67	2.51	27.08

The next two tests constitute the central point of this approach of rehabilitation (active-assistive). In these cases, the tracking is modified based on the measurements of the force sensor. The reference trajectory is the same as that presented in Figure 3.10, but modified according to equation (3.26). To simulate stiffness or spasticity from the user, an elastic band is tied from the handle of the robot (which holds the force sensor) to an external anchor point. This provides a systematic comparison, depending only on the modification of the admittance parameters. The setup allows the variation to be independent from the test subject, whose behaviour can change from one test to another. For the first test, the admittance parameters were selected to provide a high degree of help, specifically with the main diagonal of $K = [0.05\ 0.06\ 0.06\ 0.05\ 0.02\ 0.02\ 0.02]^T$and the remaining elements equal to 0, and the main diagonal of $C = [5\ 1\ 5\ 10\ 5\ 5\ 5]^T$. The remaining elements were also zero. The second test was configured to provide a low degree of help from the robot, i.e., with the main diagonal of $K = [0.1\ 0.12\ 0.12\ 0.1\ 0.04\ 0.04\ 0.04]^T$and the main diagonal of $C = [5\ 1\ 5\ 10\ 5\ 5\ 5]^T$, and the remaining elements being zero.

The results of these tests are shown in Figures 3.11 and 3.12 for high and low degrees of help, respectively. Because the opposition force to this movement is exerted on the robot, the actual trajectory is deflected from the predefined one. In these figures, the dotted line represents the desired trajectory and the solid line the actual trajectory followed by the robot, which was perturbed using the elastic band.

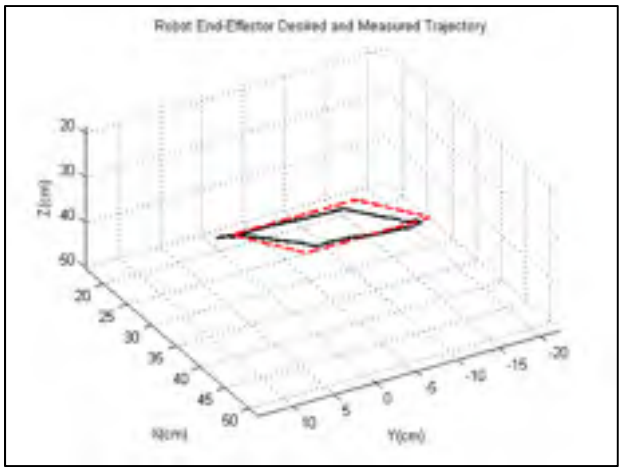

Figure 3.11 Trajectory modified with
high degree of help

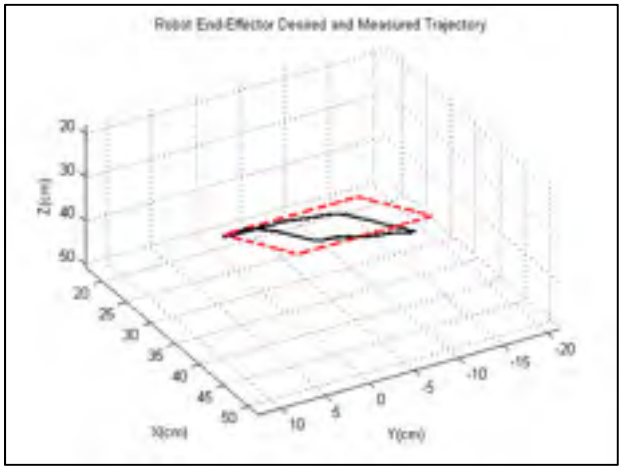

Figure 3.12 Trajectory modified with
low degree of help

For the final two tests (Figures 3.11 and 3.12), the force and torque measured with the force sensor are shown in Figure 3.13. We can see how the force input from the elastic band is very similar in both tests; nevertheless, the modification of the trajectory is different, allowing us to see the effects of modifying the admittance function coefficients.

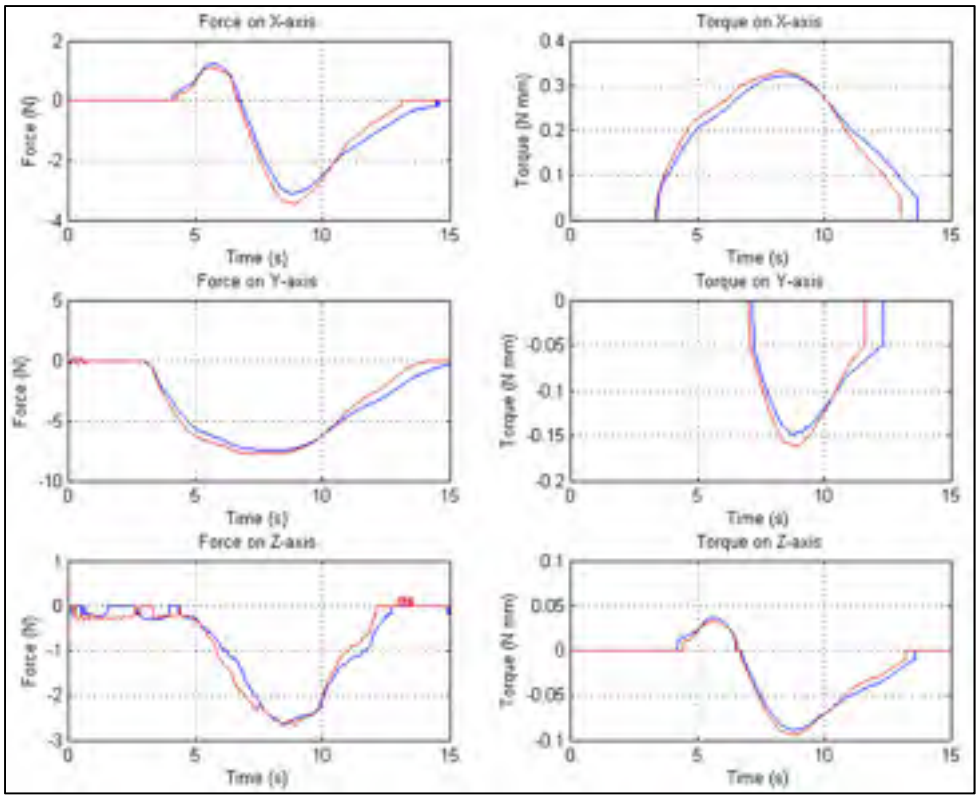

Figure 3.13 Comparison of forces-torques between high and low degree of assistance from the robot

3.5.2 Active rehabilitation, constrained free movement

In this rehabilitation mode, the user follows the trajectory by means of a virtual interface that provides the tracking of movement and incorporates a variety of exercises in a game-based environment. The active rehabilitation mode with virtual walls has two different tests: the first with the wall as an obstacle and the second, where collision with the wall indicates that the robot will assist the user, as described in section 3.4. Both setups require the subject (32-year old healthy male subject with a mass of 91 kg and height of 182 cm, in seated position) to track a straight line; the virtual wall is located parallel to the desired trajectory, 10 cm to the right.

The result for the first experiment is shown in Figure 3.14. In this mode, once the user hits the wall, the system only allows movement towards the desired trajectory. In the plots at the

bottom of the figure, the filtered force in the Y-axis of the force sensor and the position of the end-effector in the Y-axis of the reference frame are shown as a function of time. Both axes are the Y-axis, because the wall is set in the Y-direction. The Y-axis of the force sensor is parallel to the Y-axis of the reference frame, but in the opposite direction, which provides a good reference point for the comparison. Nevertheless, it is very important to remember that the force and its modification follow the transformation described in (3.25) and (3.27). It can be seen that, when the subject starts to apply force to the sensor at 12.86 seconds, the displacement of the robot starts. At 17.05 seconds, the wall is hit; the virtual wall restricts the movement of the end-effector beyond this point (at approximately 0.08 m), irrespective of an increase in the user's produced force. Finally, at 20.40 seconds, when the user starts to apply force in the opposite direction (away from the wall), the system allows the robot to continue with the movement and completes the exercise.

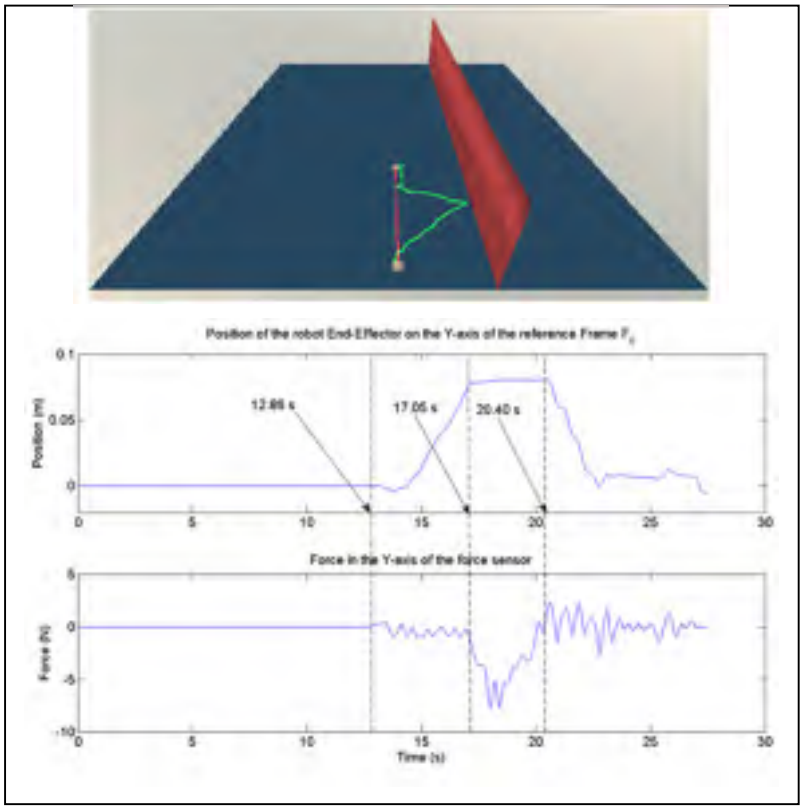

Figure 3.14 Virtual walls as obstacle
for active rehabilitation

The final test shows the assisted wall return. It can be seen in Figure 3.15 that the user starts the movement by applying force to the robot at 8.31 seconds. Once the wall is hit, at approximately 10.90 seconds, it can be seen that the movement of the robot stops, even though force continues to be exerted for some time. The system, after an idle waiting time (three seconds), resets the position to the closest point in the trajectory (two seconds), followed by another idle time (three seconds), allowing the user to be ready. After this, the user can continue the exercise when ready, in this case, at 20.06 seconds. It is important to note that in the two idle states and in the reset state, there is no input from the user to the force sensor. This shows that assistance is provided for the system without any action needed from the user. The small delays that can be observed in the state changes, especially from the applied force to the start of movement, are due to the time it takes to overcome the static friction and the filtering in the force sensor's raw data; this delay is imperceptible to the user.

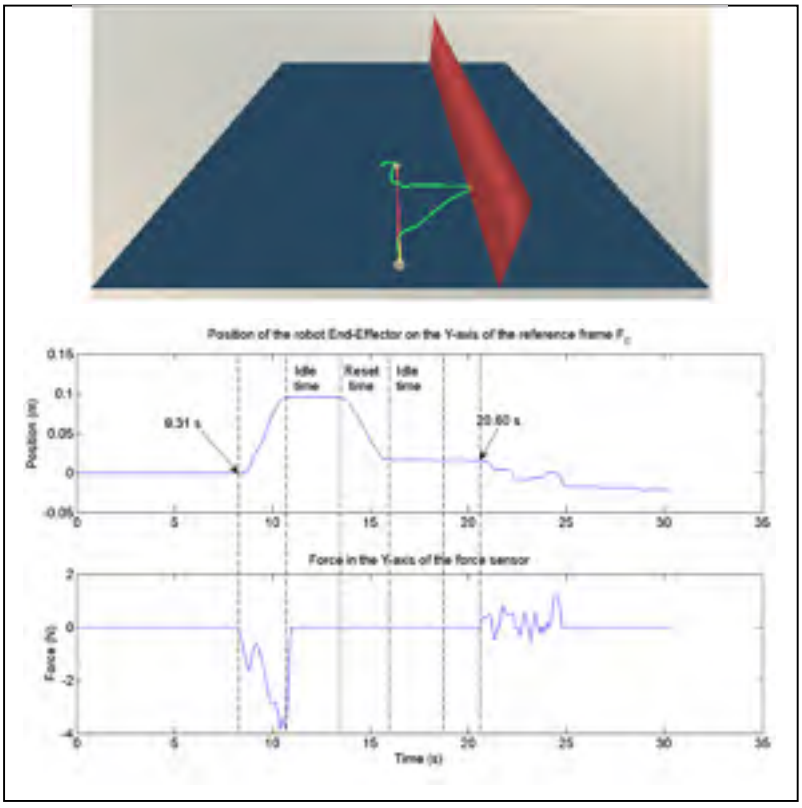

Figure 3.15 Virtual walls as obstacle and starting point
for robotic assistance in active rehabilitation

3.6 Conclusions

The experimental results confirm that the present work can actively help in different rehabilitation scenarios. For active-assistive rehabilitation, with the guidance of the ETS-MARSE, a subject can accomplish a specified trajectory. The robot can vary the assistance provided according to the evolution and the needs of future patients. It is important to note that the robot will not produce forces that are beyond the capabilities of the subject in order to fulfil a trajectory. A qualified therapist must adjust the limits according to the user's requirements. The amount of variation of the trajectory can be quantified as an excellent measurement of progression of the subject. In the case of active rehabilitation, it is shown how by means of the same admittance function, the system can work in a free movement mode. This rehabilitation mode, combined with limits (virtual walls), could indicate when patients will need assistance from the robot to complete their rehabilitation tasks. As the next step for active rehabilitation, the system will incorporate the use of electromyographic signals in order to complete the readings of the force sensor and to provide better tracking of the subject's movement intentions, and will be used on its own for subjects where the force sensor may be not enough to determine the intended movement.

CHAPTER 4

COMPLIANT CONTROL OF A REHABILITATION EXOSKELETON ROBOT ARM WITH FORCE OBSERVER

Cristóbal Ochoa-Luna[1], Maarouf Saad[1], Jawhar Ghommam[2], Mohammad Habibur Rahman[3] and Philippe S. Archambault[4,5]

[1]Department of Electrical Engineering, École de technologie supérieure,
1100 Notre-Dame West, Montreal, Quebec (H3C 1K3) Canada.

[2]National Institute of Applied Sciences and Technology, University of Carthage,
Centre Urbain Nord BP 676-1080, Tunis Cedex, Tunis, Tunisia.

[3]Mechanical Engineering Department, University of Wisconsin-Milwaukee,
3200 North Cramer Street, Milwaukee, WI (53211) USA.

[4]School of Physical & Occupational Therapy, McGill University, Canada.
3654 Prom Sir-William-Osler, Montréal, Québec (H3G 1Y5) Canada.

[5]Centre for Interdisciplinary Research in Rehabilitation (CRIR), Canada.
2275 Laurier Avenue East, Montréal, Quebec (H2H 2N8) Canada.

This paper was sent to the *IEEE/ASME Transactions on Mechatronics* in March 2016

Abstract:

In robotic rehabilitation, active rehabilitation is a phase in which interaction between human and robot allows the subjects to perform daily exercises. One key element of this interaction is the force applied by the subject. This force can be measured by a force sensor or estimated using a nonlinear force observer. In the approach presented in this paper, the nonlinear observer estimates the interaction forces between the subject and the robot, in order to understand the intention of motion of the subject. Then, by means of an admittance function, this estimation is used for compliance control, so that the robot moves while following the user's intention. This method allows the subject to perform some active isokinetic-type

rehabilitation exercises. Experimental results show the effectiveness of the proposed approach.

Keywords: Active Rehabilitation, Compliance Control, Exoskeleton Robot, Nonlinear Observer, Virtual Decomposition Control

4.1 Introduction

According to the World Health Organization, 15 million people worldwide suffer a stroke each year; of these, 5 million die and another 5 million are left with long-term disabilities (Mackay and Mensah, 2004). Stroke has been identified as one of the major causes of loss of upper extremity (UE) function. One of the most common effects after a stroke is weakness or paralysis on one side of the body (hemiparesis), which affects up to 90 percent of stroke survivors (Van der Loos and Reinkensmeyer, 2008). When rehabilitation is possible, it implies many hours of highly skilled and extensive therapy. In the last years, the demand for rehabilitation services has increased significantly. As a result, the number of clinicians available to provide therapy is not sufficient to deal with the number of patients (Bureau of Labor Statistics, 2015; Gupta, Castillo-Laborde and Landry, 2011; Landry, Ricketts and Verrier, 2007). Therefore, robotic-assisted UE rehabilitation has become very important and has shown some promising results (Huang, Tu and He, 2015; Klamroth-Marganska et al., 2014; Norouzi-Gheidari, Archambault and Fung, 2012; Patton et al., 2006). It is for that reason that we have developed the ETS - Motion Assistive Robotic-exoskeleton for Superior Extremity (ETS-MARSE). The project has been developed in different stages (Rahman et al., 2011a; Rahman et al., 2012a). The latest version comprises of a seven degree-of-freedom (DOF) exoskeleton, designed to cope with the main motion capabilities of the human UE; that is at the shoulder, elbow and wrist levels, in combination or individually. It also contains a graphic interface to a virtual environment with different rehabilitation exercises (Ferrer et al., 2013). In active rehabilitation, the subject performs a rehabilitation task and the robot interacts with the subject to control (e.g. time limits, space limits, etc.) or, as in the case of this paper, to present variable resistance to the movement (i.e. isokinetic exercise). This

behavior emphasizes the responsibility of the patient in being active to accomplish the exercise.

The interaction between the patient and the robot can be implemented through different methods: from buttons and joysticks in the first rehabilitation robots to electromyography (Kiguchi and Hayashi, 2012) and electroencephalography (Frisoli et al., 2012; He et al., 2015) in recent ones. The use of force transducers is one of the most widely used approaches (Jackson et al., 2007; Miller and Rosen, 2010; Ochoa Luna et al., 2015; Ozkul and Barkana, 2013; Zhou and Ben-Tzvi, 2015). Upper extremity rehabilitation by means of the robot-human interaction forces principally makes use of compliant control as admittance and impedance (Gupta and O'Malley, 2006; Otten et al., 2015). These systems use transducers to measure the force and torque exchanges between the exoskeleton and the user or the exoskeleton and the environment. For example, the iPAM dual robot system uses two manipulator-like robots, with a total of 6DOF, to hold the patient's arm at that level of the upper arm and forearm, with two 6DOF force transducers (Jackson et al., 2007). The RehabRoby, a 6DOF exoskeleton, uses two one-axis force sensors mounted dorsally in the forearm strip; one to measure the force applied to the elbow flexion movement and the other for the shoulder flexion movement (Ozkul and Barkana, 2013). The EXO-UL7, a 7DOF wearable upper limb exoskeleton, uses four 6-axis force/torque sensors; one at each attachment point (upper arm, lower arm and hand) and one at the tip of the exoskeleton (Miller and Rosen, 2010). In our previous studies with the ETS-MARSE, we have demonstrated the feasibility of rehabilitation work with the aid of compliance control for robotic rehabilitation with the use of a 6DOF force sensor mounted at robot's endpoint (Ochoa Luna et al., 2015). All the above-mentioned systems have shown they can provide users with satisfactory rehabilitation exercises. However, some problems with the use of force sensors may arise, such as cost, sensibility to temperature changes, noise and unstable states caused by the narrow bandwidth of force information (Katsura, Matsumoto and Ohnishi, 2007), etc. There is also the fact that small sensors, although very precise, are susceptible to be damaged during human-robot interaction.

In this paper we present the use of a nonlinear observer, that have been previously investigated for industrial applications (Alcocer et al., 2003; Chan, Naghdy and Stirling, 2013; Do and Pan, 2008; Wen-Hua et al., 2000), applied to a rehabilitation robot (ETS-MARSE) to avoid the need for a force sensor. Applications of disturbance observers for rehabilitation have been presented before (Gupta and O'Malley, 2011; Popescu et al., 2013). In the first paper, a nonlinear disturbance observer was applied successfully to control external forces to a 1DOF rehabilitation mechanism. In the second one, a trio of nonlinear observers (force observer, velocity observer, and force-disturbance observer) was used to control a hand exoskeleton system for rehabilitation. The performance of the system was demonstrated by numerical simulation. In the work presented in this paper, the force estimated by the proposed force observer was used to detect the subject's movement intention and to apply a compliance force control to move the robot-human system. This approach also simplifies the use of an admittance function to modify the current position of the robot and perform a compliant movement. Indeed, with a force observer, the torque applied to each joint can be estimated directly; i.e. it is no longer necessary to transform the force measured in Cartesian space by a force sensor to joint space using a Jacobian inverse. The impedance of the robot-human system due the admittance function is used to characterize the isokinetic-type exercises. Another key aspect is the study of the effects of the control based on the nonlinear observer in a multi-degree-of-freedom robot (7DOF). Finally, in order to better separate the effects of the friction from the human interaction forces (as these could be seen as disturbance), the friction estimated by the controller (see section 4.2) is fed back into the observer, in order to precisely discard the effects of the position controller friction-compensation part.

This paper is organized as follows. Section 4.2 presents the nonlinear position control. In section 4.3, the compliance control that includes the nonlinear force observer is described. Section 4.4 describes the hardware architecture and experimental setup of the system and its results. Finally, section 4.5 provides the conclusions and future work.

4.2 Nonlinear control: Virtual Decomposition Control and Force Observer

In this paper, the Virtual Decomposition Control (VDC) technique is used for the nonlinear control of the robot. In previous studies with the ETS-MARSE (Ochoa Luna et al., 2014b), VDC has proven that besides the performance in position control, it can successfully address two important issues: a) it facilitates the implementation in a high degree-of-freedom robot (7DOF in this case) through its subsystem decomposition, and b) it copes with the changes in the dynamics of the robot-human system due to the biomechanical and physiological characteristics of different patients through its internal dynamic-parameters adaptation. Therefore, this technique was adopted as the current control method for our robot. Additionally, as mentioned, the estimated friction parameters are used to feedback the controller friction compensation to the nonlinear observer.

This section shows only the kinematics analysis of the ETS-MARSE robot in order to present it to the reader. A detailed analysis of the VDC implemented in the ETS-MARSE is described in (Ochoa Luna et al., 2014b) and for a complete analysis of VDC, interested readers can refer to (Zhu and De Schutter, 1999; Zhu et al., 2013). The frame attachment for the ETS-MARSE is shown in Figure 4.1. The corresponding Denavit-Hartenberg modified parameters are summarized in Table 4.1.

4.2.1 Nonlinear force observer

The development of the force observer was realized following the concept presented in (Hacksel and Salcudean, 1994; Nicosia and Tomei, 1990). We can define the dynamics of a robot manipulator as:

$$M(q)\ddot{q} + C(q,\dot{q})\dot{q} + D\dot{q} + G(q) = u + J^T(q)F \tag{4.1}$$

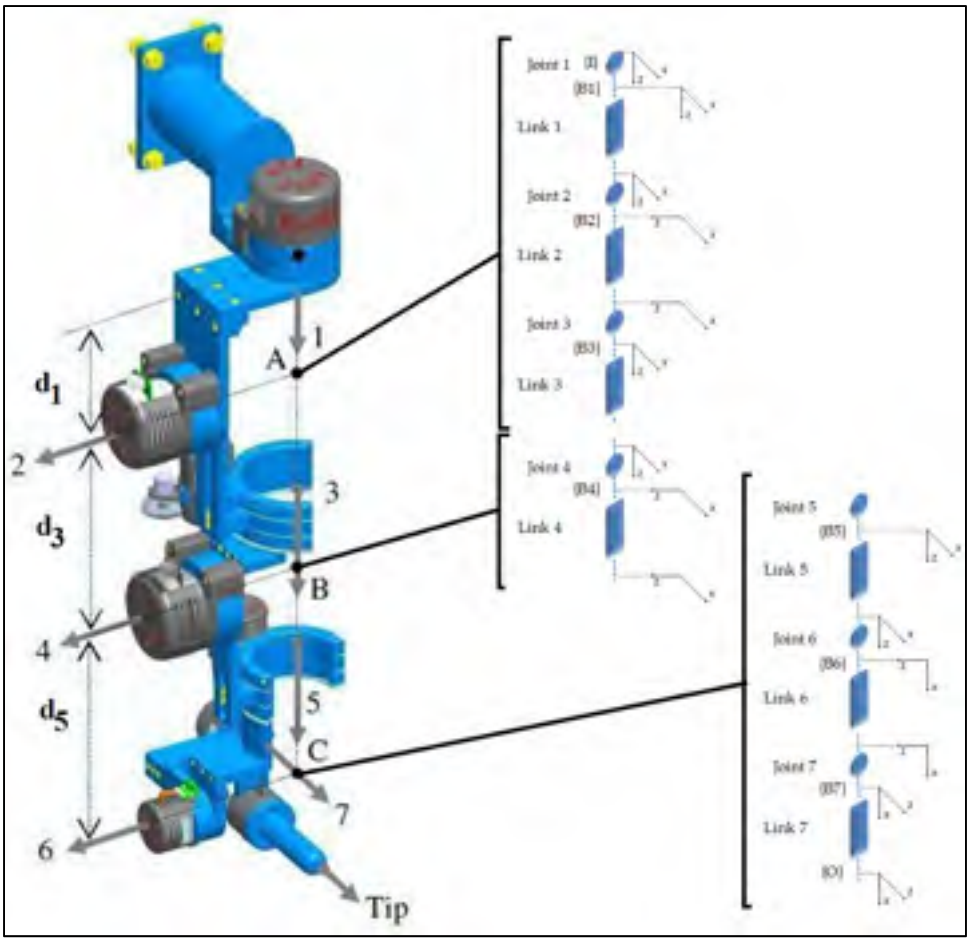

Figure 4.1 7DOF exoskeleton robot arm

Table 4.1 ETS-MARSE Denavit-Hartenberg modified parameters

i	α_{i-1}	a_{i-1}	d_i	θ_i
1	0°	0	d_1	θ_1
2	-90°	0	0	θ_2
3	90°	0	d_3	θ_3
4	-90°	0	0	θ_4
5	90°	0	d_5	θ_5
6	-90°	0	0	θ_6-90º
7	-90°	0	0	θ_7

where F is the force exerted at the end effector of the robot from the subject, $J^T(q)$ is the transpose of the Jacobian matrix of the system and u the vector of control torques. $M(q)$ is the inertia matrix of the system, $C(q,\dot{q})$ the Coriolis and centrifugal matrix in Cristoffel form, $G(q)$ the gravity vector and D represents the viscous friction coefficients. We define the state variables as:

$$x_1 = q \tag{4.2}$$
$$x_2 = \dot{q}$$

replacing (4.2) into (4.1) and solving for the joint acceleration we obtain:

$$\dot{x}_2 = M^{-1}(x_1)[-C(x_1,\dot{x}_1)\dot{x}_1 - D\dot{x}_1 - G(x_1) + u + J^T(x_1)F] \tag{4.3}$$

The state variables can be estimated as follows, considering the system without external perturbations (user exerted force):

$$\dot{\hat{x}}_1 = \hat{x}_2 + K_1\tilde{x}_1 \tag{4.4}$$
$$\dot{\hat{x}}_2 = M^{-1}(x_1)\left[-C\left(x_1,\dot{\hat{x}}_1\right)\dot{\hat{x}}_1 - D\dot{\hat{x}}_1 - G(x_1) + u + K_2\tilde{x}_1\right] \tag{4.5}$$

where K_1 and K_2 are two 7×7 symmetric positive definite gain matrices. The estimation error is defined as:

$$\tilde{x}_1 = x_1 - \hat{x}_1 \tag{4.6}$$

given from (4.2) that $\dot{x}_1 = x_2$, subtracting (4.4) from $\dot{x}_1$ yields:

$$\dot{\tilde{x}}_1 = \tilde{x}_2 - K_1\tilde{x}_1 \tag{4.7}$$

then subtracting (4.5) from (4.3) and given that in Lagrangian robotic systems, for two vectors $x \in \mathbb{R}^n$ and $y \in \mathbb{R}^n$, $C(q,x)y = C(q,y)x$ (Nicosia and Tomei, 1990) yields:

$$\dot{\tilde{x}}_2 = \dot{x}_2 - \dot{\hat{x}}_2$$
$$= M^{-1}(x_1)\left[-C(x_1,\dot{x}_1)\dot{x}_1 + C\left(x_1,\dot{\hat{x}}_1\right)\dot{\hat{x}}_1 - D\left(\dot{x}_1 - \dot{\hat{x}}_1\right) + J^T(x_1)F - K_2\tilde{x}_1\right] \quad (4.8)$$
$$= M^{-1}(x_1)\left[-C(x_1,\dot{x}_1)\dot{x}_1 + C\left(x_1,\dot{\hat{x}}_1\right)\dot{\hat{x}}_1 - D\dot{\tilde{x}}_1 + J^T(x_1)F - K_2\tilde{x}_1\right]$$
$$= M^{-1}(x_1)\left[-C(x_1,\dot{x}_1)\dot{\tilde{x}}_1 - C\left(x_1,\dot{\hat{x}}_1\right)\dot{\tilde{x}}_1 - D\dot{\tilde{x}}_1 + J^T(x_1)F - K_2\tilde{x}_1\right]$$

differentiating (4.7) with respect to time, gives:

$$\ddot{\tilde{x}}_1 = \dot{\tilde{x}}_2 - K_1\dot{\tilde{x}}_1$$
$$= M^{-1}(x_1)\left[-C(x_1,\dot{x}_1)\dot{\tilde{x}}_1 - C\left(x_1,\dot{\hat{x}}_1\right)\dot{\tilde{x}}_1 - D\dot{\tilde{x}}_1 + J^T(x_1)F - K_2\tilde{x}_1\right] \quad (4.9)$$
$$- K_1\dot{\tilde{x}}_1$$

therefore, we can obtain the force that the user applies to the robot:

$$J^T(x_1)F = M(x_1)\ddot{\tilde{x}}_1 + \left[C(x_1,\dot{x}_1) + C\left(x_1,\dot{\hat{x}}_1\right) + D + M(x_1)K_1\right]\dot{\tilde{x}}_1 + K_2\tilde{x}_1 \quad (4.10)$$

In order to simplify the computational complexity of (4.10), it has been demonstrated that a good estimation of the external force F can be obtained using only the last right-side term of it (Alcocer et al., 2003). For a slow time varying environmental force, we can obtain and estimated $\hat{F}$ as follows:

$$\hat{F} = J(x_1)^+ K_2\tilde{x}_1 \quad (4.11)$$

where $J(x_1)^+$ is the generalized Jacobian pseudo-inverse and $\hat{F}$ is the estimated force due to the human.

Remark: In our case, it is not necessary to determine the Cartesian external force, since the estimated joint torques are used directly as it will be explained in the admittance section.

Finally, the torque due to friction is often hard to model accurately. VDC provides a way to estimate the friction torque in each joint by its internal parameter estimation. To use a more precise real-time friction model, we use these parameters and the model proposed by the controller and the friction term $D\dot{\hat{x}}_1$ in (4.5) can be replaced as follows:

$$D(\dot{\hat{x}}_1) = {K_c}^T \text{sign}(\dot{\hat{x}}_1) + {K_v}^T \dot{\hat{x}}_1 + C_c \tag{4.12}$$

where K_c is the vector of estimated Coulomb friction coefficients, K_v is the vector of estimated viscous friction coefficients and C_c the vector of asymmetric Coulomb friction offsets.

4.2.2 Stability Analysis

Theorem 1: Suppose the control input u is such that the solutions for the robot dynamics (4.1) exist, and consider the observer (4.4) and (4.5) where the observer gains K_1 and K_2 are chosen such that are diagonal positive matrices and $K_2 = K_1^{-1} - \frac{1}{2}I$, where $K_1^{-1} > \frac{1}{2}I$, results in the convergence of the estimation error states $\dot{\tilde{x}}_1 \to 0$ and $\dot{\tilde{x}}_2 \to 0$ as $t \to \infty$.

Proof: To obtain the error dynamics, take the time differentiation of (4.4) as follows:

$$\ddot{\tilde{x}}_1 = \dot{\hat{x}}_2 + K_1 \dot{\tilde{x}}_1 \tag{4.13}$$

then substituting (4.5) into (4.13) we obtain:

$$\ddot{\tilde{x}}_1 = M^{-1}(x_1)\left[-C(x_1, \dot{\hat{x}}_1)\dot{\hat{x}}_1 - D\dot{\hat{x}}_1 - G(x_1) + u + K_2\tilde{x}_1\right] + K_1\dot{\tilde{x}}_1 \tag{4.14}$$

subtracting (4.14) from (4.3) we get:

$$M(x_1)\ddot{\tilde{x}}_1 + C(x_1, \dot{x}_1)\dot{x}_1 - C\left(x_1, \dot{\hat{x}}_1\right)\dot{\hat{x}}_1 = J^T(x_1)F - K_1 M(x_1)\dot{\tilde{x}}_1 - D\dot{\tilde{x}}_1 - K_2\tilde{x}_1 \tag{4.15}$$

and finally we obtain:

$$M(x_1)\ddot{\tilde{x}}_1 = J^T(x_1)F - K_1 M(x_1)\dot{\tilde{x}}_1 - C\left(x_1, \dot{\hat{x}}_1\right)\dot{\tilde{x}}_1 - C(x_1, \dot{x}_1)\dot{\tilde{x}}_1 - D\dot{\tilde{x}}_1 - K_2\tilde{x}_1 \tag{4.16}$$

Consider the following Lyapunov function candidate:

$$V = \frac{1}{2}\dot{\tilde{x}}_1{}^T M(x_1)\dot{\tilde{x}}_1 \tag{4.17}$$

the time derivative of (4.17) along the solutions of (4.16) is:

$$\dot{V} = \dot{\tilde{x}}_1{}^T M(x_1)\ddot{\tilde{x}}_1 + \frac{1}{2}\dot{\tilde{x}}_1{}^T \dot{M}(x_1)\dot{\tilde{x}}_1 \tag{4.18}$$

substituting (4.16) into (4.18) and grouping terms we have:

$$\dot{V} = -\dot{\tilde{x}}_1{}^T\left(-J^T(x_1)F + K_2\tilde{x}_1 + K_1 M(x_1)\dot{\tilde{x}}_1 + C\left(x_1, \dot{\hat{x}}_1\right)\dot{\tilde{x}}_1 + D\dot{\tilde{x}}_1\right) - \dot{\tilde{x}}_1{}^T C(x_1, \dot{x}_1)\dot{\tilde{x}}_1 + \frac{1}{2}\dot{\tilde{x}}_1{}^T \dot{M}(x_1)\dot{\tilde{x}}_1 \tag{4.19}$$

then, given that the matrix $\dot{M}(q) - 2C(q, \dot{q})$ is skew-symmetric:

$$\dot{V} = -\dot{\tilde{x}}_1{}^T\left(-J^T(x_1)F + K_2\tilde{x}_1 + K_1 M(x_1)\dot{\tilde{x}}_1 + C\left(x_1, \dot{\hat{x}}_1\right)\dot{\tilde{x}}_1 + D\dot{\tilde{x}}_1\right) \tag{4.20}$$

Taking from (4.11) that $J^T(x_1)\hat{F} = K_2\tilde{x}_1$, we obtain:

$$\dot{V} = -\dot{\tilde{x}}_1^{\,T}\left(K_1 M(x_1)\dot{\tilde{x}}_1 + C\left(x_1, \dot{\hat{x}}_1\right)\dot{\tilde{x}}_1 + D\dot{\tilde{x}}_1\right) \tag{4.21}$$

finally, it can be established that:

$$\dot{V} = -K^{-1}M(x_1)\left\|\dot{\tilde{x}}_1\right\|^2 \leq -\beta\left\|\dot{\tilde{x}}_1\right\|^2 \tag{4.22}$$

where β is a positive constant and $K = K_1^{-1} - \frac{1}{2}I > 0$. Since $M(x_1)$ is uniformly positive definite, the Lyapunov function in (4.17) is positive definite in $\dot{\tilde{x}}_1$. Since $\dot{V} \leq 0$, V is also bounded, and therefore $\dot{\tilde{x}}_1$ is bounded and therefore $\ddot{\tilde{x}}_1$ is also bounded. To apply Barbalat's lemma, let us check the uniform continuity of $\dot{V}$. Differentiating (4.22) yields:

$$\ddot{V} \leq -2\beta\dot{\tilde{x}}_1^T(\dot{\tilde{x}}_2 - K_1\dot{\tilde{x}}_1) \tag{4.23}$$

This shows that $\ddot{V}$ is bounded since $\dot{\tilde{x}}_1$ and $\dot{\tilde{x}}_2$ are bounded. Hence $\dot{V}$ is uniformly continuous. Using Barbalat's lemma, we have $\dot{\tilde{x}}_1 \to 0$. From (4.7) it can be concluded that $\dot{\tilde{x}}_2 \to 0$, from (4.8) it can be concluded that $\tilde{x}_1 \to 0$ as $t \to \infty$ and therefore by construction from (4.7) it can be inferred that $\tilde{x}_2 \to 0$ as $t \to \infty$.

4.2.3 Admittance control

In order to control the movement of the robot from the user's force, a compliance control based on admittance is used. An admittance function can be defined as a transfer function that has a force as an input signal and yields a motion as the output signal and can be expressed as follows:

$$q_a = q_p + K_3^{-1}\hat{\tau} \tag{4.24}$$

where q_a is the 7×1 vector of the new desired trajectory defined by the admittance, q_p is the 7×1 vector with the current position and the last right term of the equation, the chosen

admittance function. This is the form of a spring function in which K_3 is a 7×7 gain matrix that corresponds to the spring constant and $\hat{\tau}$ is the 7×1 vector of estimated torques exerted towards the robot joints by the subject as consequence of his intention of movement. To calculate this torque, we use the virtual work principle to substitute the left-hand side of (4.10); hence (4.11) becomes:

$$\hat{\tau} = K_2 \tilde{x}_1 \tag{4.25}$$

Because of this substitution, the Cartesian external forces don't need to be calculated and problems with the inverse of the Jacobian needed in (4.11) are eliminated. If the user stops exerting forces, $\hat{\tau} \to 0$ making the robot reduce its movement and gradually, when $q_a = q_p$ the robot remains in its last position. With this, the robot is allowed to follow the user's intention of movement while the trajectory tracking ensures the gravity compensation.

4.3 Experimental results

In this section a brief description of the system architecture is given; afterward the experimental setup is presented. The experiment consists of two scenarios. The first one is based on an active joint-space task in which the subjects were asked to perform an elbow flexion-extension and shoulder external-internal rotation. The second scenario is based on active Cartesian-space task; in this case, the subject was asked to follow a straight line presented in the virtual interface.

4.3.1 System architecture

The ETS-MARSE is shown in Figure 4.2. It is a manipulator like, open chain, 7DOF (all revolute) wearable robot. It was designed for its joints to correspond to the principal degrees of freedom of the human arm:

- 3DOF at shoulder level for horizontal flexion/extension, vertical flexion/extension and internal/external rotation,

- 1DOF for elbow flexion/extension,
- 1DOF for forearm pronation/supination, and
- 2DOF at the wrist level for radial/ulnar deviation and flexion/extension.

The exoskeleton structure has a handle mounted in the end-effector (tip) of the robot, where the users' hand must be positioned. Each DOF is driven by a brushless DC motor incorporated with a harmonic drive; each motor has a Hall Effect sensor used for position feedback of the joints. A backplane card collects analog and digital signals and connects through the proper interface cards to an NI PXI-7813R (Reconfigurable Input-Output card) placed on an NI PXI-1031 chassis. The card has an integrated FPGA in which is executed the low-level control: A PI controller for the current loop of the motors, position feedback via the Hall Effect sensors and the collection of the force sensor inputs. In the chassis is also mounted a PXI-8108 controller, which executes the high-level control: the robot operating system and the trajectory tracking controller. The force-position control is implemented with an update rate of 1ms.

A PC runs the virtual environment that is the human-machine interface in which the robot user visualizes the rehabilitation exercise. Security is a major concern. Hardware stoppers keep the range of motion in secure extent, software position and velocity limits stop the motor outputs if exceeded, and the system has a hardware emergency stop button, accessible anytime to the user.

For the following test, the perturbation observed was characterized using the force sensor of the robot. The main diagonals of the gain matrices, leaving the remaining elements in cero, were: $K_1 = [20\ 20\ 20\ 20\ 20\ 20\ 20]^T$ and $K_2 = [100\ 100\ 100\ 100\ 100\ 100\ 100]^T$ and $K_3 = [1\ 1\ 2\ 2\ 1\ 1\ 1]^T$.

Figure 4.2 Subject wearing ETS-MARSE robot arm and virtual interface

4.3.2 Joint space task

The tests in this scenario were conducted with three healthy male subjects in seated position, ages 27-34 years old, weight between 78 to 91 kg and height 179-182 cm. The subjects were requested to perform two joint movements; the first one consisted of the extension and flexion of the elbow joint (joint 4 on ETS-MARSE) followed by the external and internal rotation of the shoulder joint (joint 3 on ETS-MARSE). Two repetitions of the sequence were performed. The motion is illustrated in Figure 4.3; the left-side graphic shows the elbow movement and the right-side one the shoulder movement. The subjects were trained to perform an external-internal rotation of between 0 degrees and 50 degrees at joint 3, and an extension-flexion of between 90 degrees and 20 degrees at joint 4, staying close to 5 seconds in each part of the movement. Since this is an active rehabilitation exercise, the robot doesn't control the amplitude or the speed of the exercise. Figure 4.4 displays one subject's results. The upper-row plots show the force estimated by the observer after filtering. The force is filtered to avoid perceptible oscillations for the subject; this can also be achieved by adding a damping term to the admittance function. The left plot corresponds to joint 3 (shoulder external-internal rotation) and the right one to joint 4 (elbow extension-flexion). The movement of the joints is illustrated on the bottom-row plots that represent the position of the corresponding joints in time.

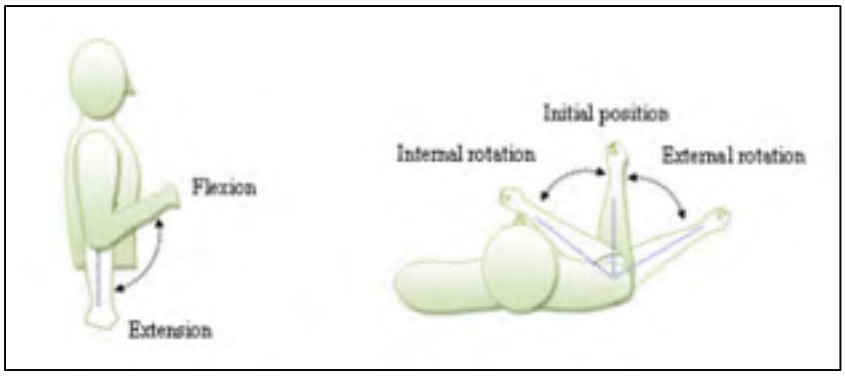

Figure 4.3 Joint space exercises

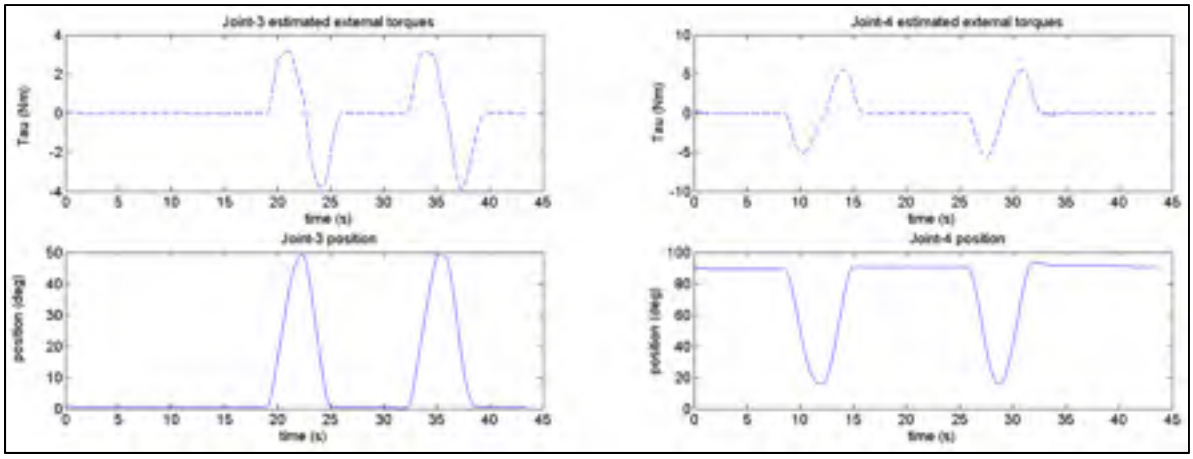

Figure 4.4 Joint space exercise estimated torques and joint positions

It is important to mention that the precision of the estimation of the torque magnitude is not a critical point in the proposed method. That is also why the simplification shown in (4.11) is valid for this approach. Estimating the torque acting on the joints by the effect of the human interaction allows us to detect the subject's movement intentions and command the robot to follow that movement.

It is then possible to change the gain of the estimated torque in order to make the system more or less sensitive to this perturbation. Indeed, variation in the admittance coefficients (spring constant) will cause variation in the resistance needed to move the exoskeleton (virtual spring effect). Using this concept, the rehabilitation exercise can be executed with

different compliances. This will translate into more or less effort for the user to move the robot.

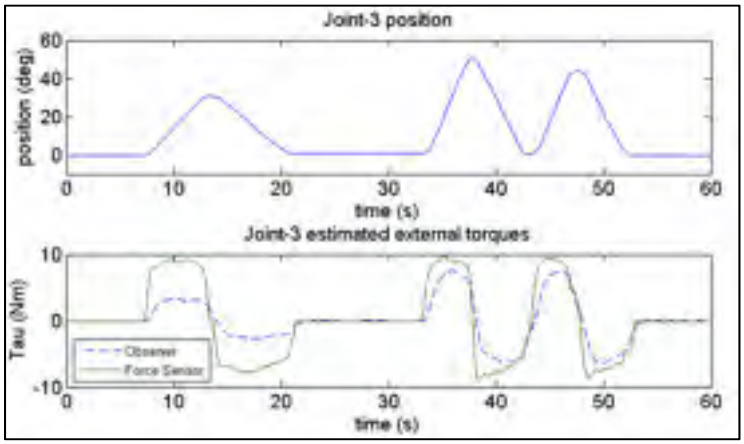

Figure 4.5 Joint 3 position and estimated and measured force for joint space test

To illustrate this behavior, the second exercise of this scenario is focused on one joint (joint 3). The subjects were requested to perform an external-internal rotation of the shoulder (as shown on the right side of Figure 4.3); then, during the same test, the value of the joint estimation gain was reduced in real-time and the user repeated the movement. In Figure 4.5, the real-time position of joint 3 is shown in the top plot, and in the bottom one, the external torque for one of the users. For reference, the reading of a 6DOF force sensor mounted on the base of the ETS-MARSE's handle (see Figure 4.2) is shown. The force sensor reading is presented in a solid line and the estimation of the observer is shown in the dotted line. It is clear that changing the gain in the observer (vertical line at approximately 27 seconds) doesn't impede on estimating the subject's movement intention. However, it is evident how the robot's movement amplitude changed between the first movement and the two subsequent ones, once the gain was changed. The force sensor reading shows how, although the external torque exerted by the user in all the cases is approximately the same, the estimation changes. Thus, with the same force, the subject produced a greater range movement; or it can also be said that with the initial gain, more effort was needed to achieve the same movement amplitude as for the last two movements. With these results, the

objective of using the force observer in combination with the admittance function to perform isokinetic exercises is demonstrated.

4.3.3 Cartesian space task

For the Cartesian space scenario, the subject was requested to follow a straight line in the virtual interface. The objective of this test was to evaluate the performance of the robot under a coordinated multi-joint movement representing a common active rehabilitation task. In this case, joints 2, 3 and 4 of the robot are allowed to move simultaneously. This test was performed with a healthy male subject, 33 years old, 98 kilograms weight, and 182 cm height in seated position. The coordinates of the straight line are expressed in the inertial frame of reference (refer to Figure 4.1). The result of this test is shown in Figure 4.6. It can be seen that the user can successfully perform the exercise. As usual in robot rehabilitation, the tracking of the test can be recorded and serve as a reference for the subject's improvement or as mentioned before, the effort required from the user to move may be improved in order to make the rehabilitation exercise more demanding.

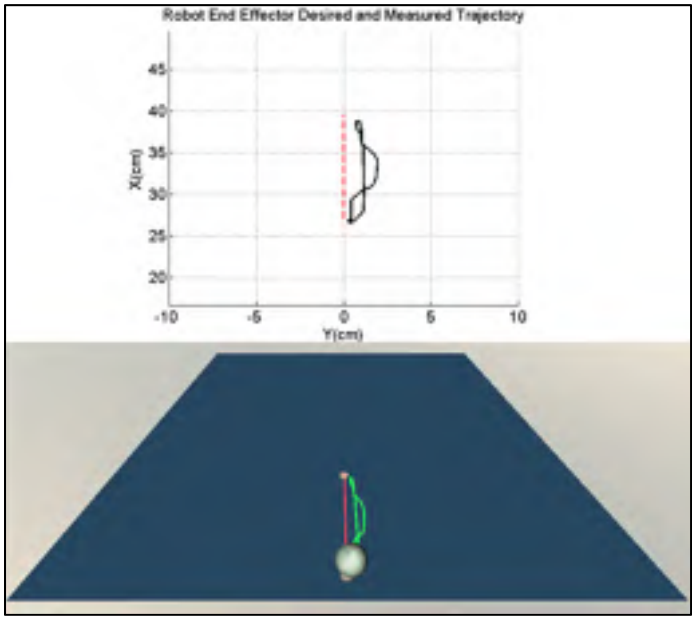

Figure 4.6 Cartesian space trajectory test results

Varying the trajectory to be followed and the joints involved in the movement significantly affects the force estimation. The nonlinear observer must be calibrated for different positions; thus, it will be necessary, in future work, to implement the dynamic adjustment of its parameters according to the arm configuration.

Finally, in order to experimentally validate the behavior of the nonlinear observer, Figure 4.7 shows the behavior of the state variable x_1 compared against the measured position. The test followed the movements described in Figure 4.3; it consisted on an elbow extension/flexion and a shoulder external/internal rotation. The right column shows information of joint 3 (shoulder external/internal rotation) and the left one of joint 4 (elbow extension/flexion). It can be seen in the upper plots that the measured position and estimated position overlaps. In order to better compare the real x_1 and estimated state $\hat{x}_1$ the estimation error $\tilde{x}_1$ is shown in the lower plots.

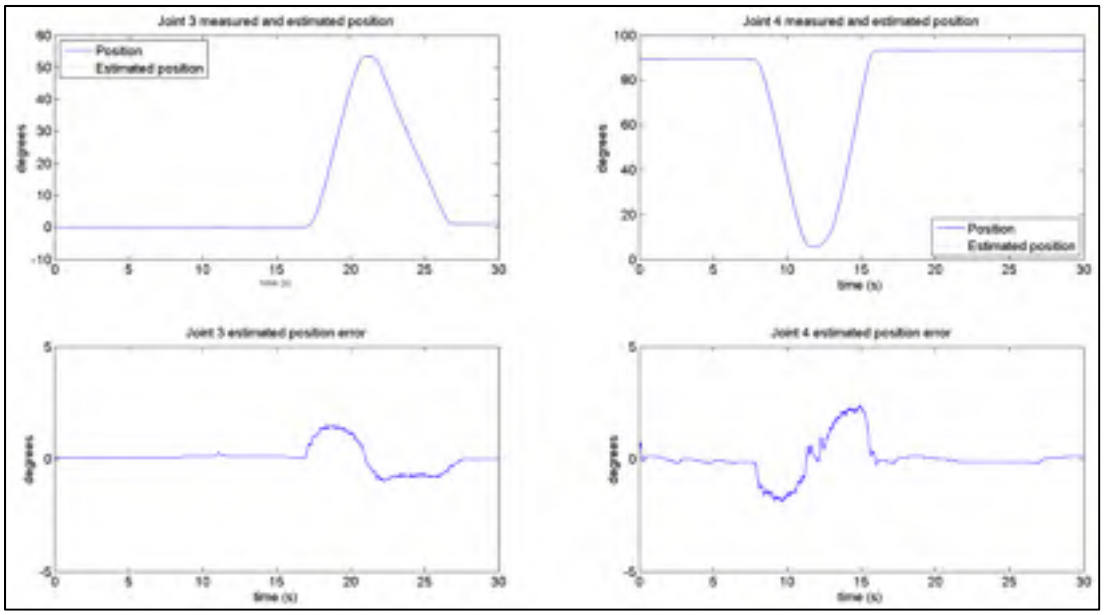

Figure 4.7 Measured and estimated position and position error

4.4 Conclusions

This paper successfully shows that a force observer can be used as an alternative to force sensors, in order to perform some active rehabilitation tasks. This advantage allows applying force directly to the robot structure, theoretically without restrictions, since patients with high spasticity can easily damage a force sensor.

Some considerations need to be taken into account. A force should be detected continuously; otherwise, the estimation will go to zero intermittently causing the robot to stop-and-go erratically; consequently, the robot should constantly present minimal (adjustable) opposition to the movement. Therefore, having a completely compliant system is not adequate for this approach unless this behavior is resolved. Hence, the importance of using the proposed method to perform resistive rehabilitation exercises (isokinetic).

A more accurate model of the robot will result in better estimation of interactive forces; nevertheless, a complete model of a robot with high degree-of-freedom is computationally heavy. This approach consumes much more resources than processing a force sensor input.

There is also a critical issue that must be addressed in order to improve this approach. As shown, when the exercises are aimed at a specific joint or sequence, the estimation of the force can be used directly. Nevertheless, as the movements become more complex, a greater complexity arises in determining the ergonomic position of the redundant robot. A solution for these cases is necessary in order to employ the robot for a wide variety of movements.

DISCUSSION OF THE RESULTS

The work presented in this thesis describes the design and implementation of a control strategy for the ETS-MARSE robot, as well as the design of active-assistive rehabilitation and active rehabilitation strategies. Moreover, passive rehabilitation is possible with the presented control law. In all rehabilitation cases (passive, active-assisted and active), some Cartesian trajectories are possible to execute according to the rehabilitation task pursued.

To achieve the described results, the methodology presented in Chapter 1 was followed. In the matter of the control technique, using VDC allowed to have robustness against changes in the robot's user characteristics. Thus, the rehabilitation provided can be more systematic and the variations depend almost completely on the patients' improvement. Passive and active rehabilitation exercises were implemented both in joint and in Cartesian space. A performance evaluation using the VDC approach against CTC and PID was presented, supporting the better performance of VDC. Also the simplification of the dynamical model of the robot through the virtual decomposition presented an advantage.

About the sensing interface, addressed in Chapter 3 and Chapter 4 of this thesis, different rehabilitation schemes were proposed for active-assistive and active rehabilitation task with the guidance of the ETS-MARSE. The rehabilitation schemes were basically presented in Chapter 3, in which was demonstrated that our robot is able to vary the assistance provided to future rehabilitation patients. The amount of variation of the trajectory can be quantified as an excellent measurement of progression of the subject. Also, the robot can perform a free movement according to the user intention of motion. The ETS-MARSE will help him to accomplish the task only when is required by the exercise specifications (virtual wall limits), letting the subject control the free motion in any other moment. At the same time, the robot will be providing help in gravity compensation; for the robot itself by default and for the patients' arm if necessary. Finally, in Chapter 4, it was shown that a force observer can be used instead of a force sensor for certain tasks. To recognize the subject's intended movement, it is not necessary a precise measurement of the force, a close estimate is

sufficient. This method allows reducing the dependency of a force sensor that can easily be damaged by the patient's condition.

CONCLUSION

This thesis work was focused on obtaining a consistent control technique for the ETS-MARSE (Motion Assistive Robotic-exoskeleton for Superior Extremity) and to obtain a reliable sensing interface that could capture the user intention of movement to provide different assisted and active-assisted rehabilitation techniques.

With the results presented in this work, different rehabilitation schemes and characteristics are offered. It is safe to say that the robot has a reliable control strategy as well as rehabilitation-task capabilities. Although investigation in the field of control and increasing the tasks that the exoskeleton can perform is always interesting and an area of many opportunities, the current developments need to be consolidated for the next phase of the robot. The ETS-MARSE is ready to move from a development environment to a test environment, with the pertinent considerations listed next in the recommendations section.

RECOMMENDATIONS

In order to continue the development of this project to fulfill the final aim of having a robotic prototype to be used in rehabilitation and possibly daily assistance, some considerations need to be made:

The advances so far (different modes of passive rehabilitation, active-assisted rehabilitation, active rehabilitation, the human-machine interface, between others) had been developed and tested with healthy human beings. An important next step is to start the validation of the techniques in trials with rehabilitation patients. To precede with this step a profound safety review is necessary.

Another important step in order to achieve full usability of the rehabilitation strategies is the development of a complete solution for the robot inverse kinematics problem. That is, the exoskeleton can reach some points of its workspace in more than one configuration of its links (redundancy). Solving this redundancy problem, will give complete ranges in admittance and Cartesian space trajectories.

As the next step for active rehabilitation, the use of electromyographic signals is a promising objective. EMG signals can be combined with force sensor readings or force observer estimations in order to provide a more detailed interpretation of the subject's movement intention. Also can be used alone for subjects in whom the force sensor may be not enough to determine the intended movement.

Continue to develop the haptic and teleoperation ideas for the ETS-MARSE is an important area of opportunity. A consolidation of the different modes of operation in the development environment (LabView) is necessary. The update of the virtual environment of the human-machine interface is also a mandatory next step to the process of maturation of the project.

APPENDIX A

ELEMENTS IN THE REGRESSOR MATRIX Y_A AND PARAMETER VECTOR θ_A

Non-zero elements in the regressor matrix $Y_A \in \mathbb{R}^{6\times 13}$ for the link linear parametrization in (2.14):

$$y_A(1,1) = \frac{d}{dt}({}^A v_r)(1) + {}^A v(5)\,{}^A v_r(3) - {}^A v(6)\,{}^A v_r(2) + {}^A g(1) \tag{A A-1}$$

$$y_A(1,2) = -{}^A v(5)\,{}^A v_r(5) - {}^A v(6)\,{}^A v_r(6) \tag{A A-2}$$

$$y_A(1,3) = -\frac{d}{dt}({}^A v_r)(6) + {}^A v(5)\,{}^A v_r(4) \tag{A A-3}$$

$$y_A(1,4) = \frac{d}{dt}({}^A v_r)(5) + {}^A v(6)\,{}^A v_r(4) \tag{A A-4}$$

$$y_A(2,1) = \frac{d}{dt}({}^A v_r)(2) + {}^A v(6)\,{}^A v_r(1) - {}^A v(4)\,{}^A v_r(3) + {}^A g(2) \tag{A A-5}$$

$$y_A(2,2) = \frac{d}{dt}({}^A v_r)(6) + {}^A v(4)\,{}^A v_r(5) \tag{A A-6}$$

$$y_A(2,3) = -{}^A v(4)\,{}^A v_r(4) + {}^A v(6)\,{}^A v_r(5) \tag{A A-7}$$

$$y_A(2,4) = -\frac{d}{dt}({}^A v_r)(4) + {}^A v(6)\,{}^A v_r(5) \tag{A A-8}$$

$$y_A(3,1) = \frac{d}{dt}({}^A v_r)(3) + {}^A v(4)\,{}^A v_r(2) - {}^A v(5)\,{}^A v_r(1) + {}^A g(3) \tag{A A-9}$$

$$y_A(3,2) = -\frac{d}{dt}({}^A v_r)(5) + {}^A v(4)\,{}^A v_r(6) \tag{A A-10}$$

$$y_A(3,3) = \frac{d}{dt}({}^A v_r)(4) + {}^A v(5)\,{}^A v_r(6) \tag{A A-11}$$

$$y_A(3,4) = -{}^A v(4)\,{}^A v_r(4) - {}^A v(5)\,{}^A v_r(5) \tag{A A-12}$$

$$y_A(4,3) = y_A(3,1) \tag{A A-13}$$

$$y_A(4,4) = -y_A(2,1) \tag{A A-14}$$

$$y_A(4,6) = y_A(3,3) \tag{A A-15}$$

$$y_A(4,7) = -y_A(2,4) \tag{A A-16}$$

$$y_A(4,8) = y_A(3,2) \tag{A A-17}$$

$$y_A(4,9) = -y_A(2,2) \tag{A A-18}$$

$$y_A(4,10) = {}^{A}v(6)\,{}^{A}v_r(6) - {}^{A}v(5)\,{}^{A}v_r(5) \quad \text{(A A-19)}$$

$$y_A(4,11) = \frac{d}{dt}({}^{A}v_r)(4) + {}^{A}v(5)\,{}^{A}v_r(6) - {}^{A}v(6)\,{}^{A}v_r(5) \quad \text{(A A-20)}$$

$$y_A(4,12) = -{}^{A}v(6)\,{}^{A}v_r(5) \quad \text{(A A-21)}$$

$$y_A(4,13) = {}^{A}v(5)\,{}^{A}v_r(6) \quad \text{(A A-22)}$$

$$y_A(5,2) = -y_A(3,1) \quad \text{(A A-23)}$$

$$y_A(5,4) = y_A(1,1) \quad \text{(A A-24)}$$

$$y_A(5,5) = -y_A(3,2) \quad \text{(A A-25)}$$

$$y_A(5,7) = y_A(1,4) \quad \text{(A A-26)}$$

$$y_A(5,8) = -y_A(3,3) \quad \text{(A A-27)}$$

$$y_A(5,9) = {}^{A}v(4)\,{}^{A}v_r(4) - {}^{A}v(6)\,{}^{A}v_r(6) \quad \text{(A A-28)}$$

$$y_A(5,10) = y_A(1,3) \quad \text{(A A-29)}$$

$$y_A(5,11) = {}^{A}v(6)\,{}^{A}v_r(4) \quad \text{(A A-30)}$$

$$y_A(5,12) = \frac{d}{dt}({}^{A}v_r)(5) + {}^{A}v(6)\,{}^{A}v_r(4) - {}^{A}v(4)\,{}^{A}v_r(6) \quad \text{(A A-31)}$$

$$y_A(5,13) = -{}^{A}v(4)\,{}^{A}v_r(6) \quad \text{(A A-32)}$$

$$y_A(6,2) = y_A(2,1) \quad \text{(A A-33)}$$

$$y_A(6,3) = -y_A(1,1) \quad \text{(A A-34)}$$

$$y_A(6,5) = y_A(2,2) \quad \text{(A A-35)}$$

$$y_A(6,6) = -y_A(1,3) \quad \text{(A A-36)}$$

$$y_A(6,8) = {}^{A}v(5)\,{}^{A}v_r(5) - {}^{A}v(4)\,{}^{A}v_r(4) \quad \text{(A A-37)}$$

$$y_A(6,9) = y_A(2,4) \quad \text{(A A-38)}$$

$$y_A(6,10) = -y_A(1,4) \quad \text{(A A-39)}$$

$$y_A(6,11) = -{}^{A}v(5)\,{}^{A}v_r(4) \quad \text{(A A-40)}$$

$$y_A(6,12) = {}^{A}v(4)\,{}^{A}v_r(5) \quad \text{(A A-41)}$$

$$y_A(6,13) = \frac{d}{dt}({}^{A}v_r)(6) + {}^{A}v(4)\,{}^{A}v_r(5) - {}^{A}v(5)\,{}^{A}v_r(4) \quad \text{(A A-42)}$$

The 13 elements of parameter vectors $\theta_A \epsilon \mathbb{R}^{13}$ are listed as:

$$\theta_{A1} = m_A \quad \text{(A A-43)}$$

$$\theta_{A2} = m_A\,{}^{A}r_{mx} \quad \text{(A A-44)}$$

$$\theta_{A3} = m_A {}^A r_{my} \quad \text{(A A-45)}$$

$$\theta_{A4} = m_A {}^A r_{mz} \quad \text{(A A-46)}$$

$$\theta_{A5} = m_A {}^A r_{mx}^2 \quad \text{(A A-47)}$$

$$\theta_{A6} = m_A {}^A r_{my}^2 \quad \text{(A A-48)}$$

$$\theta_{A7} = m_A {}^A r_{mz}^2 \quad \text{(A A-49)}$$

$$\theta_{A8} = m_A {}^A r_{mx} {}^A r_{my} - I_{Axy} \quad \text{(A A-50)}$$

$$\theta_{A9} = m_A {}^A r_{mx} {}^A r_{mz} - I_{Axz} \quad \text{(A A-51)}$$

$$\theta_{A10} = m_A {}^A r_{my} {}^A r_{mz} - I_{Ayz} \quad \text{(A A-52)}$$

$$\theta_{A11} = I_{Axx} \quad \text{(A A-53)}$$

$$\theta_{A12} = I_{Ayy} \quad \text{(A A-54)}$$

$$\theta_{A13} = I_{Azz} \quad \text{(A A-55)}$$

where m_A is the mass; ${}^A r_m = \left[{}^A r_{mx}, {}^A r_{my}, {}^A r_{mz}\right]^T \in \mathbb{R}^3$ denotes a vector pointing from the origin of frame A towards the mass centre, expressed in frame A; and $I_{Axx}, I_{Ayy}, I_{Azz}, I_{Axy}, I_{Axz}, I_{Ayz}$ are the elements of I_A.

APPENDIX B

MOTORS AND HARMONIC DRIVES SPECIFICATIONS

Table-A B-1 ETS-MARSE detailed specification for DC motors and harmonic drives

Actuators, Maxon brushless DC motors		
Specification	EC-90, flat 90 W (joints 1, 2, 4)	EC-45, flat 30 W (joints 3, 5–7)
Nominal voltage (V)	24	12
Nominal speed (rpm)	2650	2860
Torque constant (mNm/A)	70.5	25.5
Weight (g)	648	88
Harmonic drives		
Specification	CSF-2UH17–120 F (joints 1, 2)	CSF-2XH14–100 F (joint 4)	CSF-2XH11–100 F (joints 3, 5–7)
Torque at 2000 rpm (Nm)	24	7.8	5
Momentary peak torque (Nm)	86	54	25
Repeated peak torque (Nm)	54	28	11
Gear ratio	120	100	100

ANNEX I

ADITIONAL AND FUTURE WORK: ELECTROMYOGRAPHY, TELEOPERATION AND HAPTIC CAPABILITIES

The present annex describes additional work realized with the ETS-MARSE that led to the publication of other articles with the research group. The first section describes the first advances in EMG signal processing for commanding the mentioned exoskeleton. The content is presented as a straightforward report, with only a briefly overview of the problem and the general specifications of the technique used. For specific information about the application proposed, the reader should refer to the papers cited in the text. The second section briefly describes the work in the area of teleoperation of the ETS-MARSE.

A I - 1. Electromyography

We can define electromyography as a technique for evaluating and recording the electrical activity produced by skeletal muscles (Robertson, 2004). In general, the muscles are the actuators responsible of human motion; at a very basic approach, in normal conditions, the muscle contractions are activated by the cortex and transmitted by the nervous systems to reach the muscular tissue. The use of EMG signals to control exoskeleton robots have been in constant development in the present century (Khokhar, Xiao and Menon, 2010; Komada et al., 2009; Lucas, DiCicco and Matsuoka, 2004; Rosen et al., 2001). There are two kinds of EMG signals that can be collected: surface signals or intramuscular signals; being the second one an invasive method. In our project we work with surface EMG signals. There are three basic steps to use EMG signals in any task, illustrated in Figure A-I.1:

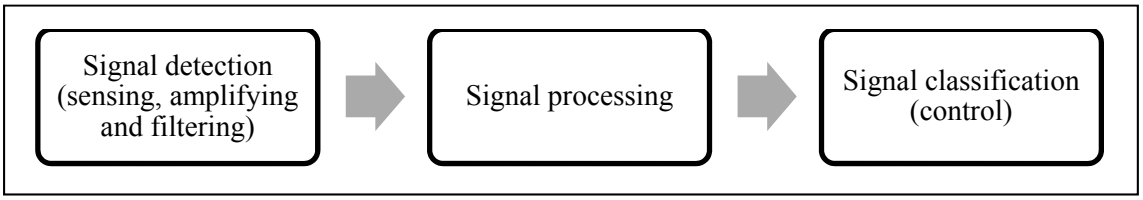

Figure-A I-1 Basic steps of EMG signal processing

The first step is to detect or sense the EMG signals from the muscles, where the activity is measured, amplified and filtered. The raw EMG signals come with lot of noise and do not have ready-to-use information. Hence, as a second step is necessary to perform processing of the signal to extract more meaningful information.

The second step is the feature detection or extraction of the EMG signals by means of which, certain information closely related with the muscular activity can be obtained. The signal can be analyzed in time domain, where the signal is usually first rectified and then analyzed with some techniques as linear envelope, root mean square (RMS), Willison amplitude (Smith et al., 2008), among others; or in frequency domain, with methods like spectral analysis of random signals, mean frequency and median frequency. Recently there are some interesting works that are achieving good results like using wavelet transform (Jiang et al., 2005) that also can be used in the detection phase (Phinyomark, Limsakul and Phukpattaranont, 2010) and particle swarm optimization (Khushaba, Al-Ani and Al-Jumaily, 2007).

Finally, the classification of the signals needs to be done in order to generate a desired control action. EMG signals are highly nonlinear and vary from one subject to another, even for the same movement. The signals also depend on the subject's physiological condition (stress, exhaustion, attention, etc.), also can fluctuate due to factors such as sweating, small changes in the positioning of the electrodes, arm position, and others.This step can go from basic methods like simple threshold or double threshold, to complex pattern recognition algorithms.

In our project, in order to perform the signal detection (first step), the Bagnoli-16 Main Amplifier Unit along with its input modules and Single Differential Surface EMG Sensors, from DELSYS® were used. The signals are collected through the backplane card described in subsections 2.4 or subsection 3.2, and sent to the NI PXI-8081 through the NI PXI-7813R input/output card, both also described in the mentioned subsections. The configuration of the voltage range of the raw EMG signals is ±5V.

For the second step, the signal processing, for this first stage of development were considered different basic filtering techniques as RMS, mean of the absolute value, moving average, and Savitzky-Golay (Savitzky and Golay, 1964). The RMS filtering (a measure of power of the signals) shows for our case the best performance, having a very small delay in the signal processing. The RMS filtering is defined as follows:

$$RMS_{EMG} = \sqrt{\frac{1}{N}\sum_{i=1}^{N} v_i^2} \qquad \text{(A I-1)}$$

where v_i is the voltage of the ith sample of the EMG signal and N is the number of samples. In our experiment, the number of samples was set to 50 with a sampling time of 0.5ms. An example of the RMS filtering is shown in Figure A-I.2, the left plot shows the raw EMG signal and the right one, the filtered signal.

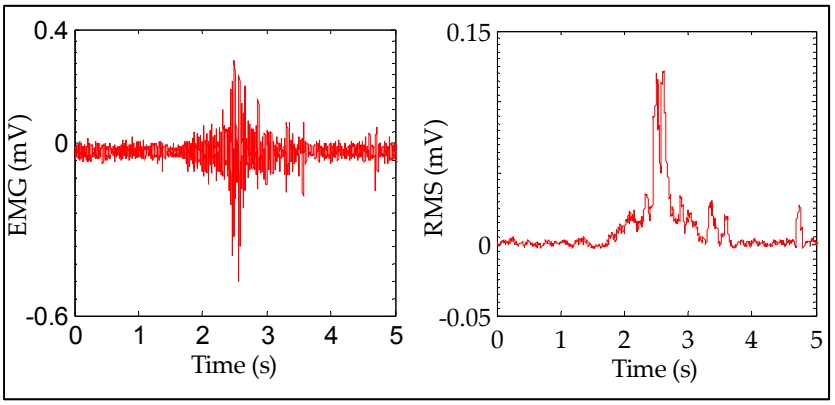

Figure-A I-2 Example of raw EMG signals and RMS value

For the final step of executing a control action with the filtered EMG signal, an approach is proposed in which agonist and antagonist muscle groups are used (as biceps for elbow flexion and triceps for elbow extension). The EMG signals processed from these groups of muscles are used as virtual force/torque applied to the corresponding joint they drive, through

a proportional constant. The results presented in the paper (Rahman et al., 2015a) shows the results of the presented approach.

Besides the mentioned paper, the EMG processing is used along with the force based control (FBC) described in Chapter 3 to analyze the effectiveness of the force control approach presented (Rahman et al., 2014).

As another use of the EMG signal processing, a neuro-fuzzy controller is being developed. A neuro-fuzzy controller can be trained to adapt to different users and different motion situations. Using the flexible and adaptable nature of this controller, it is expected to develop an effective knowledge base that can overcome aforementioned problems of an EMG based control (EBC). So far, an elementary fuzzy controller for the elbow has been tested with the first satisfactory results. In the developing process, the ETS-MARSE can be used in any of the operation modes described in this thesis (passive, active-assistive and active) to generate a motion database and use an Adaptive Neuro-Fuzzy Inference Systems (ANFIS) to generate the equivalent fuzzy inference system. The work so far in this area is in its initial state and a lot of work is necessary for the first functional rehabilitation schemes with EBC or a FBC/EBC hybrid.

A I - 2. Teleoperation and haptic capabilities

Teleoperation is an extensive area in robotics. It spans from simple remote controlled devices, to exploration robots of other planets. In the case of medical robots and devices, teleoperation has given the opportunity to perform successful remote surgeries in which haptic capabilities of the robot have played also a vital role. In the case of tele-diagnostics of physiological conditions, some devices are able to use image processing to read and diagnose, with the guide of specialists, some conditions that restrain human natural motion. Teleoperation is an option that can present an opportunity to overcome the same problem of insufficient number of qualified therapist that can perform rehabilitation processes in site.

For our device, we are proposing teleoperation capabilities that will allow the generation of predefined rehabilitation exercise in a remote way, as well as real time maneuvering of the subject that wears the exoskeleton with haptic feedback of the patient condition and evolution. To give the ETS-MARSE these capabilities a master-slave device was used first. The second step in developing of teleoperation capabilities uses the PHANTOM Omni® haptic device from Sensable® Technologies, a 6DOF positional sensing device compact and portable, with two integrated switches (buttons) that add more customization capabilities. So far, it has been developed an interface in which the user is able to select different points in the Phantom workspace and they are sent to the ETS-MARSE via UDP communication for it to perform, mapped to its own workspace, the same trajectory defined by the haptic device. These trajectories are consequently defined in the Cartesian space and can include any number of via points. Real time trajectory tracking and haptic capabilities are to be incorporated to this approach. A virtual environment for full feedback has started to be developed.

ANNEX II

VIRTUAL DECOMPOSITION CONTROL

This annex presents a more general description of VDC control. The information presented in the papers part of this thesis is specific for the application in our robot. However the technique can be extended easily. Some generalities are briefly described next according to (Zhu, 2010). This annex covers only the application for manipulator-like robots; however VDC can be applied for space robots (no gravity), humanoid robots, force-reflected bilateral teleoperation, and modular robot manipulators. The VDC approach can also be extended to distributed parameter systems and to electrical circuits.

A II - 1 Subsystem decomposition and kinematics

First, the reference frames of the robot are established. Decomposition is done by placing virtual cutting points that separate each joint and link of the system into a subsystem. The Denavit-Hartenberg parameters or the modified Denavit-Hartenberg parameters are obtained in order to obtain the homogeneous transformation matrices of the system. Using these matrices and defining any pair of frames $\{A\}$ and $\{B\}$, the force/moment transformation matrices are calculated as follows:

$$ {}^{A}U_{B} = \begin{bmatrix} {}^{A}R_{B} & 0_{3\times3} \\ ({}^{A}r_{AB}\times){}^{A}R_{B} & {}^{A}R_{B} \end{bmatrix} \in \mathbb{R}^{6\times6} \tag{A II-1} $$

where ${}^{A}R_{B}$ represents the rotation matrix from one frame to the next one and ${}^{A}r_{AB}$ the distance between them, and:

$$ ({}^{A}r_{AB}\times) = \begin{bmatrix} 0 & -{}^{A}r_{AB}(3) & {}^{A}r_{AB}(2) \\ {}^{A}r_{AB}(3) & 0 & -{}^{A}r_{AB}(1) \\ -{}^{A}r_{AB}(2) & {}^{A}r_{AB}(1) & 0 \end{bmatrix} \tag{A II-2} $$

where ${}^{A}r_{AB}(i)$ represents the i_{th} term of the ${}^{A}r_{AB}$ vector. Each force/moment transformation matrix ${}^{B_i}U_{B_{i+1}}$ for $i = 1, \dots, n-1$. The next step is to calculate ${}^{B_i}V$, the linear/angular velocity vectors of the $\{B_i\}$ frames for $i = 1, \dots, n$ as follows:

$$ {}^{B_i}V = \begin{bmatrix} {}^{B_i}v \\ {}^{B_i}\omega \end{bmatrix} \in \mathbb{R}^6 \tag{A II-3} $$

where ${}^{B_i}v$ is the linear velocity vector and ${}^{B_i}\omega$ is the angular velocity vector of the corresponding frame. Defining each joint position (angle) as q_1 to q_n and using the previous linear/angular velocity vectors in (A II-3), the augmented velocity vector is formed with the following form:

$$ \mathcal{V}_n = [\dot{q}_1 \quad \cdots \quad \dot{q}_n \quad {}^{B_1}V^T \quad \dots \quad {}^{B_n}V^T]^T \tag{A II-4} $$

Factorizing the joint velocity vector in (A II-4) it is obtained:

$$ \mathcal{V}_n = J_n \, \dot{\boldsymbol{q}} \tag{A II-5} $$

where $\dot{\boldsymbol{q}} = [\dot{q}_1 \quad \cdots \quad \dot{q}_n]^T$ is the joint velocity vector and J_n is the $49 \times n$ VDC Jacobian matrix of the system:

$$ J_n = \begin{bmatrix} & & I_n & \\ z & 0_6 & \cdots & 0_6 \\ {}^{B_1}U_{B_2}^T z & z & \ddots & \vdots \\ \vdots & \ddots & \ddots & 0_6 \\ {}^{B_1}U_{B_n}^T z & \dots & {}^{B_{n-1}}U_{B_n}^T z & z \end{bmatrix} \tag{A II-6} $$

where $z = [0 \quad 0 \quad 0 \quad 0 \quad 0 \quad 1]^T$, I_n represents the $n \times n$ identity matrix and 0_6 is a six element zero vector. Finally, for the kinematics it is necessary to calculate the required velocities, which are a function of the control requirements.

$$\dot{\boldsymbol{q}}_{\boldsymbol{r}} = \dot{\boldsymbol{q}}_{\boldsymbol{d}} + \lambda(\boldsymbol{q}_{\boldsymbol{d}} - \boldsymbol{q}) \tag{A II-7}$$

where $\dot{\boldsymbol{q}}_r = [\dot{q}_{1r} \quad \cdots \quad \dot{q}_{nr}]^T$ is the required velocity vector, $\dot{\boldsymbol{q}}_d = [\dot{q}_{1d} \quad \cdots \quad \dot{q}_{nd}]^T$ is the desired velocity vector, $\lambda > 0$ is a control parameter, $\boldsymbol{q}_d = [q_{1d} \quad \cdots \quad q_{nd}]^T$ is the desired position vector and $\boldsymbol{q} = [q_1 \quad \cdots \quad q_n]^T$ the position vector. From (A II-6) and (A II-7) the augmented required velocity vector is obtained as follows:

$$\mathcal{V}_{nr} = J_n \, \dot{\boldsymbol{q}}_{\boldsymbol{r}} \tag{A II-8}$$

From (A II-4) can be established:

$$\mathcal{V}_{nr} = [\dot{q}_{1r} \quad \cdots \quad \dot{q}_{nr} \quad {}^{B_1}V_r^T \quad \cdots \quad {}^{B_n}V_r^T]^T \tag{A II-9}$$

A II-2 Dynamics

To obtain the inverse dynamics that takes part in the control of the robot, it is necessary to calculate the required force/moment vectors for the links, ${}^{B_i}F_r$, and then the net torques required by the joints, τ_{ir}^*. The first step for the link dynamics is to obtain the required net force/moment vectors with the following equation:

$${}^{B_i}F_r^* = Y_i \, \hat{\theta}_i + K_{si}({}^{B_i}V_r - {}^{B_i}V) \tag{A II-10}$$

For $i = 1, \ldots, n$ where ${}^{B_i}F_r^*$ are the required net force/moment vectors, K_{si} is a symmetric positive-definite gain matrix, ${}^{B_i}V$ and ${}^{B_i}V_r$ are the velocities defined in (4) and (9). $Y_i \in \mathbb{R}^{6\times 13}$ is a regressor matrix composed by elements of $d/dt({}^{B_i}V_r) \in \mathbb{R}^6$, the velocity vectors ${}^{B_i}V \in \mathbb{R}^6$ and ${}^{B_i}V_r \in \mathbb{R}^6$, and terms from the vector of gravity propagation, and where $\hat{\theta}_i \in \mathbb{R}^{13}$ is the estimated parameters vector composed by the mass of the link, the elements of the vector pointing from the origin of the reference frame of the link toward its mass center, and elements of the inertia tensor of the link. To estimate the parameters in $\hat{\theta}_i$, s_i is defined as follows:

$$s_i = Y_i^T\left({}^{B_i}V_r - {}^{B_i}V\right) \tag{A II-11}$$

$$\hat{\theta}_{i\gamma} = \mathcal{P}\left(s_{i\gamma}(t), \rho_{i\gamma}, a_{i\gamma}(t), b_{i\gamma}(t), t\right) \tag{A II-12}$$

For $i = 1, \dots, n$ and $\gamma = 1, \dots, 13$ where $\hat{\theta}_{i\gamma}$ represents the γth parameter of the ith joint, $s(t) \in \mathbb{R}$ is a scalar variable, $\rho_{i\gamma}$ is the parameter update gain, $a_{i\gamma}(t)$ and $b_{i\gamma}(t)$ are the lower and upper bounds of $\hat{\theta}_{i\gamma}$ respectively, and the projection function $\mathcal{P}$, is a differentiable scalar function defined for $t \geq 0$ such that its time derivative is governed by:

$$\dot{\mathcal{P}} = \rho\, s(t)\, \mathcal{K} \tag{A II-13}$$

with:

$$\mathcal{K} = \begin{cases} 0 \;\; if\; \mathcal{P} \leq a(t) and\; s(t) \leq 0 \\ 0 \;\; if\; \mathcal{P} \geq b(t) and\; s(t) \geq 0 \\ 1 \qquad otherwise \end{cases}$$

Once this step is done, the required force/moment vectors at the cutting points are obtained as follows:

$$\begin{aligned} {}^{B_n}F_r &= {}^{B_n}F_r^* \\ {}^{B_i}F_r &= {}^{B_i}F_r^* + {}^{B_i}U_{B_{i+1}}\, {}^{B_{i+1}}F_r \end{aligned} \tag{A II-14}$$

for $i = n-1, \dots, 1$. The next step is the calculation of the dynamics of the joints. For $i = 1, \dots, n$ in (A II-15), (A II-16), (A II-17) and (A II-18), the following Y vector and parameter vector are defined:

$$Y_{ai} = [\ddot{q}_{ir} \quad sign(\dot{q}_{ir}) \quad \dot{q}_{ir} \quad 1] \tag{A II-15}$$

$$\theta_{ai} = [J_{mi} \quad k_{ci} \quad k_{vi} \quad c_i]^T \tag{A II-16}$$

where the sub-index a in the vectors is used to differentiate joint variables form the link variables introduced in (A II-10), J_{mi} is the equivalent mass or moment of inertia, $k_{ci} > 0$ denotes the Coulomb friction coefficient, $k_{ci} > 0$ the viscous friction coefficient and c_i denotes an offset that accommodates asymmetric Coulomb frictions. Defining the s function:

$$s_{ai} = Y_{ai}^T(\dot{q}_{ir} - \dot{q}_i) \tag{A II-17}$$

Then, the same procedure as above in (A II-12) and (A II-13) is used to estimate the parameters. Next the net torque for the joint τ_{ir}^* is obtained as follows:

$$\tau_{ir}^* = Y_{ai}\,\hat{\theta}_{ai} + k_{ai}(\dot{q}_{ir} - \dot{q}_i) \tag{A II-18}$$

where τ_{ir}^* is the net torque of the joint, k_{ai} denotes a feedback gain and $\hat{\theta}_{ai} \in \mathbb{R}^4$ denotes the estimate of $\theta_{ai} \in \mathbb{R}^4$.

A II-3 Control

To develop the control of the entire system, the torque resulting from the link and joint analysis are combined. First, it is required to extract the torque of the link force/moment vector.

$$\tau_{air} = z^{T\ B_i}F_r \tag{A II-19}$$

for $i = 1, \dots, n$. With $z = [0 \quad 0 \quad 0 \quad 0 \quad 0 \quad 1]^T$ that was defined before, the control torque is designed as:

$$\tau_i = \tau_{ir}^* + \tau_{air} \tag{A II-20}$$

for $i = 1, \dots, n$.

BIBLIOGRAPHY

Alcocer, A., A. Robertsson, A. Valera and R. Johansson. 2003. « Force estimation and control in robot manipulators ». In *Robot Control 2003 (SYROCO'03): A Proceedings Volume from the 7th IFAC Symposium, Wrocław, Poland, 1-3 September 2003*. (1-3 September 2003) Vol. 1, p. 55. International Federation of Automatic Control.

Artemiadis, Panagiotis K., and Kostas J. Kyriakopoulos. 2008. « Estimating arm motion and force using EMG signals: On the control of exoskeletons ». In *2008 IEEE/RSJ International Conference on Intelligent Robots and Systems (IROS 2008)*. (Nice, France, 22-26 September), p. 279-284.

Asada, Haruhiko, and Jean-Jacques E Slotine. 1986. *Robot analysis and control*. New York: J. Wiley, 277 p.

Brackbill, E. A., Mao Ying, S. K. Agrawal, M. Annapragada and V. N. Dubey. 2009. « Dynamics and control of a 4-dof wearable cable-driven upper arm exoskeleton ». In *Robotics and Automation, 2009. ICRA '09. IEEE International Conference on*. (12-17 May 2009), p. 2300-2305.

Brigham and Women's Hospital Rehabilitation Services. 2014. « Physical Therapy Standards of Care and Protocols ». < http://www.brighamandwomens.org/Patients_Visitors/pcs/rehabilitationservices/StandardsofCare.aspx >. Accessed 2 September 2014.

Brokaw, Elizabeth B., Theresa Murray, Tobias Nef and Peter S. Lum. 2011. « Retraining of interjoint arm coordination after stroke using robot-assisted time-independent functional training ». *Journal of Rehabilitation Research & Development,* vol. 48, n° 4, p. 299-316.

Bureau of Labor Statistics. 2015. « Occupational Outlook Handbook, 2014-15 Edition, Physical Therapists ». < http://www.bls.gov/ooh/healthcare/physical-therapists.htm >. Accessed February 26 2015.

Calanca, Andrea, and Paolo Fiorini. 2014. « Human-Adaptive Control of Series Elastic Actuators ». *Robotica,* vol. CJO, n° First View, p. 1-16.

Chan, Linping, Fazel Naghdy and David Stirling. 2013. « Extended active observer for force estimation and disturbance rejection of robotic manipulators ». *Robotics and Autonomous Systems,* vol. 61, n° 12, p. 1277-1287.

Chiri, Azzurra, Nicola Vitiello, Francesco Giovacchini, Stefano Roccella, Fabrizio Vecchi and Maria Chiara Carrozza. 2012. « Mechatronic Design and Characterization of the Index Finger Module of a Hand Exoskeleton for Post-Stroke Rehabilitation ». *IEEE/ASME Transactions on Mechatronics,* vol. 17, n° 5, p. 884-894.

Ciliz, M. Kemal. 2005. « Adaptive control of robot manipulators with neural network based compensation of frictional uncertainties ». *Robotica,* vol. 23, n° 02, p. 159-167.

Colombo, Roberto, Fabrizio Pisano, Silvestro Micera, Alessandra Mazzone, Carmen Delconte, M Chiara Carrozza, Paolo Dario and Giuseppe Minuco. 2005. « Robotic techniques for upper limb evaluation and rehabilitation of stroke patients ». *IEEE Transactions on Neural Systems and Rehabilitation Engineering,* vol. 13, n° 3, p. 311 - 324.

Coote, Susan, Brendan Murphy, William Harwin and Emma Stokes. 2008. « The effect of the GENTLE/s robot-mediated therapy system on arm function after stroke ». *Clinical Rehabilitation,* vol. 22, n° 5, p. 395-405.

Craig, John J. 2005. *Introduction to robotics: mechanics and control*, 3rd. Upper Saddle River, N.J.: Pearson/Prentice Hall, 408 p.

Culmer, Peter R., Andrew E. Jackson, Sophie Makower, Robert Richardson, J. Alastair Cozens, Martin C. Levesley and Bipin B. Bhakta. 2010. « A Control Strategy for Upper Limb Robotic Rehabilitation With a Dual Robot System ». *IEEE/ASME Transactions on Mechatronics,* vol. 15, n° 4, p. 575-585.

Department of Economic and Social Affairs. 2013. *World Population Ageing 2013*. Coll. « World Population Ageing ». New York: United Nations.

Dipietro, Laura, Mark Ferraro, Jerome Joseph Palazzolo, Hermano Igo Krebs, Bruce T. Volpe and Neville Hogan. 2005. « Customized interactive robotic treatment for stroke: EMG-triggered therapy ». *IEEE Transactions on Neural Systems and Rehabilitation Engineering,* vol. 13, n° 3, p. 325-334.

Do, K D, and J Pan. 2008. « Nonlinear control of an active heave compensation system ». *Ocean Engineering,* vol. 35, n° 5, p. 558-571.

Eschweiler, Jörg, Kurt Gerlach-Hahn, Arne Jansen-Toy and Steffen Leonhardt. 2014. « A survey on robotic devices for upper limb rehabilitation ». *Journal of neuroengineering and rehabilitation,* vol. 11, n° 1, p. 3.

Feriančik, Miloslav, and Ondrej Líška. 2014. « Automatic rehabilitation device based on robot and machine vision ». In *2014 International Conference on Mechatronics and Robotics, Structural Analysis (MEROSTA 2014)*. (Santorini Island, Greece, 17-21 July 2014), sous la dir. de Mastorakis, Nikos, Kleanthis Psarris, George Vachtsevanos, Philippe Dondon, Valeri Mladenov, Aida Bulucea, Imre Rudas, Olga Martin, Bogdan Epureanu, Cho W Solomon To and Hyung Hee Cho, p. 201-203. Coll. « Advances in Robotics, Mechatronics and Circuits ».

Ferrer, Steven Bruce, Cristobal Ochoa-Luna, Mohammad Habibur Rahman, Maarouf Saad and Philippe S Archambault. 2013. « HELIOS: The human machine interface for MARSE robot ». In *Human System Interaction (HSI), 2013 The 6th International Conference on*. (6-8 June 2013), p. 117-122.

Frisoli, A., C. Loconsole, D. Leonardis, F. Banno, M. Barsotti, C. Chisari and M. Bergamasco. 2012. « A New Gaze-BCI-Driven Control of an Upper Limb Exoskeleton for Rehabilitation in Real-World Tasks ». *Systems, Man, and Cybernetics, Part C: Applications and Reviews, IEEE Transactions on,* vol. 42, n° 6, p. 1169-1179.

Garrec, P., J. P. Friconneau, Y. Measson and Y. Perrot. 2008. « ABLE, an innovative transparent exoskeleton for the upper-limb ». In *IEEE/RSJ International Conference on Intelligent Robots and Systems, 2008. IROS 2008.* (22-26 September 2008), p. 1483-1488.

Garrec, Philippe. 2010. « Design of an anthropomorphic upper limb exoskeleton actuated by ball-screws and cables ». *University" Politehnica" of Bucharest Scientific Bulletin, Series D: Mechanical Engineering,* vol. 72, n° 2, p. 23-34.

Gopura, R. A. R. C., and K. Kiguchi. 2007. « Development of an exoskeleton robot for human wrist and forearm motion assist ». In *Industrial and Information Systems, 2007. ICIIS 2007. International Conference on*. p. 535-540.

Gorinevsky, Dimitry M., Alexander M. Formalsky and Anatoly Yu Schneider. 1997. *Force control of robotics systems*. Boca Raton, FL: CRC Press, 363 p.

Gupta, Abhishek, and Marcia K. O'Malley. 2006. « Design of a haptic arm exoskeleton for training and rehabilitation ». *IEEE/ASME Transactions on Mechatronics,* vol. 11, n° 3, p. 280-289.

Gupta, Abhishek, and Marcia K O'Malley. 2011. « Disturbance-observer-based force estimation for haptic feedback ». *Journal of Dynamic Systems, Measurement, and Control,* vol. 133, n° 1, p. 014505.

Gupta, Neeru, Carla Castillo-Laborde and Michel Landry. 2011. « Health-related rehabilitation services: assessing the global supply of and need for human resources ». *BMC Health Services Research,* vol. 11, n° 1, p. 276.

Hacksel, P. J., and S. E. Salcudean. 1994. « Estimation of environment forces and rigid-body velocities using observers ». In *1994 IEEE International Conference on Robotics and Automation*. p. 931-936. IEEE.

He, W., Y. Zhao, H. Tang, C. Sun and W. Fu. 2015. « A Wireless BCI and BMI System for Wearable Robots ». *Systems, Man, and Cybernetics: Systems, IEEE Transactions on,* vol. PP, n° 99, p. 1-11.

Health Canada. 2006. « It's Your Health - Stroke ». < http://www.hc-sc.gc.ca/hl-vs/iyh-vsv/diseases-maladies/stroke-vasculaire-eng.php >. Accessed 22 September 2015.

Hesse, Stefan, Henning Schmidt and Cordula Werner. 2006. « Machines to support motor rehabilitation after stroke: 10 years of experience in Berlin ». *Journal of Rehabilitation Research & Development,* vol. 43, n° 5, p. 671-678.

Hu, X. L., K. Y. Tong, R. Song, X. J. Zheng and K. H. Lui. 2008. « Robot-assisted wrist training for chronic stroke: A comparison between electromyography (EMG) driven robot and passive motion ». In *Biomedical Robotics and Biomechatronics, 2008. BioRob 2008. 2nd IEEE RAS & EMBS International Conference on*. (19-22 October 2008), p. 637-641.

Hu, X. L., K. Y. Tong, R. Song, X. J. Zheng, K. H. Lui, W. W. F. Leung, S. Ng and S. S. Y. Au-Yeung. 2009. « Quantitative evaluation of motor functional recovery process in

chronic stroke patients during robot-assisted wrist training ». *Journal of Electromyography and Kinesiology,* vol. 19, n° 4, p. 639-650.

Hu, X. L., K. Y. Tong, X. J. Wei, W. Rong, E. A. Susanto and S. K. Ho. 2013. « The effects of post-stroke upper-limb training with an electromyography (EMG)-driven hand robot ». *Journal of Electromyography and Kinesiology,* vol. 23, n° 5, p. 1065-1074.

Hu, Xiaoling, Kai Yu Tong, Rong Song, Vincent S. Tsang, Penny O. Leung and Le Li. 2007. « Variation of muscle coactivation patterns in chronic stroke during robot-assisted elbow training ». *Arch Phys Med Rehabil,* vol. 88, p. 1022 - 1029.

Huang, J., X. Tu and J. He. 2015. « Design and Evaluation of the RUPERT Wearable Upper Extremity Exoskeleton Robot for Clinical and In-Home Therapies ». *Systems, Man, and Cybernetics: Systems, IEEE Transactions on,* vol. PP, n° 99, p. 1-10.

Jackson, A E, R J Holt, P R Culmer, S G Makower, M C Levesley, R C Richardson, J A Cozens, Mon M Williams and B B Bhakta. 2007. « Dual robot system for upper limb rehabilitation after stroke: the design process ». *Proceedings of the Institution of Mechanical Engineers, Part C: Journal of Mechanical Engineering Science,* vol. 221, n° 7, p. 845-857.

Jiang, M. W., R. C. Wang, J. Z. Wang and D. W. Jin. 2005. « A Method of Recognizing Finger Motion Using Wavelet Transform of Surface EMG Signal ». In *Engineering in Medicine and Biology Society, 2005. IEEE-EMBS 2005. 27th Annual International Conference of the*. (17-18 January 2006), p. 2672-2674.

Katsura, S., Y. Matsumoto and K. Ohnishi. 2007. « Modeling of Force Sensing and Validation of Disturbance Observer for Force Control ». *Industrial Electronics, IEEE Transactions on,* vol. 54, n° 1, p. 530-538.

Kazerooni, H., and Jenhwa Guo. 1993. « Human Extenders ». *Journal of Dynamic Systems, Measurement, and Control,* vol. 115, n° 2B, p. 281-290.

Khokhar, Z. O., Z. G. Xiao and C. Menon. 2010. « Surface EMG pattern recognition for real-time control of a wrist exoskeleton ». *Biomed Eng Online,* vol. 9, p. 41.

Khushaba, Rami N., Ahmed Al-Ani and Adel Al-Jumaily. 2007. « Swarm Intelligence based Dimensionality Reduction for Myoelectric Control ». In *Intelligent Sensors, Sensor*

Networks and Information, 2007. ISSNIP 2007. 3rd International Conference on. (3-6 December 2007), p. 577-582.

Kiguchi, K., and Y. Hayashi. 2012. « An EMG-Based Control for an Upper-Limb Power-Assist Exoskeleton Robot ». *Systems, Man, and Cybernetics, Part B: Cybernetics, IEEE Transactions on,* vol. 42, n° 4, p. 1064-1071.

Klamroth-Marganska, Verena, Javier Blanco, Katrin Campen, Armin Curt, Volker Dietz, Thierry Ettlin, Morena Felder, Bernd Fellinghauer, Marco Guidali, Anja Kollmar, Andreas Luft, Tobias Nef, Corina Schuster-Amft, Werner Stahel and Robert Riener. 2014. « Three-dimensional, task-specific robot therapy of the arm after stroke: a multicentre, parallel-group randomised trial ». *The Lancet Neurology,* vol. 13, n° 2, p. 159-166.

Komada, S., Y. Hashimoto, N. Okuyama, T. Hisada and J. Hirai. 2009. « Development of a Biofeedback Therapeutic-Exercise-Supporting Manipulator ». *IEEE Transactions on Industrial Electronics,* vol. 56, n° 10, p. 3914-3920.

Krebs, H. I., J. J. Palazzolo, L. Dipietro, M. Ferraro, J. Krol, K. Rannekleiv, B. T. Volpe and N. Hogan. 2003. « Rehabilitation Robotics: Performance-Based Progressive Robot-Assisted Therapy ». *Autonomous Robots,* vol. 15, n° 1, p. 7-20.

Krebs, H. I., B. T. Volpe, D. Williams, J. Celestino, S. K. Charles, D. Lynch and N. Hogan. 2007. « Robot-Aided Neurorehabilitation: A Robot for Wrist Rehabilitation ». *Neural Systems and Rehabilitation Engineering, IEEE Transactions on,* vol. 15, n° 3, p. 327-335.

Kurnicki, Adam, Bartłomiej Stanczyk and Bartosz Kania. 2014. « Manipulator development for telediagnostics ». In *2014 International Conference on Mechatronics and Robotics, Structural Analysis (MEROSTA 2014)*. (Santorini Island, Greece, 17-21 July 2014), sous la dir. de Mastorakis, Nikos, Kleanthis Psarris, George Vachtsevanos, Philippe Dondon, Valeri Mladenov, Aida Bulucea, Imre Rudas, Olga Martin, Bogdan Epureanu, Cho W Solomon To and Hyung Hee Cho, p. 214-218. Coll. « Advances in Robotics, Mechatronics and Circuits ».

Kwakkel, Gert, Boudewijn J. Kollen and Hermano I. Krebs. 2008. « Effects of Robot-Assisted Therapy on Upper Limb Recovery After Stroke: A Systematic Review ». *Neurorehabilitation and Neural Repair,* vol. 22, n° 2, p. 111-121.

Landry, Michel D, Thomas C Ricketts and Molly C Verrier. 2007. « The precarious supply of physical therapists across Canada: exploring national trends in health human resources (1991 to 2005) ». *Human Resources for Health,* vol. 5, n° 1, p. 23.

Li, Z., S. S. Ge, M. Adams and W. S. Wijesoma. 2008. « Robust adaptive control of uncertain force/motion constrained nonholonomic mobile manipulators ». *Automatica,* vol. 44, n° 3, p. 776-784.

Lo, Ho Shing, and Sheng Quan Xie. 2012. « Exoskeleton robots for upper-limb rehabilitation: State of the art and future prospects ». *Medical Engineering & Physics,* vol. 34, n° 3, p. 261-268.

Loureiro, Rui, Farshid Amirabdollahian, Michael Topping, Bart Driessen and William Harwin. 2003. « Upper Limb Robot Mediated Stroke Therapy—GENTLE/s Approach ». *Autonomous Robots,* vol. 15, n° 1, p. 35-51.

Lucas, L., M. DiCicco and Y Matsuoka. 2004. « An EMG-Controlled Hand Exoskeleton for Natural Pinching ». *Journal of Robotics and Mechatronics,* vol. 16, n° 5, p. 482-488.

Lum, Peter S., Charles G. Burgar, Peggy C. Shor, Matra Majmundar and Machiel Van der Loos. 2002. « Robot-assisted movement training compared with conventional therapy techniques for the rehabilitation of upper-limb motor function after stroke ». *Archives of Physical Medicine and Rehabilitation,* vol. 83, n° 7, p. 952-959.

Lum, PS, CG Burgar and PC Shor. 2004. « Evidence for improved muscle activation patterns after retraining of reaching movements with the MIME robotic system in subjects with post-stroke hemiparesis ». *IEEE Trans Neural Syst Rehabil Eng,* vol. 12, n° 2, p. 186 - 194.

Mackay, Judith, and George A. Mensah. 2004. « The Atlas of Heart Disease and Stroke ». In., p. 112. Geneva, Switzerland: World Health Organization. < http://www.who.int/cardiovascular_diseases/resources/atlas/en/ >.

Masiero, Stefano, Mario Armani and Giulio Rosati. 2011. « Upper-limb robot-assisted therapy in rehabilitation of acute stroke patients: focused review and results of new randomized controlled trial ». *Journal of Rehabilitation Research & Development,* vol. 48, n° 4, p. 355-366.

Masiero, Stefano, Andrea Celia, Giulio Rosati and Mario Armani. 2007. « Robotic-Assisted Rehabilitation of the Upper Limb After Acute Stroke ». *Archives of Physical Medicine and Rehabilitation,* vol. 88, n° 2, p. 142-149.

Miller, Levi Makaio, and Jacob Rosen. 2010. « Comparison of multi-sensor admittance control in joint space and task space for a seven degree of freedom upper limb exoskeleton ». In *Biomedical Robotics and Biomechatronics (BioRob), 2010 3rd IEEE RAS and EMBS International Conference on*. (Tokyo, Japan, 26-29 September 2010), p. 70-75.

Mistry, M., P. Mohajerian and S. Schaal. 2005. « An exoskeleton robot for human arm movement study ». In *Intelligent Robots and Systems, 2005. (IROS 2005). 2005 IEEE/RSJ International Conference on*. p. 4071-4076.

National Stroke Association®. 2012. « Effects of Stroke - Paralysis ». Internet. < http://www.stroke.org/site/PageServer?pagename=paralysis >. Accessed 10 June 2014.

Nef, Tobias, Marco Guidali, Verena Klamroth-Marganska and Robert Riener. 2009. « ARMin - Exoskeleton Robot for Stroke Rehabilitation ». In *World Congress on Medical Physics and Biomedical Engineering, September 7 - 12, 2009, Munich, Germany*, sous la dir. de Dössel, Olaf, and WolfgangC Schlegel. Vol. 25/9, p. 127-130. Coll. « IFMBE Proceedings »: Springer Berlin Heidelberg.

Nicosia, S, and P Tomei. 1990. « Robot control by using only joint position measurements ». *Automatic Control, IEEE Transactions on,* vol. 35, n° 9, p. 1058-1061.

Norouzi-Gheidari, Nahid, Philippe S. Archambault and Joyce Fung. 2012. « Effects of robot-assisted therapy on stroke rehabilitation in upper limbs: systematic review and meta-analysis of the literature ». *Journal of Rehabilitation Research & Development,* vol. 49, n° 4, p. 479-496.

Ochoa Luna, Cristóbal, Mohammad Habibur Rahman, Maarouf Saad and Philippe S Archambault. 2014a. « Robotic assisted trajectory tracking for human arm rehabilitation ». In *2014 International Conference on Mechatronics and Robotics, Structural Analysis (MEROSTA 2014)*. (Santorini Island, Greece, 17-21 July 2014), under the direction of Mastorakis, Nikos, Kleanthis Psarris, George Vachtsevanos, Philippe Dondon, Valeri Mladenov, Aida Bulucea, Imre Rudas, Olga Martin, Bogdan Epureanu, Cho W Solomon To and Hyung Hee Cho, p. 51-55.

Ochoa Luna, Cristóbal, Mohammad Habibur Rahman, Maarouf Saad, Philippe S Archambault and Steven Bruce Ferrer. 2015. « Admittance-based upper limb robotic active and active-assistive rehabilitation ». *International Journal of Advanced Robotic Systems,* vol. 12, p. 117.

Ochoa Luna, Cristóbal, Mohammad Habibur Rahman, Maarouf Saad, Philippe S Archambault and Wen-Hong Zhu. 2014b. « Virtual decomposition control of an exoskeleton robot arm ». *Robotica,* vol. CJO, p. 1-23.

Otten, Alexander, Carsten Voort, Arno Stienen, Ronald Aarts, Edwin van Asseldonk and Herman van der Kooij. 2015. « LIMPACT:A Hydraulically Powered Self-Aligning Upper Limb Exoskeleton ». *IEEE/ASME Transactions on Mechatronics,* vol. 20, n° 5, p. 2285-2298.

Ozkul, Fatih, and Duygun Erol Barkana. 2013. « Upper-Extremity Rehabilitation Robot RehabRoby: Methodology, Design, Usability and Validation ». *International Journal of Advanced Robotic Systems,* vol. 10, p. 1-13.

Patton, James L, Mary Ellen Stoykov, Mark Kovic and Ferdinando A Mussa-Ivaldi. 2006. « Evaluation of robotic training forces that either enhance or reduce error in chronic hemiparetic stroke survivors ». *Experimental Brain Research,* vol. 168, n° 3, p. 368-383.

Perry, Joel C, and Jacob Rosen. 2006. « Design of a 7 Degree-of-Freedom Upper-Limb Powered Exoskeleton ». In *Biomedical Robotics and Biomechatronics, 2006. BioRob 2006. The First IEEE/RAS-EMBS International Conference on*. (20-22 February 2006), p. 805-810.

Perry, Joel C, Jacob Rosen and Stephen Burns. 2007. « Upper-Limb Powered Exoskeleton Design ». *Mechatronics, IEEE/ASME Transactions on,* vol. 12, n° 4, p. 408-417.

Phinyomark, A., C. Limsakul and P. Phukpattaranont. 2010. « EMG signal estimation based on adaptive wavelet shrinkage for multifunction myoelectric control ». In *Electrical Engineering/Electronics Computer Telecommunications and Information Technology (ECTI-CON), 2010 International Conference on*. (19-21 May 2010), p. 322-326.

Pons, José L. (1, 5). 2008. *Wearable Robots: Biomechatronic Exoskeletons*. Hoboken, N. J.: Wiley, xviii, 338 p. p.

Popescu, N., D. Popescu, M. Ivanescu, D. Popescu, C. Vladu and I. Vladu. 2013. « Force observer-based control for a rehabilitation hand exoskeleton system ». In *Control Conference (ASCC), 2013 9th Asian*. (23-26 June 2013), p. 1-6.

Rahman, M. H., T. K. Ouimet, M. Saad, J. P. Kenne and P. S. Archambault. 2011a. « Dynamic Modeling and Evaluation of a Robotic Exoskeleton for Upper-Limb Rehabilitation ». *International Journal of Information Acquisition,* vol. 8, n° 1, p. 83-102.

Rahman, Mohammad Habibur. 2012. « Development of an exoskeleton robot for UPPER-LIMB rehabilitation ». Doctor of Philosophy thesis. Montréal, École de technologie supérieure, (xx, 186) p.

Rahman, Mohammad Habibur, Kazuo Kiguchi, Md Mozasser Rahman and Makoto Sasaki. 2006. « Robotic Exoskeleton for Rehabilitation and Motion Assist ». In *Industrial and Information Systems, First International Conference on*. (8-11 August 2006), p. 241-246.

Rahman, Mohammad Habibur, Thierry Kittel-Ouimet, Maarouf Saad, Jean-Pierre Kenné and Philippe S Archambault. 2011b. « Dynamic Modeling and Evaluation of a Robotic Exoskeleton for Upper-limb Rehabilitation ». *International Journal of Information Acquisition,* vol. 8, n° 1, p. 83-102.

Rahman, Mohammad Habibur, Thierry Kittel-Ouimet, Maarouf Saad, Jean-Pierre Kenné and Philippe S. Archambault. 2012a. « Development and Control of a Robotic Exoskeleton for Shoulder, Elbow and Forearm Movement Assistance ». *Applied Bionics and Biomechanics,* vol. 9, n° 2012, p. 275-292.

Rahman, Mohammad Habibur, Cristóbal Ochoa Luna, Mohammad Jahidur Rahman, Maarouf Saad and Philippe Archambault. 2014. « Force-position control of a robotic exoskeleton to provide upper extremity movement assistance ». *International Journal of Modelling, Identification and Control,* vol. 21, n° 4, p. 390-400.

Rahman, Mohammad Habibur, Cristobal Ochoa Luna, Maarouf Saad and Philippe S Archambault. 2015a. « EMG Based Control of a Robotic Exoskeleton for Shoulder and Elbow Motion Assist ». *Journal of Automation and Control Engineering,* vol. 3, n° 4, p. 270-276.

Rahman, Mohammad Habibur, Mohammad Jahidur Rahman, Cristóbal Ochoa Luna, Maarouf Saad, Jean-Pierre Kenné and Philippe S Archambault. 2015b. « Development of a whole arm wearable robotic exoskeleton for rehabilitation and to assist upper limb movements ». *Robotica,* vol. 33, n° 01, p. 19-39.

Rahman, Mohammad Habibur, Maarouf Saad, Jean-Pierre Kenné and Philippe S Archambault. 2012b. « Nonlinear Sliding Mode Control Implementation of an Upper Limb Exoskeleton Robot to Provide Passive Rehabilitation Therapy ». In *Intelligent Robotics and Applications*, sous la dir. de Su, Chun-Yi, Subhash Rakheja and Honghai Liu. Vol. 7507, p. 52-62. Coll. « Lecture Notes in Computer Science », 7507: Springer Berlin Heidelberg.

Rahman, Mohammad Habibur, Maarouf Saad, Jean-Pierre Kenné, Philippe S Archambault and Thierry Kittel-Ouimet. 2012c. « Development of a 4DoFs exoskeleton robot for passive arm movement assistance ». *International Journal of Mechatronics and Automation,* vol. 2, n° 1, p. 34-50.

Riener, Robert, T Nef and G Colombo. 2005. « Robot-aided neurorehabilitation of the upper extremities ». *Medical & Biological Engineering & Computing,* vol. 43, n° 1, p. 2-10.

Robertson, D. Gordon E. 2004. *Research methods in biomechanics*. Champaign, Ill.: Human Kinetics, x, 309 p. p.

Rocon, E., J. M. Belda-Lois, A. F. Ruiz, M. Manto, J. C. Moreno and J. L. Pons. 2007. « Design and Validation of a Rehabilitation Robotic Exoskeleton for Tremor Assessment and Suppression ». *Neural Systems and Rehabilitation Engineering, IEEE Transactions on,* vol. 15, n° 3, p. 367-378.

Rosen, Jacob, Moshe Brand, Moshe B Fuchs and Mircea Arcan. 2001. « A myosignal-based powered exoskeleton system ». *IEEE Trans Systerms, Man, and Cybernetics,* vol. 31, n° 3, p. 210 - 212.

Sankai, Yoshiyuki. 2006. « Leading Edge of Cybernics: Robot Suit HAL ». In *SICE-ICASE, 2006. International Joint Conference*. (Bexco, Busan, Korea, 18-21 October 2006), p. P-1-P-2.

Sarakoglou, Ioannis, Sophia Kousidou, Nikolaos G Tsagarakis and Darwin G Caldwell. 2007. « Exoskeleton-based exercisers for the disabilities of the upper arm and hand ». In *Rehabilitation Robotics*, sous la dir. de Kommu, Sashi S. p. 499-522. I-Tech

Education and Publishing.
< http://www.intechopen.com/books/rehabilitation_robotics >.

Savitzky, Abraham, and Marcel J. E. Golay. 1964. « Smoothing and Differentiation of Data by Simplified Least Squares Procedures ». *Analytical Chemistry,* vol. 36, n° 8, p. 1627-1639.

Seamone, W., and G. Schmeisser. 1985. « Early clinical evaluation of a robot arm/worktable system for spinal-cord-injured persons ». *Journal of rehabilitation research and development,* vol. 22, n° 1, p. 38-57.

Seraji, Homayoun. 1994. « Adaptive admittance control: an approach to explicit force control in compliant motion ». In *1994 IEEE International Conference on Robotics and Automation*. (San Diego, CA., 8-13 May 1994) Vol. 4, p. 2705-2712. IEEE.

Siciliano, Bruno, and Oussama Khatib. 2008. *Springer Handbook of Robotics*. Berlin, Heidelberg: Springer Science+Business Media.

Smith, Ryan J., Francesco Tenore, David Huberdeau, Ralph Etienne-Cummings and Nitish V. Thakor. 2008. « Continuous decoding of finger position from surface EMG signals for the control of powered prostheses ». In *30th Annual International Conference of the IEEE Engineering in Medicine and Biology Society, 2008. EMBS 2008.* (British Columbia, Canada, 20-24 August 2008), p. 197-200. IEEE.

Song, Zuoshi, Jianqiang Yi, Dongbin Zhao and Xinchun Li. 2005. « A computed torque controller for uncertain robotic manipulator systems: Fuzzy approach ». *Fuzzy Sets and Systems,* vol. 154, n° 2, p. 208-226.

Sun, F. C., Z. Q. Sun and G. Feng. 1999. « An adaptive fuzzy controller based on sliding mode for robot manipulators ». *Systems, Man, and Cybernetics, Part B: Cybernetics, IEEE Transactions on,* vol. 29, n° 5, p. 661-667.

Tsagarakis, N., D. G. Caldwell and G. A. Medrano-Cerda. 1999. « A 7 DOF pneumatic muscle actuator (pMA) powered exoskeleton ». In *8th IEEE International Workshop on Robot and Human Interaction RO-MAN '99.* (Pisa, Italy, 27-29 September 1999), p. 327-333. IEEE.

Uzmay, Ibrahim, and Recep Burkan. 2002. « Parameter estimation and upper bounding adaptation in adaptive-robust control approaches for trajectory control of robots ». *Robotica,* vol. 20, n° 06, p. 653-660.

Van der Loos, H. Machiel , and David J. Reinkensmeyer. 2008. « Rehabilitation and Health Care Robotics ». In *Springer Handbook of Robotics*, sous la dir. de Siciliano, Bruno, and Oussama Khatib. p. 1225-1227. Berlin Heidelberg: Springer. < http://books.google.ca/books?id=Xpgi5gSuBxsC >.

Vitiello, N., T. Lenzi, S. Roccella, S. M. M. De Rossi, E. Cattin, F. Giovacchini, F. Vecchi and M. C. Carrozza. 2013. « NEUROExos: A Powered Elbow Exoskeleton for Physical Rehabilitation ». *Robotics, IEEE Transactions on,* vol. 29, n° 1, p. 220-235.

Wege, A., K. Kondak and G. Hommel. 2006. « Force Control Strategy for a Hand Exoskeleton Based on Sliding Mode Position Control ». In *Intelligent Robots and Systems, 2006 IEEE/RSJ International Conference on*. p. 4615-4620.

Wen-Hua, Chen, D. J. Ballance, P. J. Gawthrop and J. O'Reilly. 2000. « A nonlinear disturbance observer for robotic manipulators ». *Industrial Electronics, IEEE Transactions on,* vol. 47, n° 4, p. 932-938.

Younggeun, Choi, James Gordon, Kim Duckho and Nicolas Schweighofer. 2009. « An Adaptive Automated Robotic Task-Practice System for Rehabilitation of Arm Functions After Stroke ». *IEEE Transactions on Robotics,* vol. 25, n° 3, p. 556-568.

Zhang, Bin, Rong Xiong and Jun Wu. 2011. « Kinematics analysis of a novel 7-DOF humanoid manipulator for table tennis ». In *2011 International Conference on Electronics, Communications and Control (ICECC)*. (Ningbo, China, 09-11 September 2011), p. 1524-1528. IEEE.

Zhang, Mingming, T Claire Davies and Shane Xie. 2013. « Effectiveness of robot-assisted therapy on ankle rehabilitation - a systematic review ». *Journal of NeuroEngineering and Rehabilitation,* vol. 10, p. 30.

Zhijun, Li, S. S. Ge, M. Adams and W. S. Wijesoma. 2008. « Adaptive Robust Output-Feedback Motion/Force Control of Electrically Driven Nonholonomic Mobile Manipulators ». *Control Systems Technology, IEEE Transactions on,* vol. 16, n° 6, p. 1308-1315.

Zhou, Ma, and Pinhas. Ben-Tzvi. 2015. « RML Glove - An Exoskeleton Glove Mechanism With Haptics Feedback ». *IEEE/ASME Transactions on Mechatronics,* vol. 20, n° 2, p. 641-652.

Zhu, Wen-Hong (387-389). 2010. *Virtual Decomposition Control: Toward Hyper Degrees of Freedom Robots*. Coll. « Springer Tracts in Advanced Robotics », 60. Berlin Heidelberg: Springer, 448 p.

Zhu, Wen-Hong, and Joris De Schutter. 1999. « Adaptive control of mixed rigid/flexible joint robot manipulators based on virtual decomposition ». *IEEE Transactions on Robotics and Automation,* vol. 15, n° 2, p. 310-317.

Zhu, Wen-Hong, and Joris De Schutter. 2002. « Experimental verifications of virtual-decomposition-based motion/force control ». *IEEE Transactions on Robotics and Automation,* vol. 18, n° 3, p. 379-386.

Zhu, Wen-Hong, and Tom Lamarche. 2007. « Modular Robot Manipulators Based on Virtual Decomposition Control ». In *Robotics and Automation, 2007 IEEE International Conference on*. (10-14 April 2007), p. 2235-2240.

Zhu, Wen-Hong, Tom Lamarche, Erick Dupuis, David Jameux, Patrick Barnard and Liu Guangjun. 2013. « Precision Control of Modular Robot Manipulators: The VDC Approach With Embedded FPGA ». *IEEE Transactions on Robotics,* vol. 29, n° 5, p. 1162-1179.

Zhu, Wen-Hong, Jean-Claude Piedboeuf and Yves Gonthier. 2006. « A dynamics formulation of general constrained robots ». *Multibody System Dynamics,* vol. 16, n° 1, p. 37-54.

Zhu, Wen-Hong, Xi Yu-Geng, Zong-Jun Zhang, Bien Zeungnam and Joris De Schutter. 1997. « Virtual decomposition based control for generalized high dimensional robotic systems with complicated structure ». *IEEE Transactions on Robotics and Automation,* vol. 13, n° 3, p. 411-436.

Zhu, Wen-Hong, Bien Zeungnam and Joris De Schutter. 1998. « Adaptive motion/force control of multiple manipulators with joint flexibility based on virtual decomposition ». *IEEE Transactions on Automatic Control,* vol. 43, n° 1, p. 46-60.